

**Responses of a Locust Looming Sensitive Neuron, Flight Muscle  
Activity and Body Orientation to Changes in Object Trajectory,  
Background Complexity, and Flight Condition**

A Thesis Submitted to the College  
of Graduate and Postdoctoral Studies  
in Partial Fulfillment of the Requirements  
for the Degree of Doctor of Philosophy  
in the Department of Biology  
University of Saskatchewan  
By Cody William Manchester

© Copyright Cody William Manchester, May 2019 All Rights Reserved

## PERMISSION TO USE

In presenting this thesis in partial fulfillment of the requirements for a Postgraduate degree from the University of Saskatchewan, I agree that the Libraries of this University may make it freely available for inspection. I further agree that permission for copying of this thesis in any manner, in whole or in part, for scholarly purposes may be granted by the professor or professors who supervised my thesis work or, in their absence, by the Head of the Department or the Dean of the College in which my thesis work was done. It is understood that any copying or publication or use of this thesis or parts thereof for financial gain shall not be allowed without my written permission. It is also understood that due recognition shall be given to me and to the University of Saskatchewan in any scholarly use which may be made of any material in my thesis.

Requests for permission to copy or to make other uses of materials in this

thesis in whole or part should be addressed to:

Head of the Department of Biology,  
112 Science Place, University of Saskatchewan,  
Saskatoon, Saskatchewan, Canada S7N 5E2

OR

Dean of College of Graduate and Postdoctoral Studies,  
116 Thorvaldson Building, 110 Science Place, University of Saskatchewan,  
Saskatoon, Saskatchewan, Canada S7N 5C9

## ABSTRACT

Survival is one of the highest priorities of any animal. Interaction in the environment with conspecifics, predators, or objects, is driven by evolution of systems that can efficiently and rapidly respond to potential collision with these stimuli. Flight introduces further complexity for a collision avoidance system, requiring an animal to compute air speed, wind speed, ground speed, as well as transverse and longitudinal image flow, all within the context of detecting an approaching object. Understanding the mechanisms underlying neural control and coordination of motor systems to produce behaviours in response to the natural environment is a main goal of neuroethology. Locusts have a tractable nervous system, and a robust, reproducible collision avoidance response to looming stimuli. This tractable system allows recording from the nerve cord and flight muscles with precision and reliability, allowing us to answer important questions regarding the neuronal control of muscle coordination and, in turn, collision avoidance behaviour during flight. In flight, a collision avoidance behaviour will most often be a turn away from the approaching stimulus. I tested the hypothesis that during loosely tethered flight, synchrony between flight muscles increases just prior to the initiation of a turn and that muscle synchronization would correlate with body orientation changes during flight steering. I found that hind and forewing flight muscle synchronization events correlated strongly with forewing flight muscle latency changes, and to pitch and roll body orientation changes in response to a lateral looming visual stimulus. These findings led me to investigate further the role of the looming-sensitive descending contralateral movement detector (DCMD) neuron in flight muscle coordination and the initiation of forewing asymmetry in rigidly tethered locusts that generate a flight-like rhythm. By conducting simultaneous recordings from the nerve cord, forewing flight muscles, and visually recording the wing positions within the same flying animal, I hypothesized

that DCMD burst properties would correlate with flight muscle activity changes and the initiation of wing asymmetry associated with turning behaviour. Furthermore, I accessed the effect of manipulating background complexity of the locust's visual environment, looming object trajectory, and the putative effect of mechanosensory feedback during flight, on DCMD burst firing rate properties. DCMD burst properties were affected by changes in background complexity and object trajectory, and most interestingly during flight. This suggests that reafferent feedback from the flight motor system modulates the DCMD signal, and therefore represents a more naturalistic representation of collision avoidance behaviour. A pivotal discovery in my study was the temporal role of bursting in collision avoidance behaviour. I found that the first burst in a DCMD spike train represents the earliest detectable neuronal event correlated with muscle activity changes and the creation of wing asymmetry. I found strong correlations across all object trajectories and background complexities, between the timing of the first bursts, flight muscle activity changes and the initiation of wing asymmetry. These findings reinforce the importance of the temporal properties of DCMD bursting in collision avoidance behaviour.

## AKNOWLEDGEMENTS

This has been an adventure of a lifetime, that wouldn't have been possible without love and support along the way. I want to thank my parents for inspiring me from when I was young, staying the course with me through every move, from apartment to apartment and degree to degree, never wavering to be there for me when I needed it. Thank you to my sister for always being on the other end of the phone when I was having a low day and always being a voice of reassurance. I want to thank my supervisor Professor Jack Gray. He believed in me and gave me a chance to pursue my scientific passions. I will be forever thankful for his guidance and mentorship from the first day I stepped into the lab to the last day. Thank you to my committee members, Professor Tracy Marchant, Professor Doug Chivers, and Professor John Howland, who have supported me through thick and thin, always making themselves present whenever I had a question or concern. Thank you for your honesty and pushing me when I needed to be pushed. Survival in the lab is dependent on those you work with. Thank you to all of my lab mates over the years for always providing a helping hand when needed, and for getting me through the most frustrating of days.

## TABLE OF CONTENTS

PERMISSION TO USE.....	i
ABSTRACT .....	ii
ACKNOWLEDGEMENTS .....	iv
TABLE OF CONTENTS .....	v
LIST OF FIGURES .....	viii
LIST OF TABLES .....	x
LIST OF EQUATIONS.....	xi
LIST OF ABBREVIATIONS AND SYMBOLS .....	xii
CHAPTER 1. GENERAL INTRODUCTION .....	1
1.1 NEUROETHOLOGY .....	1
1.2.1 PRINCIPLES OF FLIGHT .....	1
1.2.2 INSECT FLIGHT.....	2
1.3 NEURAL CONTROL OF MOTION .....	5
1.3.1 SENSORY ENVIRONMENTS.....	5
1.3.2 VISION .....	6
1.3.3 SENSORY CODING .....	8
1.3.4 CENTRAL PATTERN GENERATION .....	10
1.3.5 SENSORY MOTOR INTEGRATION .....	12
1.4 LOCUST BIOLOGY.....	13
1.4.1 LOCUST BIOLOGY AND ANATOMY .....	13
1.4.2 FLIGHT BEHAVIOUR AND COLLISION AVOIDANCE.....	23
1.4.3 DCMD AND LOOMING SENSITIVITY .....	24
1.5 OBJECTIVES .....	30
CHAPTER 2 .....	32
FLIGHT MUSCLE COORDINATION AND BODY ORIENTATION CHANGES OF LOCUST MIGRATORIA DURING COLLISION AVOIDANCE BEHAVIOUR .....	32
2.1 ABSTRACT .....	32
2.2 INTRODUCTION .....	33

<b>2.3 MATERIALS AND METHODS</b>	35
2.3.1 ANIMALS	35
2.3.2 PREPARATION	35
2.3.3 VISUAL STIMULI	36
2.3.4 RECORDING TECHNIQUES	39
2.3.5 EMG ANALYSIS	39
2.3.6 VIDEO ANALYSIS	44
2.3.7 STATISTICAL ANALYSIS	45
<b>2.4 RESULTS</b>	47
2.4.1 GENERAL BEHAVIOUR	47
2.4.2 RESPONSE TIME AND DURATION	47
2.4.3 BODY ORIENTATION	48
2.4.4 DEPRESSOR MUSCLE ACTIVITY	53
2.4.5 TIMINGS AND CORRELATIONS	53
<b>2.5 DISCUSSION</b>	57
<b>CHAPTER 3</b>	64
<b>RESPONSE OF A LOCUST MOTION SENSITIVE NEURON, FLIGHT MUSCLE ACTIVITY, AND WING ASYMMETRY DURING FLIGHT STEERING</b>	64
<b>3.1 ABSTRACT:</b>	64
<b>3.2 INTRODUCTION</b>	65
<b>3.3 MATERIAL AND METHODS</b>	70
3.3.1 ANIMALS	70
3.3.2 PREPARATION	70
3.3.3 VISUAL STIMULUS	71
3.3.4 RECORDING TECHNIQUES	72
3.3.5 VISUAL ANALYSIS	72
3.3.6 SPIKE TRAIN ANALYSIS	76
3.3.7 STATISTICAL ANALYSIS	79
<b>3.4 RESULTS</b>	80
3.4.1 GENERAL BEHAVIOUR	80
3.4.2 MUSCLE ACTIVITY AND TIMING	82
3.4.3 DCMD BURSTING ACTIVITY AND TIMING	83

4.4 DCMD BURSTING, MUSCLE ACTIVITY AND WING ASYMMETRY .....	89
<b>3.5 DISCUSSION .....</b>	<b>97</b>
<b>CHAPTER 4. GENERAL DISCUSSION.....</b>	<b>105</b>
4.1 FLIGHT MUSCLE COORDINATION IN COLLISION AVOIDANCE BEHAVIOR.....	105
4.2 THE EFFECT OF BEHAVIOUR ON THE SENSORY SYSTEM.....	107
4.3 FUTURE DIRECTIONS.....	107
.....	110
<b>REFERENCES.....</b>	<b>111</b>



## LIST OF FIGURES

<b>Figure 1.1:</b> Locust anatomy and degrees of freedom during flight. ....	15
<b>Figure 1.2:</b> Locust thoracic muscle anatomy. ....	17
<b>Figure 1.3:</b> Motion sensing neurons in the locust nervous system .....	18
<b>Figure 1.4:</b> The apposition compound eye of a locust. ....	21
<b>Figure 1.5:</b> Flight is produced by central pattern generators in the thoracic ganglia. ....	22
<b>Figure 1.6:</b> Visual expansion properties of a looming stimulus and corresponding DCMD responses. ....	26
<b>Figure 1.7:</b> Relationship between DCMD activity and locust jumping responses to looming stimuli. ....	28
<b>Figure 1.8:</b> DCMD and behavioural responses during gliding. ....	29
<b>Figure 2.1:</b> Diagram of experimental set up to record muscle activity and wing kinematics during collision avoidance. ....	38
<b>Figure 2.2:</b> Body position, body orientation and muscle activity data from one locust producing a left turn. ....	41
<b>Figure 2.3:</b> Plots of synchrony versus time from one animal responding to a lateral looming disc. ....	43
<b>Figure 2.4:</b> Graphs showing body orientation changes over time in response to a lateral looming disc. ....	46
<b>Figure 2.5:</b> Temporal properties of behaviour and body orientation parameters. ....	49
<b>Figure 2.6:</b> Changes in instantaneous wing beat frequency for all pure left turns .....	51
<b>Figure 2.7:</b> Average changes in locust body orientation during initiation of a turn to the left....	52
<b>Figure 2.8:</b> Linear regressions of temporal properties of muscles activity and body orientation.. ....	55
<b>Figure 2.9:</b> Order of muscle and body orientation events that occur during collision avoidance .....	63

<b>Figure 3.1:</b> A top and front view of the experimental set up .....	68
<b>Figure 3.2:</b> Behavioural and physiological data from one locust during a left turn in response to a sphere looming 45° from the left.....	73
<b>Figure 3.3:</b> A Graph representing the change in angular difference between the left and right forewing, during a presentation of a leftwards 45° loom, in a simple background. ....	75
<b>Figure 3.4:</b> EMG and DCMD recordings showing extractable parameters of muscle timing and DCMD bursting. ....	77
<b>Figure 3.5:</b> Comparison of wing asymmetry timing and maximum angular difference between different stimulus conditions. ....	81
<b>Figure 3.6:</b> Comparison of muscle activity properties across different presentation conditions. ....	85
<b>Figure 3.7:</b> DCMD firing rate and intraburst firing rate for each presentation and flight condition. ....	88
<b>Figure 3.8:</b> Effects of stimulus background complexity, object trajectory, and flight on DCMD burst parameters. ....	91
<b>Figure 3.9:</b> Relative timing of DCMD bursting, flight muscle synchrony and latency, and behaviour during different presentation conditions. ....	93
<b>Figure 3.10:</b> Correlations between DCMD events, muscle events and wing asymmetry timings under varying presentation conditions. ....	95
<b>Figure 4.1:</b> Diagram illustrating the timing of events leading to collision avoidance behaviour for three looming trajectories.....	109

## LIST OF TABLES

<b>3.1:</b> Neural, muscle, and wing asymmetry timing (PPM) correlations .....	94
--	----

## LIST OF EQUATIONS

<b>1.1:</b> Calculation of Reynolds Number .....	2
<b>2.1:</b> Calculation for Michelson contrast ratio .....	36
<b>2.2:</b> Calculation of yaw, pitch, and roll body orientations.....	44
<b>3.1:</b> Calculation of wing asymmetry difference.....	72

## LIST OF ABBREVIATIONS AND SYMBOLS

<b>WBF</b>	Wing Beat Frequency
<b>TOFB</b>	Time of first burst
<b>TOS</b>	Time of synchrony
<b>TOL</b>	Time of Latency
<b>TOWA</b>	Time of wing asymmetry
$\theta$	Wing angle
$\psi$	Yaw
$X$	Pitch
$\eta$	Roll
<b>LGMD</b>	Lobula giant movement detector
<b>DCMD</b>	Descending contralateral movement detector
<b>Re</b>	Reynolds number
<b>TSDN</b>	Target selective descending neurons
<b>IPSP</b>	Inhibitory postsynaptic potential
<b>EPSP</b>	Excitatory post synaptic potential
<b>ISI</b>	Inter spike interval
<b>PPM</b>	Pearson product moment

## **CHAPTER 1. GENERAL INTRODUCTION**

### **1.1 NEUROETHOLOGY**

Neuroethology is the study of the neural basis of natural animal behaviour, using combinations of powerful neurophysiological and behavioural techniques to uncover the underlying mechanisms responsible for behaviour within a natural environment. Neuroethology assists in answering question in more complex vertebrate systems, like spatial orientation and learning in rats (Dudchenko and Wallace, 2018) and navigation in bats (Genzel et al., 2018). Invertebrates, which contain tractable nervous systems, allow for unambiguous identification of specific neurons and processes responsible for the production of behaviours such as swimming control in jelly fish (Satterlie, 2002), cray fish tail flip escape behaviour (Zucker, 1971) and flight control in insects (Wilson, 1968). Insects are particularly ideal, given the tractable neural architecture capable of producing complex behaviours such as navigation and flight maneuvering.

#### **1.2.1 PRINCIPLES OF FLIGHT**

Flying objects must generate enough lift to become airborne. In technology and nature, airfoils (wings) are the dominant structures that produce lift. Wings manipulate the flow of air deflecting off of their surface, creating pressure differences between the top and bottom surfaces. These pressure differences create an air velocity ratio that results in a relatively lower pressure on the upper wing surface, thus generating lift and overcoming drag (Cayley, 1809). Two important principles, steady-state and non steady-state aerodynamics, typically differentiate artificial and biological flight, respectively. Steady-state aerodynamics are typical of fixed wing aircraft and result from a fixed body reference frame where linear and angular velocity vectors remain constant and there is no net acceleration during forward flight - forces of drag, lift, thrust

and weight cancel out (Bernard, 2005). During turning, centripetal acceleration is created as a product of the magnitude of the true air speed and radius of the turn (McClamroch, 2011). Non steady-state aerodynamics arise from changes in wing positions and the forces are not constant. Instead, air moves, ventral to dorsal, across the wings, resulting in a net rotation of air around the airfoil surface. These net rotations form vortices, which are the origins of lift generation in insects (Dudley, 2000). Non-steady flight provides more maneuverability and, during optimal wing motions, reduces energy required for aerodynamically generated forces by 27% (Pesavento and Wang, 2009). Insect flight capabilities are constrained by the Reynolds number associated with the size and shape of the wings. The Reynolds number ( $Re$ ) represents the relationship between inertial forces and the viscous forces on the wings and is dependent on the characteristic wing length and the surrounding kinematic viscosity the air (Sommerfeld, 1908).

$$R_e = \frac{\rho VL}{\mu} \dots\dots\dots (1.1)$$

At low  $Re$ , laminar, viscous flow dominates, whereas high  $Re$  results in turbulent flows dominated by inertial forces. Large variations in wing size across the Class Insecta means that insects fly within a range of  $Re$  that spans 3 orders of magnitude, from 10 to 10,000 (Dudley, 2000). Even at low  $Re$ , inertial forces are roughly an order of magnitude higher than viscous forces (Sane, 2003a), though viscous forces still have an effect on the structuring of air flow and effect small and large insects differently (Sane, 2003a).

### 1.2.2 INSECT FLIGHT

Flying insects (Pterygota), have monophyletic origins from as far back as 480 million years ago (Whiting et al., 1997), and have since greatly diversified and developed many adaptations to challenges that exist in aerial environments. For example, dragonflies (Order Odonata) engage in complex prey hunting behaviours due to their ability to hover, fly backwards and perform rapid directional changes (Usherwood and Lehmann, 2008). To accomplish successful flight behaviours, insects modify movement of the wings and thorax to generate appropriate aerodynamic forces. Insects make use of non-steady state high lift aerodynamics, resulting from wing accelerations during the flapping cycle, and steady-state aerodynamics during behaviours such as glides (Cooter and Baker, 1977). To sustain flapping flight, insects rely on five aerodynamic principles: added mass, absence of stall, rotational circulation, clap and

fling, and wing-wake interactions (Chin and Lentink, 2016). These principles exist within a quasi-steady state model, created to better explain how insects are capable of flight outside of steady state aerodynamics. During flapping flight, wings undergo two translational movements (upstroke and downstroke) and two rotational movements (pronation and supination) (Chin and Lentink, 2016). The wings leading edge generates a rotational vortex, stabilized by axial flow which reinforces lift generation during the downstroke (Ellington et al., 1996). Added mass refers to pressure forces acting on the wing as a result of the air closest to the wings decelerating or accelerating more than air further from the wings. (Lehmann, 2004; Sane, 2003a; Sane and Dickinson, 2001) and, therefore, influencing aerodynamic force generation. During flight, leading edge vortices created at the beginning of a wing stroke can build up to a point where the flow is no longer attached to the wing, creating a stall (Ellington et al., 1996). Insects solve this issue by creating revolving motions about the base of the wings that induce centripetal and coriolis forces, thus stabilizing the growing leading edge vortex (Chin and Lentink, 2016; Ellington et al., 1996; Kruyt et al., 2015; Lentink and Dickinson, 2009). Significant control of lift is accomplished by changing the timing of rotations of the wings, manipulating the Kramer Effect, which is the creation of additional air circulation about the wings, ensuring that air flows smoothly across the surface at the trailing edge (Sane, 2003b; Sane and Dickinson, 2002) When these rotations occur within wing phases (pre or post upstroke or downstroke), positive or negative lift can be generated, respectively (Sane, 2003b; Sane and Dickinson, 2001). Certain species of insects invoke a clap and fling method of flapping, resulting in increased lift generation (Lighthill, 1973; Weis-fogh, 1973). When wings reach the top of the upstroke, the wings respective leading edge vortices negate one another, reducing the vorticity and allowing for more rapid generation of air circulation during the downstroke (Lehmann, 2004). Although beneficial, clap and fling is used primarily during takeoff and when executing more advanced behaviours (Chin and Lentink, 2016; Lehmann, 2004; Sunada et al., 1993; Wakeeling and Ellington, 1997). The final consideration for insect flight is wing-wake interactions. This process involves the recapturing of wakes dissipating from the wings at the end of a stroke (Dickinson et al., 1999a). In hovering insects, a combination of clap and fling with wake recapture is responsible for up to 25% of lift generation (Sane and Dickinson, 2001), and occurs during wing stroke reversal (Dickinson et al., 1999b). Main aerodynamic principles notwithstanding, insects presented with unique challenges have developed specific adaptations for flight. Smaller insects,



flying with low  $Re$ , have developed morphological adaptations to compensate for their wing size to body ratio. Specialized structures on the wings such as cilia or setae, increase the porosity (also known as leakiness) of the wings, allowing for more air to flow through the wings, reducing drag and maintaining a lower inertial load (Cheer and Koehl, 1987). Concurrently, the development of a clutch like system within the thorax in some species allows for independent control of each wing, coordinating and moving the wings at a faster rate, circumventing frequency limitations of the nervous system (Deora et al., 2015).

Although insect dependent, insect flight musculature mainly consists of large power muscles (~15 pairs) responsible for cyclical power generation, and a higher number of control muscles that act either directly (~13 pairs) or indirectly (~18 pairs) to gate the force output to the wings for steering (Chapman, 1998; Dickinson and Tu, 1997; Hedenström, 2014; Pringle, 1957). The underlying control and coordination of these muscles comes from motor neurons with axons projecting from the thoracic ganglia, activating flight muscles either neurogenically or myogenically (Burrows, 1996). Flight muscles that are controlled by neurogenic input, are under complete control of the nervous system and are synchronous muscles (Wilson, 1968b). For example, a motor neuron will propagate an action potential to the flight muscle surface, which is followed by the generation of a muscle action potential, resulting in a twitch (Pringle, 1954). Flight muscles controlled by myogenic input enable faster muscle activation, outside the refractory period restraints of neurons. These flight muscles are asynchronous and make use of mechanical click mechanisms (e.g. stretch) (Wilson, 1968b). This mechanism engages muscular responses that require an initial trigger from the motor neuron, which creates a time window where a mechanical signal induces a muscle contraction. Evolutionarily derived insects such as Diptera, Coleoptera, Hymenoptera, Thysanoptera, Psocoptera and Hemiptera, utilize synchronous muscles for flight steering, whilst utilizing asynchronous power muscles (Ellington, 1985). Evolutionarily ancestral insects such as Odonata, Orthoptera and Lepidoptera utilize synchronous flight muscles (Ellington, 1985). Three different types of wing muscles are coordinated by the motor neurons, direct, indirect and accessory muscles (Wilson and Weis-Fogh, 1962). Three different types of wing muscles are coordinated by the motor neurons, direct, indirect and accessory muscles (Wilson and Weis-Fogh, 1962). As the name implies, direct muscles directly depress or elevate the wings, whereas indirect muscles deform the thorax and accessory muscles-supinate or pronate the wing surface (Burrows, 1996).

Insect systems provide the opportunity to study underlying physiological mechanisms of flight behaviour. For example, in dragon flies, target detection and discrimination requires 16 sensory neurons, 8 descending each side of the nerve cord, known as target-selective descending neurons (TSDN's) (Nordstrom, 2013; Olberg, 1986). These neurons synapse with motor neurons in the thoracic ganglia, which contain motor outputs to the flight muscles (Nordstrom, 2013). The flight muscles are activated to engage a robust characteristic prey capture behaviour involving complex aerial maneuvers, resulting in 97% prey capture success (Combes et al., 2013; Olberg et al., 2000). The tractability of this and other insect systems enables comprehensive investigation of fundamental principles of the neural control mechanisms responsible for flight muscle coordination that underly adaptive behaviour within complex sensory environments.

## **1.3 NEURAL CONTROL OF MOTION**

### **1.3.1 SENSORY ENVIRONMENTS**

Animals' natural environments contain complex sensory cues, requiring organisms to detect, filter and process salient information about their surroundings in order to survive. Within each sensory environment, there exist different sensory modalities in the form of visual, auditory, gustatory (taste), pressure (touch), olfactory (smell), and electrosensory stimuli. The presentation of these stimuli may be singular (unimodal) or combined with other stimuli (multimodal). Visual stimuli carry information in the form of photons and waves in the electromagnetic (EM) spectrum, whereas auditory information is carried in the form of mechanical vibrations of particles associated with the surrounding medium. Gustatory and olfactory stimuli rely on chemical compounds that convey information during feeding or communication. Information from touch requires physical contact and will depend on the physical properties of the object or environment an organism is interacting with. Some species have specialized to environments requiring electrosensory detection, allowing them to sense perturbations in the electric fields produced by themselves, conspecifics, or predators (Lissmann and Machin, 1958).

Animals have evolved essential structural adaptations to thrive in these sensory environments. For example, nocturnal owls have specialized auditory systems for detection and localizations of prey. Containing specialized facial ruff, consisting of stiff sound reflective feathers, they are able to collect sound information and relay it to asymmetrically placed ears

(Volman, 1994). This asymmetry creates interaural time differences, which are detected by specialized low-order binaural auditory receptors (Konishi, 1998). These receptors are fine tuned to detect specific interaural time differences in the horizontal plane and interlevel pressure differences in the vertical plane, assisting in the localization of prey. Taste is an important distinguishing tool that can be used to determine the presence of potentially harmful compounds during feeding. Bitter taste receptors (T2R's) are found in mammals, frogs, chickens and teleost fish and are extremely important in the detection of potential toxins (Dong et al., 2009). Bee's need to extract information about food sources, potential dangers, and social interaction, all from chemical compounds associated with olfaction. In insects, odor receptors relay information to the structures in the brain, known as mushroom bodies, where complex processing and extraction of relevant information is performed to influence behavioural output (Erber, 1985; Sandoz, 2011). Crustaceans such as crabs and lobsters have developed specialized glomeruli in the brain which perform first order processing of olfactory information (Krieger et al., 2015). In aquatic environments, some species have developed the ability to detect and manipulate electric fields. They accomplish this with ampullary electroreceptors in the skin, which are capable of detecting weak electric fields as low as 5nV/cm (Kramer, 1996). Some terrestrial animals, such as the spider (*Cupiennis salei*), have specialized mechanoreceptors to detect vibrations during predatory behaviour and mating (Speck-Hergenröder and Barth, 1987). To cope with the bombardment of sensory information, there is a high pass vibration filter built into this system composed of a viscoelastic membrane that preferentially responds to higher frequencies (McConney et al., 2009). In a rare, yet finely tuned example, the fossorial cape golden mole (*Georychus*) can sense and communicate using seismic Rayleigh waves (Willi et al., 2006). A specialized sensory epithelium uses multi modal mechanical response properties of sensory hairs to extract information from the waves, and invoke a response (Willi et al., 2006).

### 1.3.2 VISION

Vision contains a wide range of environmental information, conveyed through different properties of the EM spectrum, not all of which is visible to every animal. Detection of light wavelengths can range within animals from extreme ultraviolet at 10nm to extreme infrared at 1mm (Garstang, 2010). Differences in wavelength can convey differences in colour and discrimination of an object. The luminance reflects the amplitude of a light wave and is a

measure of the amount of energy the wave can deliver to a unit area of a surface (Stevens, 1966). Different levels of luminance between a background and an object can convey contrast information that is important for object recognition and discrimination. Changing contrasts within a visual receptive field can be important for visual motion detection (De valois and Jacobs, 1986).

Vertebrates have camera like eyes containing two specialized types of photoreceptors (rods and cones). Cones are specialized for colour differentiations and high-resolution imaging, whereas the rods are more sensitive to light and motion. Different distributions of rods and cones reflect environmental adaption. For example, nocturnal animals typically have higher numbers of rods to increase visual acuity at night. Within aquatic environments, cyprinid fish use both ultraviolet (UV) and polarized light receptors that work in tandem to help discriminate small invertebrate prey from the background environment (Hawryshyn and McFarland, 1987). Vision is composed of matrices of visual channels, where the density of these channels determines the spatial resolution (Warrant, 1999). Whereas vertebrates have camera like eyes that have matrixes composed of retinal ganglion cells, invertebrates have compound eyes with channels composed of ommatidia (Warrant, 1999). Higher numbers of channels increase spatial resolution, but also permits spatial summation, the coupling of channels to increase photon capture over a wider viewing angle, in low light conditions. Moreover, by increasing the duration of time photons are being captured and increasing the integration time (temporal summation) can improve dim light vision as well (Warrant, 1999). Invertebrates have a wide spectral sensitivity ranging from UV to red. UV light, for example, in both terrestrial and flying invertebrates is used for navigation, foraging and mate selection (Salcedo et al., 2003). On the extreme end of light sensitivity, the photoreceptors of nocturnal dung beetles are capable of detecting the polarization field of the milky way to navigate to and from food sources (Dacke et al., 2013). Moreover, when required to rapidly respond to a looming object, locusts can extract visual expansion properties of objects within tens of milliseconds to avoid a collision.

### 1.3.3 SENSORY CODING

Organisms must be able to detect and process sensory information, in the form of mechanical, chemical, thermal or electrical energy, to produce appropriate adaptive behaviours. Matched filtering involves stimulus-specific sensory structures that absorb and filter sensory energy, as well as peripheral neural circuitry that transduces this energy into electrical signals (Wehner, 1987). Therefore, matching allows for salient stimuli to be rapidly recognized and selected for further processing, while also mitigating effects of sensory noise within a particular environment (Wehner, 1987). Transduction of sensory signals can result in the hyperpolarization or depolarization of sensory cells, which are neuronal or non-neuronal. In mammals, photons of light are converted into action potentials via phototransduction pathways, mediated by g-coupled proteins that can result in either depolarization or hyperpolarization (Arshavsky et al., 2002), whereas in fly ommatidia, rhodopsin and phospholipase are coupled to open transient receptor potential channels, hyperpolarizing the cell and decreasing neurotransmitter release (Montell, 2012). Signals resulting from these pathways are amplified through signal transduction cascades that cause greater hyperpolarization downstream with the activation of only a few number of g-protein coupled receptors (Arshavsky et al., 2002). Action potentials are threshold based, all or nothing electrical signals that typically encoded information through the firing rate (Stein et al., 2005). Action potential generation occurs in the spike initiation zone of the soma, where cation influx brings the membrane potential above the threshold voltage, resulting in rapid depolarization. Cation influx is a result of the sum of inhibitory and excitatory post synaptic potentials (IPSP's, EPSP's), in a process known as postsynaptic integration. Following initial depolarization, the propagation of the action potential results from the opening of voltage gated ion channels, building a positive charge on the inner membrane surface and a negative charge on the outer membrane surface. The action potential is regenerated in the adjacent region and a refractory period maintains a unidirectional propagation direction.

Action potentials compose the language of nervous system, referred to as a neural code. Temporal sequences of action potentials can be categorized into different firing code types that reflect presynaptic inputs. A rate code is one example of how to characterize a neuron's response to a stimulus and represents the rate at which action potentials occur within a defined time window, measured in spikes/sec (Isreal and Burchiel, 2004). Rate coding and firing rate

averaging can be important for stimuli that change over long time periods but may be unsuitable for rapidly changing stimuli. Whereas average firing rate parameters can be associated with particular behaviours, responses may take place too quickly for sensory processes to access and integrate information from the neuronal firing rate. (VanRullen et al., 2005). Another example of coding is a time code, in which specific timing of spikes or the interspike intervals (ISIs) convey information about the stimulus (Stein et al., 2005). Time codes can respond to rapidly changing stimuli and evoke behaviours with short time delays. Rate and time codes can individually represent different aspects of a stimulus, and may be multiplexed for the proper execution of behaviour output (Krahe and Gabbiani, 2004; Stein et al., 2005; VanRullen et al., 2005). Complex sensory information often requires correlated firing of groups of neurons to encode information (Sanger, 2003). This is referred to as population coding. Population codes can represent information from several different neurons, and each neuron's contribution can be ranked in order of arrival to create a population time code (VanRullen, 2005). At a basic level, sensory processing can be viewed as a binary code of information transferred through a channel of many active neurons (Stein et al., 2005). The presence or absence of spikes can be represented by a (1) or (0), respectively. When considering a binary code over a period of 3ms of 001, (no-spike, no spike, spike), this would be interpreted as a rate of one spike occurring in 3 ms. This rate could also be represented by 010 or 100. In this type of rate code, the number of spikes occurring over a period of time is monitored, rather than the arrival times of the spikes. Variability in firing rates and inter spike intervals limit the amount of information that a neuron can transfer and signal variability plays an important role in how the environment is interpreted by the sensory system (Stein et al., 2005). For examples, noise associated with a signal may actually enhance the sensitivity of the system to weak signals (Stein et al., 2005). Known as stochastic resonance, this concept describes how sensory processing centers intake sensory information probabilistically by use of Bayesian interference. This method allows signals to be collected, each time increasing the probability of the best choice interpretation (Körding and Wolpert, 2004). Networks of neurons demonstrate high amounts of temporal complexity, which is important to consider when responses of a neuron depend on the rate at which excitatory and inhibitory inputs synapse with it. Therefore, the timing of these inputs also have an important effect on the response of the post synaptic neuron (Salinas and Sejnowski, 2010).

Sensory information can also be encoded in spike bursts. Bursts are sequences of high frequency spikes occurring in quick succession for a short duration. Bursts are separated by a distinct time window (the interspike interval - ISI) (McMillan and Gray, 2015; Zeldenrust et al., 2018). As with rate and time codes, rapid sensory processing can be accomplished through multiplexing of signals into two channels, a channel containing bursts, and a channel containing isolated spikes (Marsat and Pollack, 2012). Bursts have been shown to play important roles in many different systems, such as neural network responses in the rat neocortex (Connors and Gutnick, 1990), feature extraction in weakly electric fish (Gabbiani et al., 1996), visual fixation in primates (Martinez-Conde et al., 2002), auditory detection in crickets (Marsat and Pollack, 2012) and velocity and trajectory changes of visual stimuli in the locust collision avoidance system (McMillan and Gray, 2015). In the locust optic lobe, a looming sensitive interneuron, the lobula giant movement detector (LGMD), is involved in collision avoidance behaviour and known to be an intrinsically bursting neuron, capable of spike frequency adaptation (Gabbiani and Krapp, 2006). In addition to bursting, spike frequency adaption can play an important role in processing sensory stimuli (Gabbiani, 2006), including the processing of changing stimulus parameters, safeguarding the neuron from firing frequency saturation and tuning sensory responses to features of a specific stimulus (Gabbiani and Krapp, 2006; Sobel and Tank, 2006; Wang et al., 2002). An important tool in neuroethology is the use of models to study neural coding and develop testable hypotheses. Models are invaluable tools to help predict the outputs of neural activity and behaviour based on known and controllable inputs to a system. For example, two compartment models have been applied to make predictions of how intrinsic properties of a neuron will adapt to changes in stimulus parameters in pyramidal neurons in the cat visual cortex (Wang, 1998). The same model has been applied to the locust LGMD, yielding a linear relationship between attenuation and the time constant of spike frequency adaptation in the collision avoidance system (Gabbiani, 2006). These examples indicate the importance of dynamic intrinsic properties of neurons.

### **1.3.4 CENTRAL PATTERN GENERATION**

Central pattern generators (CPGs) contain neural circuits that produce coordinated patterns of rhythmic output and are essential for the production and maintenance of behaviours such as breathing, navigating, walking, swimming, or flight (Ijspeert, 2008). CPGs receive input



from ascending neurons (carrying information to the CNS) and descending neurons (carrying information to motor output), and are modulated by changes from sensory motor integration (Marder and Bucher, 2001). The neural circuitry involved in these generators produce three distinct types of motor outputs: tonic firing, antiphase oscillations, and synchronous oscillations (Marder and Bucher, 2001). Tonic firing shows a sustained response throughout the duration of a stimulus, seen in locus coeruleus output in rat sensory networks (Devilbiss and Waterhouse, 2010). Antiphase oscillations activate non synchronously, and activate antagonistic muscles through reciprocal inhibition (Li et al., 2014). Terrestrial and aquatic locomotion make use of antiphase oscillatory left-right activation of flexor and extensor muscles to induce leg movements in insects on land or whole-body movement in fish in water (Kiehn, 2006). Synchronous oscillations result in simultaneous left and right activation, seen in behaviours such as hopping in frogs or amphibious swimming (Kullander, 2012). Fish have a hind brain central pattern generator associated with vocalizations involved with communication (Bass et al., 1997), whereas *Xenopus* tadpoles exhibit CPGs that produce antiphase oscillation activity from the left and right sides of the body for locomotion. Although the existence of CPGs was postulated by Brown in 1914, the first successful experiments to show the presence of central pattern generation were conducted in 1966 using locusts. A deafferented locust (sensory input removed by severing relevant sensory nerves) can produce rhythmic motor output to the flight system, with non-rhythmic stimulation of the nerve cord (Wilson, 1966). Although motor outputs can be generated in the absence of sensory feedback (classically defined as fictive behaviour), pattern initiation requires the presence of neuromodulators (Ryckebusch and Laurent, 1993). In lampreys, using D-glutamate as an initiator, four separate segments of the spinal cord are capable of producing rhythmic motor patterns (Cohen and Wallen, 2004), and production is continual despite the presence of longitudinal midline lesions, suggesting independence of these outputs in the absence of their contralateral segment (Harris-Warrick, 1991). In locusts, the CPGs responsible for rhythmic leg and wing movement are located in the meso- and metathoracic ganglia. Although inputs from descending neurons in the brain and proprioceptor feedback from the appendages synapse directly with motor neurons that drive the legs and wings (Rowell and Reichert, 1991), locusts are able to generate flight-like rhythms following removal of the brain, subesophageal and abdominal ganglia (Wilson, 1961). Simultaneous intracellular recordings of elevator and depressor motor neurons and extracellular electromyograms (EMG) of the



corresponding flight muscles of a locust demonstrate clear rhythmic output in the absence of sensory feedback (Robertson and Pearson, 1982). Multiple CPGs can be used in tandem to coordinate a behaviour. Walking in stick insects (Order Phasmatodea) requires coordination from ascending and descending neurons, alongside the coupling of oscillators (Kalmus, 1972). However, during more complex behaviours, moving antagonistic muscle groups and appendages require separate pattern generators to work in concert - these are known as unit burst generators (Grillner, 1981). Furthermore, stick insects have multiple CPGs in the segmental ganglia, each controlling a leg joint (Bässler, 1993). Using a combination of weak central coupling and sensory feedback, these CPGs are coordinated through reflex like pathways and make direct contact with CPG structures (Marder and Bucher, 2001). The importance of sensory feedback in maintaining CPG patterning has been shown in locusts (Burrows, 1975). A single locust flight muscle stretch receptor can synapse across all ipsilateral thoracic ganglia during flight. This creates a two-way exchange of information between fore and hind wings and potentially reinforces the centrally determined flight rhythm (Burrows, 1975).

### **1.3.5 SENSORY MOTOR INTEGRATION**

Sensory motor integration involves combining both sensory and motor input, culminating in an appropriate behaviour output. The way in which sensory information is integrated depends on the target systems and required behavioural output (Flanders, 2011). Whereas feature extraction may depend on integrating information from more than one sensory source (e.g visual and auditory), information involved in motor commands will depend on the state of the motor system (Flanders, 2011).

Production of appropriate motor output requires access to the current state and position of the body, which is accomplished by continual creation of efference copies. Also known as corollary discharge, efference copies relay information about the current motor state to the brain and reduce the amount sensory processing of reafferent information (proprioceptive feedback) required (Flanders, 2011; Pynn and DeSouza, 2013). Memory filters can be used to better refine the output such that older memories can be modified, or new memories can be formed based on information from the efference copy. From a computational perspective, the current state, dictated by the efference copy, is subtracted from the desired target state to produce a more appropriate motor command (von Holst and Mittelstaedt, 1950). For example, if a human hand is

held stationary above a cup, and the motor command is to reach for the cup, the efference copy will provide positional information so that the hand makes the appropriate movement from its stationary position to the cup. The implementation of motor output in all animals must take into consideration many variables, including, posture (Matheson, 2003), time sampling of the environment (Srinivasen, 1999), behavioural state (Huston and Jayaramen, 2011), self generated versus external stimuli (Huston and Jayaramen, 2011), and experience (Giurfa, 2007). For example, in rats, cells located throughout the brain, referred to as HD cells, integrate both sensory and motor input, and discharge during horizontal head movement (Taube, 2007). Information is then sent to the entorhinal cortex and the hippocampal region to assist in navigation (Taube, 2007). In locusts, the generation of a collision avoidance response requires the visual detection of a moving object, assessment of its current state relative to the object, and production of an appropriate movement. To accomplish this the locust must process and filter the above-mentioned variables rapidly, within tens of milliseconds.

## **1.4 LOCUST BIOLOGY**

### **1.4.1 LOCUST BIOLOGY AND ANATOMY**

*Locusta migratoria* belongs to the Order Orthoptera, and the Family Acrididae. Orthopterans are more ancestral compared to many other insects and are the most diverse order among the polyneopteran groups. Orthopterans undergo incomplete metamorphosis, transitioning from an egg to nymph and, following 5 moulting cycles, to the winged adult stage. Locust are widespread across Africa, East Asia, and parts of Australia and New Zealand, where they pose serious threats to the agricultural economies. Locust-focused research gained its initial momentum from the necessity for the development of control strategies. Locusts are distinguished from other grasshoppers since they exhibit a unique density dependent polymorphic trait, allowing them to adapt to changes in resources and environment (Pener and Yerushalmi, 1998). Two different phenotypes result from this polyphenism. At low densities locusts display the solitary phase phenotype, prioritizing increased camouflage and avoiding contact with other locusts. Flight behaviour is reduced and relegated to nocturnal activity (Uvarov, 1977). Conversely, at high densities, the gregarious phase phenotype is displayed. This phase results in formations of swarms in which locusts fly long distances in search of food. Swarms are capable of containing up to 80 million individuals, spanning over 20 km and

travelling as much as 100 km per day (Topaz et al., 2008). These journeys are primarily during daylight and produce longer flight times and speeds than during the solitary phase (Matheson et al., 2004). Two main sensory pathways are involved in inducing changes from solitary to gregarious, cerebral and thoracic (Van Hiel et al., 2015). The cerebral pathway is induced by the olfactory and visual stimuli, whereas the thoracic pathway is induced by tactile sensation (Van Hiel et al., 2015). When locusts are exposed to crowding, a prominent serotonin spike occurs in the optic lobes of the brain and serotonin injections alone are able to induce gregarious behaviour (Anstey et al., 2009; Guo et al., 2013; Rogers, 2004). Following the serotonin spike, concurrent epigenetic effects (DNA methylation and histone modification), change gene expression, resulting in hormone release. Juvenile hormone is responsible for green colouration in solitary locusts, whereas corazonin is responsible for the darkening of colour in gregarious locusts. The combination of these effects result in behavioural changes within hours, colour changes within the life span of locusts, and muscle and skeletal changes over two to three generations (Van Hiel et al., 2015). Generations that follow these triggers are imprinted epigenetically, via the priming of the ovary by egg foam factor (Miller et al., 2008). As with other insects, the locust body consists of three major segments; the head, thorax and abdomen (Fig. 1.1A). The head consists of sensory structures (two compound eyes, two antennae, and a mouth containing maxillary and labial palps also involved in olfaction) and internally, the brain. The thorax is composed of 3 sections, the prothorax, mesothorax and the metathorax and contain spiracles that allow for air exchange. The prothorax contains a pair of legs, the mesothorax contains a pair of legs and a pair of forewings, and the metathorax contains a pair of legs and a pair of hind wings (Uvarov, 1977). The prothoracic and mesothoracic legs are primarily used in ground locomotion, substrate grip, and landing post flight (Reichel et al., 2017). The hind legs are used in locomotion, substrate grip, and more importantly, to catapult the locust into the air during jumps (Reichel et al., 2017).

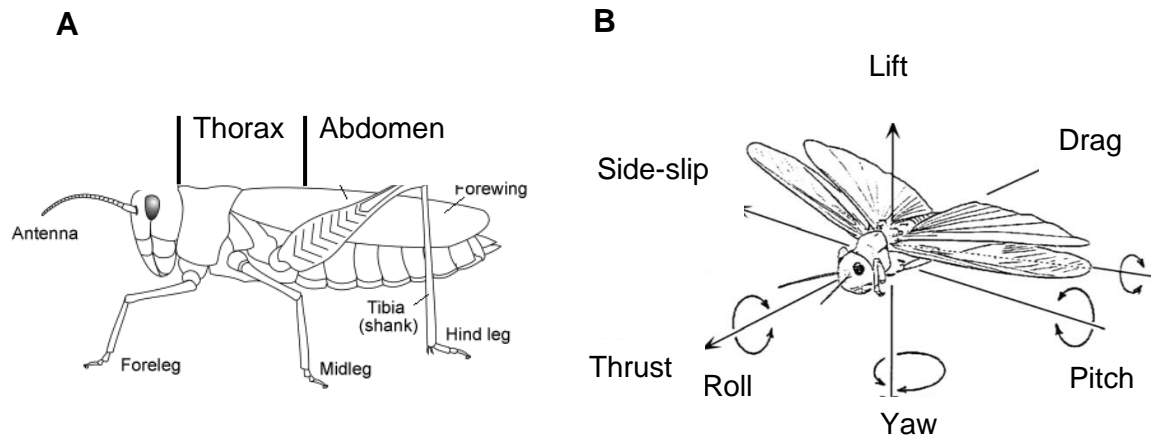


**Figure 1.1: Locust anatomy and degrees of freedom during flight.** A) Diagram of locust general anatomy. B) Flying locusts maneuver in six degrees of freedom, including three translational (drag, thrust and side-slip), and three rotational (yaw, pitch and roll). (A) [www.daff.gov.au](http://www.daff.gov.au) and (B) was provided by Indika Benaragama, 2011.

The abdomen of the locust consists of 11 segments that contain spiracles on segments 1-8 and the reproductive organs on segment 11. Forewings primarily function in flight steering and thrust generation, whereas the hind wings assist in flight stabilization and lift generation. Locusts use a near clap, partial peel (Clap and Peel) method of wing movement during forward flight, where the wings peel apart starting at the leading edge (Cooter and Baker, 1977). This method of wing beat assists in the augmentation of lift forces during flight (Miller and Peskin, 2009). Mechanosensory feedback from the legs prevents the wings from beating if the legs are in contact with a surface. Initiation of flight in locusts typically results from wind passing over the head, which contains specialized sensory hairs for detection of air flow. These hair shafts are embedded in sockets, separated by formative trichogen-tormogen cells, and contain a central channel which descends downwards to make contact with a sensory neuron, where mechanical vibrations from airflow are transduced (Horsmann et al., 1983). The sensory neuron transmits information to the dorsal tegumentary nerve, which contains neurons that synapse with downstream motor neurons that, in turn, innervate indirect flight muscles groups, such as the large dorsal longitudinal muscle (m81) and small oblique muscle (m82) (Guthrie, 1964). A locusts wing beat rhythm modulates the wind reaching wind sensitive hairs through nodding head movements. Phasic proprioceptive inputs from these hairs have a tonic effect in how flight frequency is maintained, using a cycle by cycle acceleration of the intrinsic motor pattern (Horsmann et al., 1983). During flight, locusts can move within 6 degrees of freedom, three translational (thrust, sideslip, and lift) and three rotational (yaw, pitch and roll) (Fig. 1.1B). Movement within these planes allows for the production of complex aerial maneuvers, and requires coordination of direct, indirect and accessory muscles (Fig. 1.2A,B). Direct flight muscles connect directly to the base of the wings and, via their rhythmical contractions, produce the upstroke and downstroke. Indirect and accessory muscles invoke wing movement by distorting the thorax. For example, dorsoventral muscles pull down the tergum, which indirectly and mechanically assists in the upstroke of the wing (Hoyle, 1955). Conversely, the dorsal longitudinal muscle attaches between the two phragmata of the thorax and their contraction pulls the tergum up, influencing the power of the downstroke (Hoyle, 1955). Hind wing cycles have

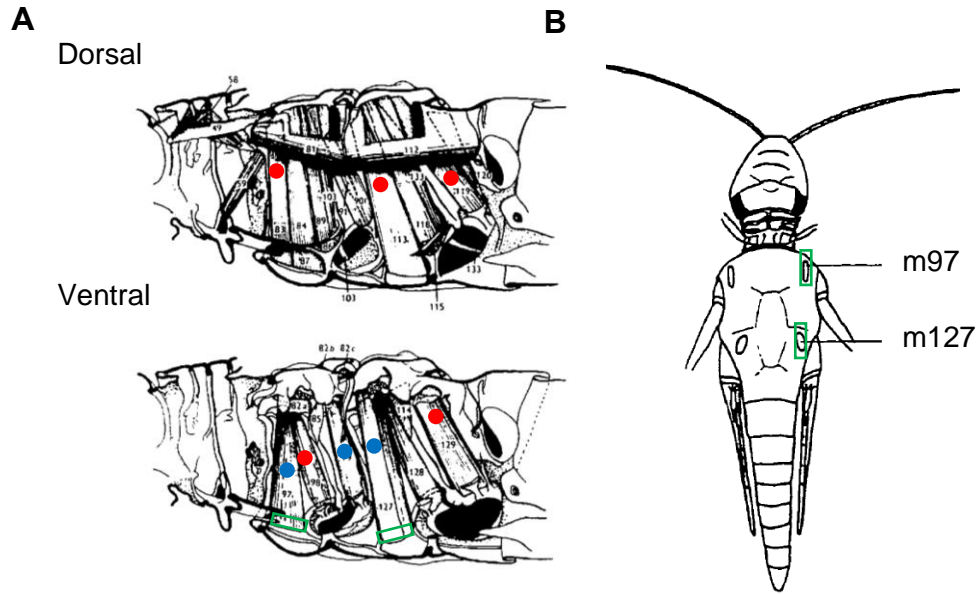


**Figure 1.2: Locust thoracic muscle anatomy.** A) Side view of the locust thorax showing muscle architecture. Direct flight depressor (blue circles) and elevator (red circles) muscles are oriented dorsoventrally. B) Ventral view of a locust. Sculpting of the ventral thorax externally identifies attachment points of specific flight muscles. In this example depressors m97 (forewing) and m127 (hindwing) are indicated by the green rectangles in (A) and (B).

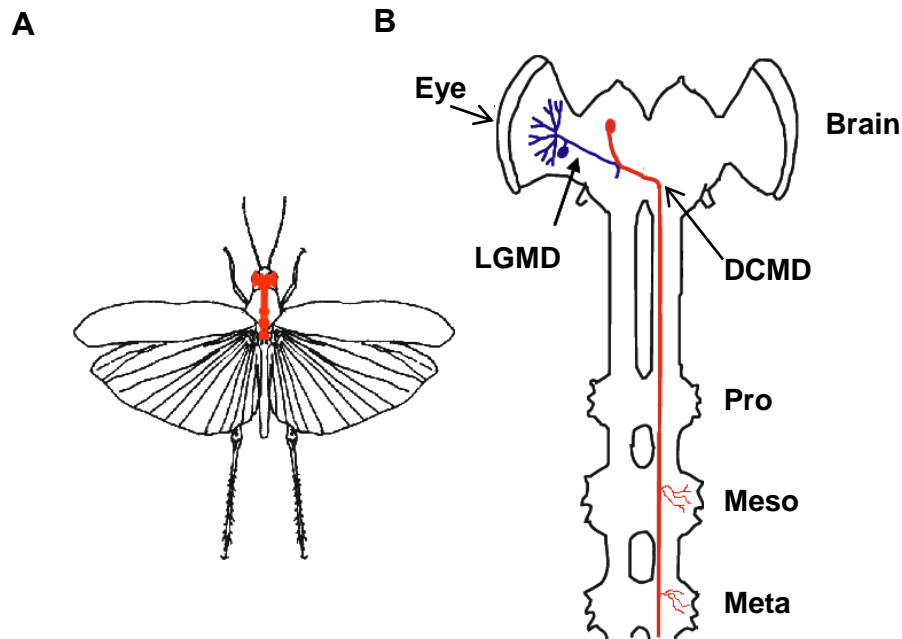


**Figure 1.3: Motion sensing neurons in the locust nervous system.** A) Top view of locust with the central nervous system (CNS) highlighted in red. B) Magnified view of the CNS highlighted in (A). Visual sensory information from each ommatidium converges onto the Lobula Giant Movement Detector (LGMD, blue), which synapses with a 1:1 spike ratio onto the Descending Contralateral Movement Detector (DCMD, red). The DCMD, in turn, connects to wing and leg interneurons and motorneurons in the mesothoracic and metathoracic ganglia. Modified from McMillan (2009)

larger stroke amplitudes ( $100^{\circ}$ - $130^{\circ}$ ) than the forewing cycles ( $70^{\circ}$ -  $80^{\circ}$ ) (Cooter and Baker, 1977). The locust nervous system consists of two major divisions: central and peripheral.

The central nervous system consists of the brain and ventral nerve cords, the latter of which contains the thoracic and abdominal ganglia, whereas the peripheral nervous system consists of the motor systems and the sensory systems (Fig1.3B) (Burrows, 1996). The locust nervous system consists of two major divisions: central and peripheral. The central nervous system consists of the brain and ventral nerve cord, the latter of which contains the thoracic and abdominal ganglia, whereas the peripheral nervous system consists of the motor systems and the sensory systems (Fig1.3B) (Burrows, 1996). The brain has 3 major divisions: the protocerebrum, deutocerebrum and tritocerebrum. The protocerebrum contains the mushroom bodies, central complex and optic lobes. Mushroom bodies are primarily involved in olfactory processing and short term odor trace memory (Schürmann and Elekes, 1987) as well as context generalization in visual learning and regulation of locomotion transitions from active to inactive states (Troy Zars, 2000), whereas the central complex serves a role in integration of information between left and right sides of the brain, coordination of locomotion and potentially processing of polarized light (Vitzthum et al., 2002). The locust has two compound apposition eyes consisting of 8500 light-gathering structure (ommatidia, Fig.1.4), each containing its own lens which samples  $1.25^{\circ}$  of the visual field (Horridge, 1978). In addition to the compound eyes, locusts contain a second set of simple eyes known as ocelli (Wilson et al., 1978). Although significantly underfocused, the ocelli are capable of resolving gratings of relatively small spatial wavelengths (Berry et al., 2007). Furthermore, ocelli temporally outperform compound eyes in both speed and sensitivity, rapidly conducting information to wing motor ganglia through large diameter ocellar interneurons (Wilson, 1978).

The optic lobes are divided into 3 neuropile masses: the lamina, medulla and lobula complex. The lamina consists of hexagonally arranged P-units, each of which contains a combined photoreceptor and lamina monopolar (L) neuron (Rind et al., 2016), and retinula cells, that terminate in the lamina and are arranged by ommatidia into cartridges. Ommatidia contain 4 cone cells, 2 primary pigment cells, 16 secondary pigment cells and 8 retinula cells (Wilson et al., 1978), alongside axons projecting to the medulla that synapse with monopolar cells. Small field monopolar cells receive input from one cartridge, whereas wide-field monopolar cells receive



input from multiple cartridges (Gilbert et al., 1992). Of the eight photoreceptors below each lens, six project to the lamina, and two project through to the medulla (Rind, 2002). The pattern of neural signals that represents an image is maintained in the medulla, known as retinotopic mapping, meaning that projections from the medulla to the lobula complex carry information regarding specific aspects of a visual stimuli. The most well characterized locations of motion detection is in the lobula (Gewecke et al, 1990; Gewecke and Hou, 1993; O'Shea and Williams, 1974; Rind, 1987, 1990a,b), where small and widefield interneurons project significant portions from the visual field to descending motor control neurons in the deutocerebrum (Rind, 2002). The last brain region is the tritocerebrum, which contains connections from the circumesophageal to the subesophageal ganglion (Chapman, 1998).

The thoracic ganglia (pro, meso and meta) act as microprocessing centers, and contain leg and wing CPGs that are composed of interneurons which carry motor commands via direct synapses with motor neurons controlling the legs and wings (Chapman, 1998). Flight muscles are controlled neurogenically, with a one to one spike ratio between the motor neuron and the muscle and motor neuron outputs in the locusts are modulated by octopamine, a neuromodulator secreted by dorsal unpaired median neurons (Rand et al., 2003). Octopamine also plays a major role in regulation of flight rhythm generation in the metathoracic and mesothoracic ganglia (Rillich et al., 2013). Specifically, this neuromodulator effects innervation of the dorsal longitudinal muscles and is known to be involved in early mobilization of lipids from fat bodies before the release of adipokinetic hormone, which coordinates fuel transport in the hemolymph. Thoracic flight interneurons are classified into three organizational categories 1) serially homologous groups, responsible for control of forewings and hind wings, 2) unique interneurons, and 3) serially homologous interneurons in the first 3 abdominal neuromeres and the metathoracic ganglion (Robertson and Pearson, 1983). Furthermore, flight control interneurons are divided into two main functional groups, premotor interneurons, responsible for inhibitory and excitatory drive to motor neurons, and pattern generator neurons, responsible for rhythmic motor output (Robertson and Pearson, 1983) (Fig. 1.5). Motor pattern interneurons in the thoracic ganglia have also been shown to respond to wind stimulus applied to the head of a locust (Robertson and Pearson, 1983). During flight, the flight rhythm must be modified to induce changes in flight behaviour.

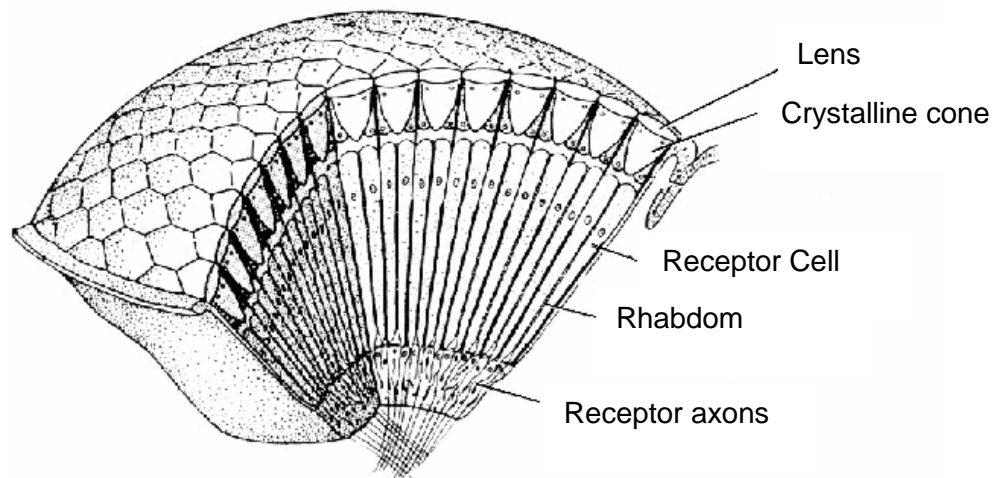


**Figure 1.4: The apposition compound eye of a locust.** The locust eyes consists of an array of image forming units (ommatidia), individually isolated by pigment cells. Each ommatidium contains a light gathering component (lens and crystalline cone) and a light sensing component (rhabdom). Ommatidial orientation around the periphery of the eye increases the field of view for light capture (Burrows, 1996). (Modified from Land and Nilsson, 2002).

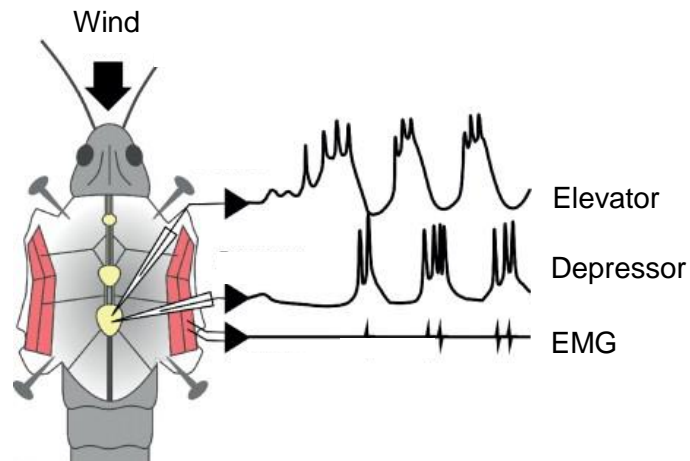


**Figure 1.5: Flight is produced by central pattern generators in the thoracic ganglia.** The locust is fixed in place and nerves carrying afferent sensory information from the wings are severed. In this deafferented preparation, rhythmic and phasic elevator and depressor motor neuron activity (top two traces) can be monitored extracellularly using electromyographic (EMG) electrodes (bottom trace). (Modified from Robertson and Pearson, 1982)

## 1.4.2 FLIGHT BEHAVIOUR AND COLLISION AVOIDANCE

Locusts utilize both fore and hind wings to initiate and maintain flight following a jump that catapults them into the air (Burrows, 1996). Removal of tarsal contact from a surface, and concurrent stimulation of aerodynamic organs located on the head of the locust, initiates flight rhythm generation (Uvarov, 1977). Seventy percent of lift and thrust during flight is generated during the downstroke of the hindwings (Burrows, 1996). During a turn, symmetrical increases in the pronation of the inside of the forewings are correlated with early wing pronation and lift and thrust reduction of the inner wing and asymmetric changes in pronation of the outside of a turn increases thrust and lift (Dawson et al., 1997; Robertson and Reye, 1992; Taylor, 2001). Correctional steering is accomplished by ruddering of the hind legs and abdomen (Arbas, 1986; Dugard, 1967; Gewecke and Phillippen, 1978) combined with alterations of wing kinematics (Schmidt and Zarnack, 1987; Thüning, 1986; Wilson, 1968c).

The locust initiates complex correctional steering movements within swarms of millions of individual locusts, that span up to 1200 square miles, with spacing between each locust averaging 30cm (Waloff, 1972; Uvarov, 1977). Despite this high density, locusts can navigate through complex environments without constantly colliding with one another (Uvarov, 1977). Locusts must avoid high speed collisions with conspecifics and predators, and therefore, rely on an efficient visual detection system, in conjunction with dedicated neural circuitry and musculature, to alter the flight path and thus avoid collision.

When stationary or when locomoting, animals must be able to avoid predators and impending collisions with conspecifics or features of the environment. Dedicated visual motion-sensitive neural circuitry exists in many different species. In non-flying animals, such as semi-terrestrial crabs, tangential neurons in the lobula, respond preferentially to moving stimuli (Oliva et al., 2007) and downstream of the visual center, wide field movement detector neurons are related to the behavioural escape responses (Oliva et al., 2007). Pigeons have dedicated neurons in the nucleus rotundus region of the midbrain that preferentially respond to looming objects (Wang and Frost, 1992). Visually-evoked escape responses may depend on the time to collision with the animal (Hatsopoulos et al., 1995; Lee, 1976; Wang and Frost, 1992), or when the approaching object passes a threshold subtense angle (Glantz, 1974; Nalbach). The retinal speed

of the approaching object can also be used to initiate a behavioural response (Hemmi, 2005) (Hemmi, 2005b).

Locusts are prey for many other animals and thus have evolved effective and rapid avoidance behaviours crucial to survival (Gibson, 1979). When on the ground, locusts will initiate a jumping response to a looming object (Burrows and Rowell, 1973; Burrows, 1995), where mechanical energy is stored in the legs and used to catapult the locust into the air, and initiate flight (Cofer et al., 2010). During flight, a locust can change its body orientation within one wing beat to avoid a collision (Mohr and Gray, 2003; McMillan et al. 2013), which is accomplished by evoking one of three main flight maneuvers. The locust may invoke a turn away from or towards the stimulus, by changing its rotational angles in the yaw, pitch and roll planes (Robertson and Reye, 1992; Robertson and Johnson, 1993; Gray et al., 2001, McMillan et al. 2013). Although a turn away from an approaching stimulus appears intuitive, turning towards the object could cause a predator to overshoot the collision and miss contact with the locust. Gliding behaviours, where the locust keeps the wings extended perpendicular to the long axis of the body, induces a controlled drop in altitude and forward motion (Santer et al., 2005; Simmons et al., 2010; Chan and Gabbiani, 2013). Lastly, the locust may stop flying, folding the wings back along the sides, causing an immediate drop in altitude. This behaviour is thought to be a last-ditch effort to avoid the collision (McMillan et al., 2013).

### **1.4.3 DCMD AND LOOMING SENSITIVITY**

Some of the best studied neurons involved in motion detection are found in the locust lobula and are categorized into two divisions. One division responds to small field motion (e.g. looming stimuli) and the other, wide field motion, such as background optic flow. Looming is defined by an object moving along a collision trajectory at a constant velocity and produces edge acceleration over the retina. From the medulla there are two further projections that synapse onto the lobula. The Lobula Giant Movement Detector (LGMD) has been identified in locusts as a wide field interneuron that responds preferentially to motion in depth (O'Shea and Williams, 1974; Rind and Simmons, 1992). The LGMD processes information based on object edge expansion over the ommatidia, which is a change in the subtense angle of an object in the field of view and changes in time with object diameter and velocity (Fig. 1.6)(Dick and Gray, 2014; Simmons et al., 2010). The LGMD receives visual inputs from presynaptic visual afferents that

are retinotopically arranged fibers sensitive to local motion (Rind and Simmons, 1992) and presynaptic excitatory afferents undergo lateral inhibition, reducing responses to objects that translate (Gabbiani et al., 2002). The connection to its postsynaptic partner, the Descending Contralateral Movement Detector (DCMD) produces a 1:1 pre-postsynaptic spike ratio at frequencies as high as 500 spikes/s (Gabbiani et al., 2001; Money et al., 2004) through a mixed chemical and electrical synapse (Rind, 1984). The DCMD, in turn, crosses the midline and descends along the contralateral nerve cord, where it synapses with interneurons and motor neurons in the thoracic ganglia (Burrows & Rowell, 1973; Simmons, 1980). The DCMD is a well characterized looming-sensitive neuron (reviewed in Rind & Simmons, 1999), with the largest diameter of all the neurons in the locust ventral nerve cord (VNC).

Cable properties dictate that a larger diameter axon will create a higher amplitude spike, making the DCMD spike the largest in an extracellular recording. This provides a unique advantage in isolating the DCMD signal from those of other active neurons. The DCMD spike rate characteristically increases during an object's approach, peaking near the time of collision (TOC) (Gray et al., 2010; Guest and Gray, 2005; Rind and Simmons, 1992; Rind and Simmons, 1996). Looming artificial stimuli presented to a locust are sufficient to initiate a DCMD response (Gabbiani et al., 1999; Judge and Rind, 1997) and the magnitude of this response decreases when the object trajectory moves further away from the midpoint of the eye, demonstrating a preferential response to objects approaching on a collision course (Judge and Rind, 1997). The DCMD is capable of encoding complex visual cues (Rind and Simmons, 1992), including paired objects and compound object shapes (Guest and Gray, 2006) and objects moving along compound trajectories (McMillan and Gray, 2012). DCMD activity can also encode information about the distance and timing of objects that transition from translating to looming trajectories (McMillan and Gray, 2012). These modulations are reflected in changes in timing and peak amplitude of the firing rate relative to time of object collision (TOC) (McMillan & Gray, 2012).

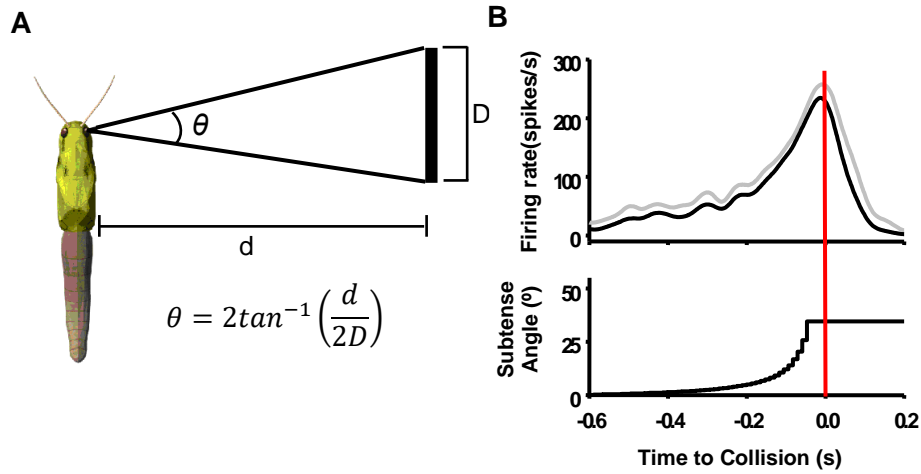


**Figure 1.6: Visual expansion properties of a looming stimulus and corresponding DCMD responses.** A) The visual subtense angle of the object ( $\theta$ ) can be calculated using basic trigonometry (equation), where  $d$  is the distance from the locust eye and  $D$  is the diameter of the object. As the object approaches,  $d$  decreases and  $\theta$  increases. B) As  $\theta$  increases (lower graph) the DCMD firing rate (upper graph) increases to a peak value that occurs before time of collision (red vertical line). Black line is the average response from 20 animals and the grey line is the positive standard deviation. (Modified from Dick and Gray, 2012)

The ability to create stimuli artificially provides a high level of control of the stimulus parameters, including size, trajectory and velocity. Furthermore, the background complexity can also be adjusted in this paradigm by the introduction of a flow field. A flow field, containing repeated wide-field visual patterns that move from front to back, simulates forward movement through an environment. Flow fields affect DCMD responses to looming objects, resulting in a decreased peak firing rate, delays in the time of the peak, shorter rise phases and longer fall phases (Silva et al., 2015). Bursting is also an important property of the DCMD. Specifically, the intra burst firing rate is modulated by changes in object parameters (McMillan and Gray, 2015). Since bursting activity may be a way of gating information into the downstream flight circuitry, these modulations likely play an important role in the collision avoidance response (Santer et al., 2005).

Linking neural activity to the output of behaviour is the ultimate goal in neuroethology. There is a relationship between DCMD activity and flexor and extensor muscle activation during initiation of jumping behaviour (Fotowat and Gabbiani, 2007). Specifically, particular phases of DCMD activity are associated with the onset of muscle activation involved in jumping escape responses. Jumping phases are evoked at specific thresholds of angular size of the looming stimulus over the retina (Fotowat and Gabbiani, 2007) (Fig. 1.7 B,D).

Since active phases in the DCMD are involved in the onset of preparatory phases in jumping, it is reasonable to assume that the DCMD is involved in other escape behaviours. More complex escape behaviour during flight presents greater challenges with respect to rapid collection and processing of sensory information concurrently with behavioural output. For example, in the locust, strong bursts of activity in the elevator motor neuron m84 is associated with the onset of a glide in response to a looming object and follows prolonged burst of DCMD activity (Santer et al, 2005) (Fig. 1.8). Although there is a relationship between DCMD activity and the initiation of escape responses in both non-flying and flying locusts, it has yet to be investigated during flight steering. Understanding the underlying neural activity associated with the onset of the most common aerial avoidance behaviour (a turn), will allow us to better understand the implementation and efficiency of the collision avoidance system.



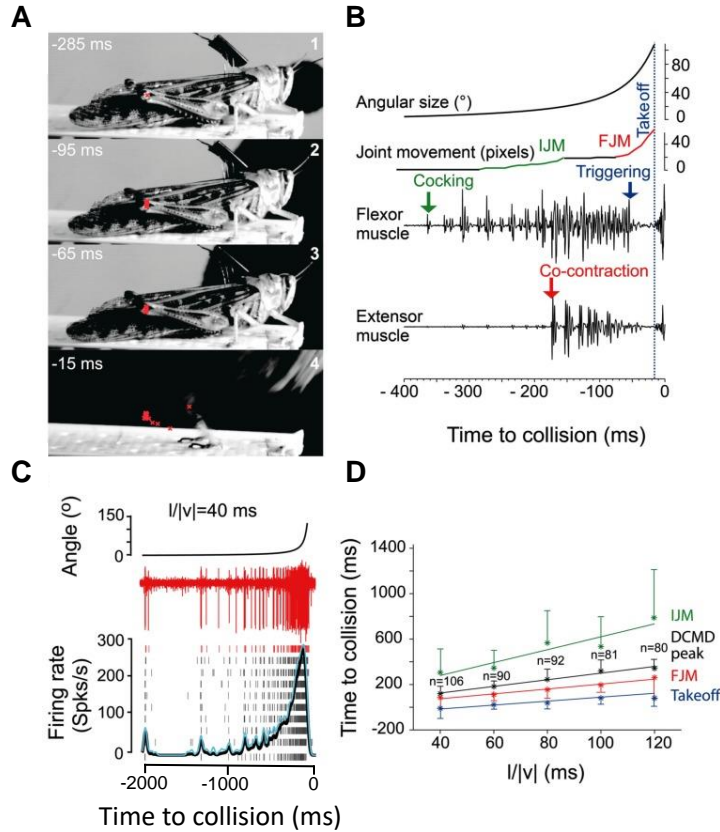


**Figure 1.7: Relationship between DCMD activity and locust jumping responses to looming stimuli.** A) Four highspeed video frame captures of a locust producing a jump in response to a looming disc. Top to bottom represents time progression measured in milliseconds to time of collision (TOC). Red markers represent position of tibia-femur joint. B) Recordings of activation of tibia flexor and extensor muscles time aligned with angular size of the stimulus and movement of the tibia. C) Raw DCMD recording and mean perievent time histogram and subtense angle of looming stimuli aligned to TOC. Rasters show DCMD spike times for each of 10 presentations to one locust. The top raster (red) corresponds to spike times extracted from the sample raw DCMD recording. D) Relationships between the ratio of the half size of the object ( $I$ ) and the absolute velocity ( $|v|$ ) and the times (relative to TOC) of peak DCMD firing rate, takeoff, initial joint movement and final joint movement. (Modified from Fotowat and Gabbiani, 2007)

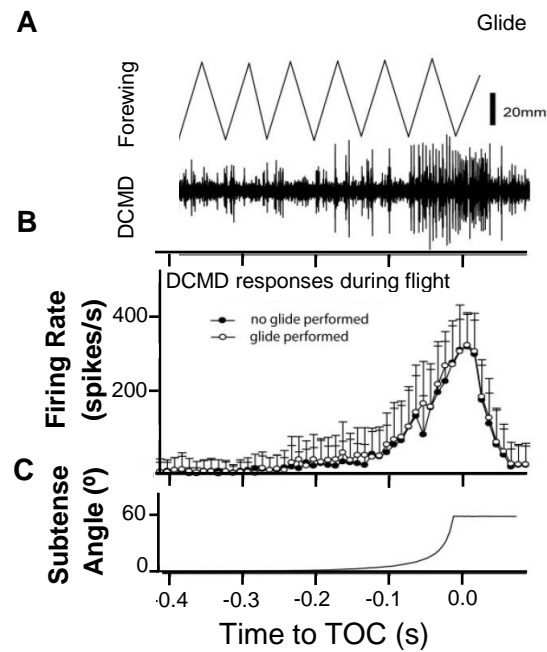


**Figure 1.8: DCMD and behavioural responses during gliding.** A) Top trace shows forewing movements measured at maximum elevation and depression. Bottom trace is an extracellular recording of the DCMD response to a 5 m/s looming disk. B) Perievent histogram of mean DCMD response during a glide behaviour or an absence of response. (C) Change in subtense angle during object approach. All time relative to TOC (0.0 s). (Modified from Santer et al, 2006).

## 1.5 OBJECTIVES

***Objective 1: Understand how flight muscles coordinate and shape motor output to produce body orientation changes that underly collision avoidance behaviour***

A locust must respond rapidly to potential collisions from both prey and conspecifics in a swarm and muscles must be coordinating to complete complex aerial maneuvers. Depression of the forewings is partially controlled by the flight muscle m97 and correlates with changes in body orientation in the yaw, pitch and roll planes (McMillan et al., 2013). Specifically, differences in muscle timings, creating a latency between the right and left sides, are correlated strongly with the initiation of a roll (McMillan et al., 2013). This leads to the question of how the right and left, hind and forewings coordinate. Moreover, are there particular muscle events that signal the initiation of changes in muscles activity and body orientation. **I hypothesize that synchrony between flight steering muscles will increase prior to intentional flight steering behaviours, and that timing and synchrony of flight muscle activity correlates with whole body orientation changes during collision avoidance behaviour.** Simultaneous EMG recordings from two forewing and one hind wing flight muscle pair, combined with high speed video recordings of body orientation, will help reveal important relationships between flight muscle coordination and the production of appropriate collision avoidance responses.

***Objective 2: Elucidate the role of looming sensitive neurons in coordinating collision avoidance behaviour during flight steering***

The DCMD is involved in both non-flying and flying collision avoidance behaviours (Fotowat and Gabbiani, 2007; Santer et al., 2005a), but has yet to be related to flight steering when the animal is flying. It is reasonable to assume that modulations of the DCMD would affect the signals to the motor neurons in the thoracic ganglia, potentially initiating crucial muscle events. We also know that trajectory changes (Dick and Gray, 2014) and complex backgrounds (Silva et al., 2014), modulate DCMD responses. **Therefore, I hypothesize that input from the flight system will modulate the DCMD responses to a looming object and, moreover, that parameters of the DCMD response will correlate with changes in muscle activity associated with turning during collision avoidance behaviour.** Left and right forewing asymmetry is associated with the onset on turn (McMillan et al., 2013), and therefore is an indicator of the

locusts behaviour output. Measuring DCMD activity, muscle activity, and behaviour output allows us to connect the activity of a single neuron, through to behaviour output. **Therefore, I hypothesize that DCMD activity correlates with timing of changes in forewing angle asymmetry, in response to a looming object.** Furthermore, changing looming object trajectories, background complexity, and flight condition may tease out plasticity of neural responses. Will changes in these parameters effect the magnitude or timing of neural responses?

Both parameters from DCMD and DCMD burst rate codes, concurrent with a potential time code of bursts, can be related to muscle events resulting in wing asymmetries associated with turns. Concomitantly, the difference in DCMD and DCMD bursting parameters between non-flying and flying paradigms will inform about the effects of flight, and potential effects of corollary discharge on the locust's collision avoidance response. Overall, these experiments will elucidate crucial relationships between neural circuitry, flight muscle coordination and the production of aerial collision avoidance behaviour.

Each of the two objectives use a different experimental set up. Both set ups allow for precise control of a looming object to evoke collision avoidance responses and both allow for EMG and video recording to be conducted. The setup for Objective 1 uses a loose flight tether, whereas a rigid tether is used for objective 2 to enable simultaneous extracellular recordings to be taken from the ventral nerve cord. More detailed information regarding these set ups are discussed in the methods sections of chapter 2 and 3. Simultaneous extracellular recordings from the DCMD and two forewing flight muscles, the right and left m97, combined with high speed video recordings of the wing positions during flight will be conducted within the same animal. How collision avoidance behaviours are initiated and executed from the level the nervous system will expand our understanding of the neural control of behaviour.

## CHAPTER 2

### FLIGHT MUSCLE COORDINATION AND BODY ORIENTATION CHANGES OF LOCUST MIGRATORIA DURING COLLISION AVOIDANCE BEHAVIOUR

(Manuscript in preparation for the Journal of Experimental Biology)

Gray, J.R., supervised the project and conceived of the original experimental design. Manchester, C.W., developed and carried out all experimentation and analysis. Results were discussed by both authors in the formulation of the final manuscript.

#### 2.1 ABSTRACT

Animals display a variety of adaptive behaviours responsible for collision avoidance with predators and conspecifics. Complex neural control mechanisms underly these behaviours, which are controlled by specialized neural circuits. *Locusta migratoria* is a tractable organism for examining flight muscle coordination of collision avoidance behaviour. Loose tether experiments have shown that locusts free to manoeuvre in 3-dimensional space will adjust wing beat frequency, coordinate timing of a single bilateral pair of flight muscles, and coordinate forewing asymmetry during the downstroke (McMillan et al., 2013). Current experiments were designed to test two hypotheses: 1) Synchrony between flight steering muscles increases prior to initiation of intentional flight steering behaviour. I analyzed EMG recordings from 3 bilaterally paired forewing m97 (1<sup>st</sup> basalar), m99 (subalar), and hindwing m127 (1<sup>st</sup> basalar) steering muscles. 2) Timing and synchrony of flight muscle activity correlate with body orientation changes during intentional flight steering. Concurrent electromyographic (EMG) and high-speed video allowed for simultaneous measurements of muscle activity and body orientation changes.

I found that during turns, ipsilateral synchronization between fore (Lm97) and hind (Lm127) occurs, followed by bilateral synchrony between left and right forewing flight muscles Lm97 and Rm97. These synchrony events correlate strongly with onset of turns and body orientation changes within the pitch and roll rotational planes. My findings demonstrate the earliest detectable muscle activity event that predicts the initialisation of turning during collision avoidance behaviour.

## 2.2 INTRODUCTION

Many animals utilize strategies to avoid predators and, at times, conspecifics while moving within environments containing complex visual stimuli. Neural circuits sensitive to looming objects, objects approaching on a direct collision course at constant velocity, exist in a range of taxa, including: tadpoles (Khakhalin et al., 2014), pigeons (Xiao et al., 2006), crabs (Olivia et al., 2007) and locusts (Robertson and Reye, 1992; Gray et al., 2001; Santer et al., 2005,2006; Simmons et al., 2010; Fotowat et al., 2011; Chan and Gabbiani, 2013). Extensive and detailed studies on neural responses to looming notwithstanding, relatively few studies describe downstream behavioural outcomes of looming detection. The migratory locust (*Locusta migratoria*, L.) can accomplish complex flight maneuvers, controlled by a tractable and well understood nervous system (Burrows, 1973). Locusts must detect and integrate salient information and produce avoidance behaviour rapidly while flying. Moreover, flight steering must be accomplished within swarms containing millions of con-specifics and potential concurrent aerial predation (Stower & Greathead, 1969; Despland et al., 2000). Studies have examined various types of behaviours associated with locust collision avoidance, such as kicking and jumping (Burrows & Rowell, 1997; Santer et al., 2008), and flight steering (Robertson and Reye, 1992; Robertson and Johnson, 1993; Gray et al., 2001; Santer et al., 2005; Simmons et al., 2010; McMillan et al., 2013, Benaragama & Gray, 2014).

Neuroanatomy and function are linked to behavioural output. For example, prey catching in toads is stimulated by spatiotemporal stimulus changes which are recognized by tectal neurons triggering the tectal bulb to signal motor output (Ewart, 2007). In fish, fin rays use proprioceptive mechanosensory feedback to modify rhythmic fin oscillations during hovering behaviour and disrupting this feedback alters the ability to properly abduct while hovering (Williams & Hale, 2015). Locusts receive visual information from compound eyes containing

ommatidia. Receptors from the eyes synapse retinotopically with the Lobula Giant Movement Detector (LGMD), which synapses in a 1:1 spike ratio with the Descending Contralateral Movement Detector (DCMD). The DCMD crosses the midline of the brain and synapses with interneurons and motoneurons in the thoracic ganglia that are responsible for control and movement of the legs and wings (Burrows & Rowell, 1973; Simmons 1980). The motor neuron outputs from the ganglia are neurogenic, synapsing 1:1 with flight depressor muscles such as the m97, m99 and m127. Several studies have analyzed aspects of muscle activity and body orientation with rigid tethers (Robertson and Johnson, 1993; Hedwig and Becher, 1998; Gray et al., 2001; Santer et al., 2005; Santer et al., 2006; Simmons et al., 2010; Ribak et al., 2012), although simultaneous recordings of a flight muscle pairs and body orientation have only recently been examined in conditions where the locust are free to maneuver in three-dimensional space.

One study showed that during collision avoidance behaviour a locust coordinates muscle timing of a single pair of flight muscles, adjusts wing beat frequency, and induces wing asymmetry associated with movement in three rotational degrees of freedom (roll, pitch and yaw, McMillan et al., 2013). These findings suggest that coordination across suites of muscles drives complex flight steering. A study of multiple flight muscles during collision avoidance behaviour found that bulk shifts in activation of forewing depressors were responsible for wing asymmetries associated with intentional steering away from a heat source (Shoemaker, 1998). Synchronization of motor output is utilized across different taxa, such as muscle motor units in human grasping tasks (Santello & Fuglevand, 2004), sound production in toad fish (Gainer et al. 1965), and shiver and flight responses in bees (Esch & Goller, 1991). Whereas left-right wing latency of a single pair of muscles has been shown to drive turning behaviour in locusts (McMillan et al., 2013), synchronization as a precursor to bilateral muscle timing is not yet known. It is possible that putative synchronization events correlate with whole body motion during flight steering. Using electromyogram recordings (EMG) in tandem with high speed video analysis, I observed relationships between 3 bilateral flight depressor muscles, first basalar m97 and subalar m99 (forewing), and first basalar m127 (hindwing) and whole-body motion in response to a simulated lateral looming object. I found that hind and forewing synchrony, and bilateral synchrony correlated with forewing muscle latency and pitch and roll body orientation changes.

## 2.3 MATERIALS AND METHODS

### 2.3.1 ANIMALS

Experiments were conducted on 17 adult male locusts (*L. Migratoria*). Animals were selected 3 weeks past their imaginal moult from a crowded colony maintained at the University of Saskatchewan in Saskatoon, Canada. The colony was maintained between 25-28°C and a 16h:8h light: dark cycle. Experiments were conducted at 28°C within a 5-hour period in the afternoon to remove putative effects of locusts flying at night (Gaten et al., 2012).

### 2.3.2 PREPARATION

Locusts were removed from their rearing cages and placed in a wire mesh container within the experimental room and acclimated for one hour. The legs of the locust were removed to prevent dislodging of electrodes, and a metal tether ring (1.2 cm diameter, 0.45 g) was attached to the dorsum of the pronotum using low melting point beeswax (McMillan et al., 2013). The locust was then positioned ventral side up for EMG insertion. Electromyographic (EMG) electrodes (100 µm gauge fine copper wire; Belden, St Laurent, QB, Canada) were inserted into the following muscles; first basalar m97 (depression and pronation of forewing), first basalar m127 (hind wing depression and pronation), and subalar m99 (depression and supination of the forewing). Muscle location was easily identified by the sculpting pattern of the external cuticle (Fig. 2.1B). Bilateral timing of m97 flight muscles are known to be associated with attempted flight steering in rigidly tethered locusts (Dawson et al., 1997; Dawson et al., 2004; McMillan et al., 2013; Möhl and Zarnack, 1977; Schmidt and Zarnack, 1987; Shoemaker and Robertson, 1998). The ground wire was inserted on the ventral side of the lower thorax, lateral to the midline. EMG and ground electrodes were held in place with low melting point beeswax. The locust was suspended from the top of the wind tunnel by a 45 cm length of 0.2 mm diameter, fishing line (Berkley Trilene XT Extra Tough Line, Pure Fishing, Columbia, SC, USA; 0.02 g). The fishing line was attached to the tether ring, which was marked with 4 equidistant fiducial points (Fig 2.1C). The total weight of tether with beeswax (0.02 g), metal ring (0.45 g) and electrode wires (0.24 g), was 0.71 g. The average weight of intact locust was 2.1 g and 1.76 g after removal of the legs (0.34 g). Therefore, the locust carried an additional 0.37 g after removal of the legs, which equated to 18% of the total intact weight. This extra weight is within



a range that locusts are able to carry aloft and generate steering maneuvers in 3-dimensional space (McMillan et al, 2013). The locust was located at a 0.9 x 0.9 x 3m upwind section of a wind tunnel within a 15 x 15 cm area used to create calibration frame. The locust was suspended equidistant (45 cm) from the wind source, ceiling and a 96 x 63 cm projection screen located to the right of the locust on the wall of the tunnel (Fig. 2.1A). The wind speed was measured using a hot-wire anemometer (VWR Scientific, Edmonton, AB, Canada) and maintained at 3m s<sup>-1</sup>, which emulates the locust's natural flight speed (Baker et al., 1981). Locusts consistently oriented upwind during flight. Room lights were turned off during experimentation and two 250-watt halogen lights were placed behind the locust to illuminate the tether.

### 2.3.3 VISUAL STIMULI

A 1.2-ms pulse was integrated into each video frame, and the vertical refresh synchronization pulse (Vsynch) from the video card (NVIDIA GeForce4 Ti4200 128 MB) were used to align the physiological recordings with video recordings. The visual stimulus was generated by VisionEgg in tandem with Python programming software (Straw, 2008). VisionEgg allows for the projection of customized python coded stimuli, manipulating object velocity, size, orientation, and trajectory. Stimuli were projected against a white projection screen 96 x 63cm, located 90° to the right of the locust.

The visual stimulus consisted of a 14 cm diameter black disc, presented against a white background. Stimuli were presented using a Sony VPL-PX11 data projector positioned 0.9m away from the projection screen and connected to a stimulus generation computer via VGA connector. A Quantum Instruments PMLX photometer (B & H Photo, New York, NY, USA) placed at the projection screen was used to measure the luminance of the black disc ( $I_{min} = 3.8 \text{ cd m}^{-2}$ ) and the white background ( $I_{max} = 36.4 \text{ cd m}^{-2}$ ), providing a Michelson contrast ratio ( $C_m$ ) of 0.81, calculated using the maximum and minimum luminance's between the stimuli and the background.

$$C_m = \frac{I_{max} - I_{min}}{I_{max} + I_{min}} \dots\dots\dots(2.1)$$

The black disk was projected at a pixel ratio of 1024 x 1024, scaled to a white background, rendered at 85 frames s<sup>-1</sup>, which is above the flicker fusion frequency of the locust compound eye (Miall, 1978). The looming disc approached the locust at 3m/s ( $l/|v| = 23\text{ms}$ ),

along a collision course  $90^\circ$  to the right eye. The stimulus was presented after 3 minutes of stable straight flight. Stable flight consisted of small deviations in the x ( $\pm 0.5$ cm), y ( $\pm 0.1$  cm), z ( $\pm 0.4$  cm) axes associated with corrective steering. Objects began 12 m away from the locust, with a visual subtense angle of  $<1^\circ$  of the field of view, which is the approximate acceptance angle of each ommatidium (Horridge, 1978). Looming objects reliably evoke collision avoidance behaviour when they pass through a subtense angle of  $10^\circ$  ( $\sim 40$ cm away at  $3 \text{ m s}^{-1}$ ) (Robertson and Johnson, 1993).

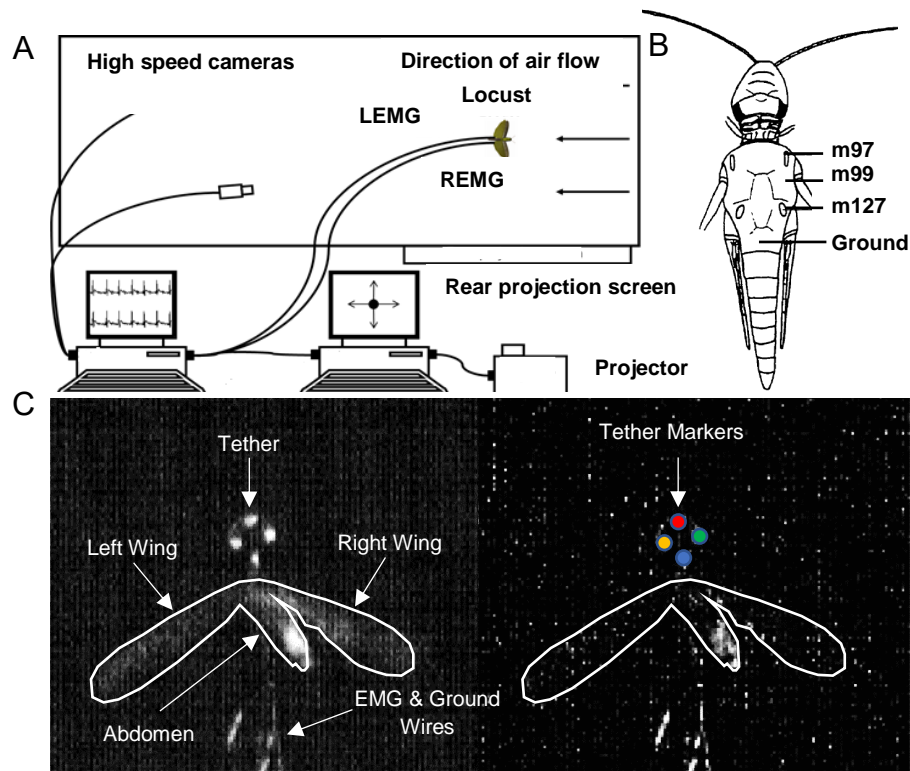


**Figure 2.1: Diagram of experimental set up to record muscle activity and wing kinematics during collision avoidance.** A) Top view schematic of the wind tunnel showing the locust position with respect to wind direction and rear projection screen. Computers shown were used for acquisition of video and EMG data (left), and visual stimulus generation (right). B) Anatomical diagram of the ventral side of the locust, showing the EMG insertion sites of the three flight muscles. A grounding wire was inserted into the ventral base of the abdomen. See text for muscle descriptions. C) Rear view screen-captured images at 480 x 420 pixel resolution from high speed video (250 fps), of a locust from the left cameras during straight flight. White lines represent the outline of the locust with extended wings. Coloured circles (right frame) indicate 4 points on the tether used for 3D body orientation analysis. Raw images (left) were filtered using a grey scale stretch and a prewitts filter to enhance edge detection of the tether markers (right).

### **2.3.4 RECORDING TECHNIQUES**

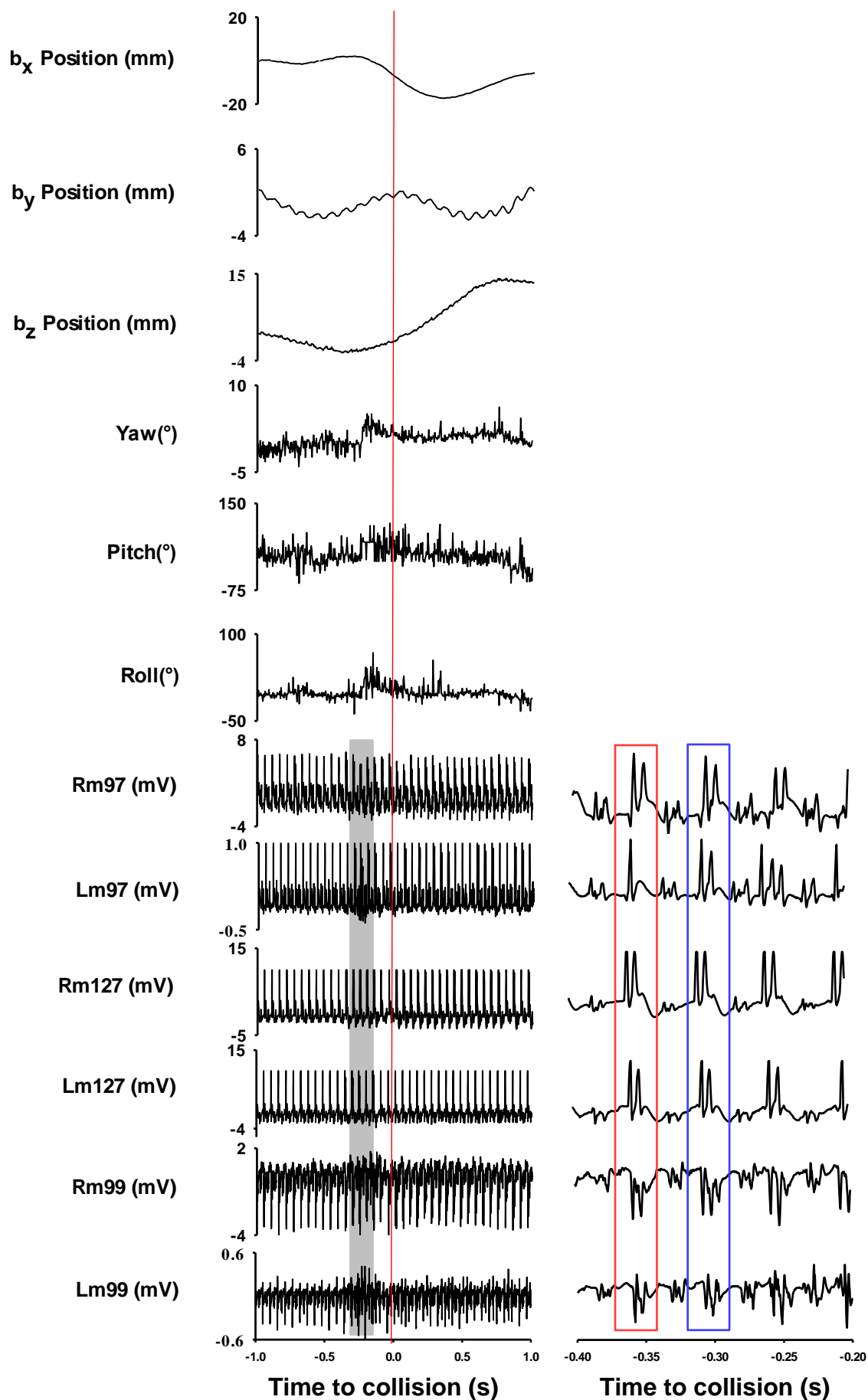
I recorded flight behavior using two high speed digital cameras (Motion Scope, Red Lake Camera, San Diego, CA, USA). Cameras were positioned 1.5m behind locust, each at a 15° angle to the midline of the wind tunnel. Cameras recorded at 250 fps, with a 8.191s buffer, and were connected via MIDAS 2.0 breakout box to the data recording computer. EMGs were simultaneously recorded through 6 channels of a DAQ A/D converter (National Instruments Vaudreuil Dorion, QB, Canada), at 25,000 samples/s. EMG signals were amplified using a A-M systems differential amplifier model 1700 (Low cut off = 10Hz, high cut off = 5000Hz, gain = x1000) (Carlsborg, WA, USA). Video and EMG synchronization was achieved by use of square wave pulses embedded within each stimulus frame, recorded using an additional DAQ input channel. Video recordings were automatically time aligned to EMG recordings using MIDAS 2.0 event capture software (Xcitex, Cambridge, MA, USA). Stimulus pulses were time aligned to EMG and video recordings using peak threshold analysis in DataView (version 10.3.1 St. Andrews, UK). Within the stimulus paradigm, time of collision (TOC) occurs 800 ms before the last stim pulse, therefore 800 ms was subtracted from the timing of the last stim pulse to determine when TOC occurred. All data collected were time aligned to TOC (Fig. 2.2).

### **2.3.5 EMG ANALYSIS**

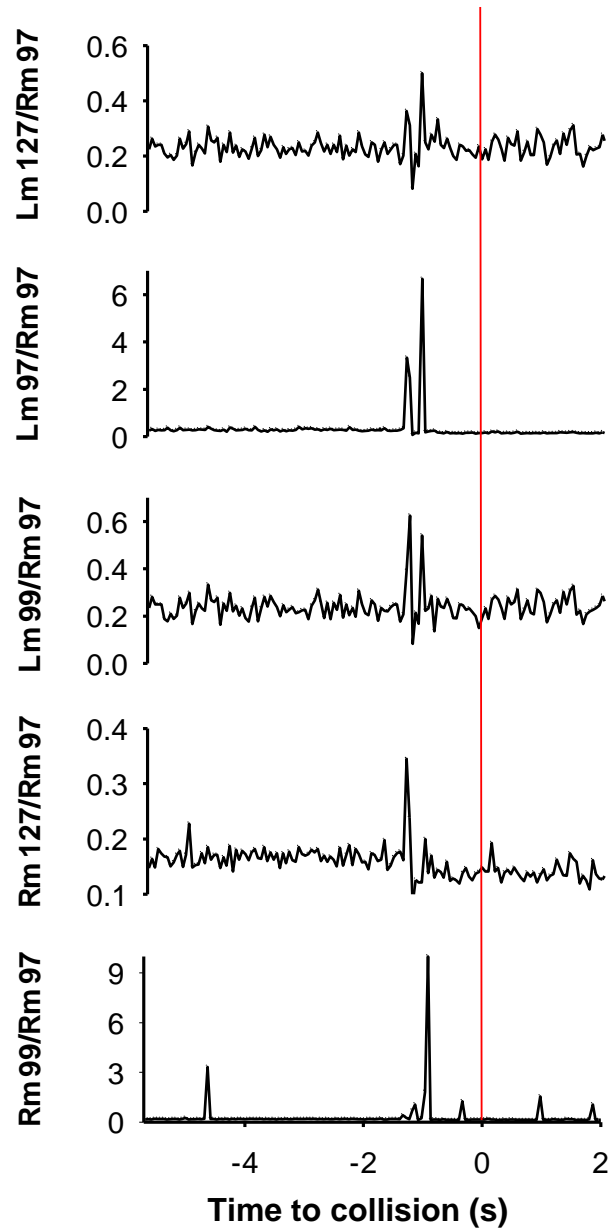
EMG spike timing analysis was conducted using DataView, using merged files containing stimulus, sync pulse and EMG channels. Spike times were differentiated using threshold analysis on EMG spikes of each flight muscle. Spike time markers were exported to NeuroExplorer spike train analysis software (Version 4.0, Madison, AL, USA), and analyzed for synchronization using inverted synchrony versus time analysis. Distance between spikes were inverted, creating positive inflections for small distances between spikes (Fig. 2.3). The timestamps of these peaks were extracted from each muscle group to indicate the occurrence of a synchrony event. Synchrony events were defined as spikes occurring within 3ms of each other (~6% of the wing stroke duration).

Identified synchrony events were exported to Sigma Plot (Version 10.0, Systat Software, Richmond, CA, USA), and time aligned to time of collision (TOC). When analyzing synchrony across both bilateral and ipsilateral muscle synchrony, Rm97 was chosen as an arbitrary

reference, whereas ipsilateral synchrony, Rm97 was chosen as a reference for the right and Lm97 was chosen for the reference of the left. Latency represents the difference in bilaterally paired flight muscle timing and was determined by subtracting the time of the left EMG spike from the time of an associated right EMG spike. General timing and the magnitude of positive and negative latency values (negative indicating a left turn and positive indicating a right turn) were collected using NeuroExplorer and transferred to Sigma Plot 12.5 to be time aligned to TOC. Wing beat frequency was extracted in NeuroExplorer by analyzing the instantaneous frequency of EMG spikes of the Lm97 from each animal. Each EMG spike represents one depression of the forewing, and in turn, a wing beat. Timing and magnitude of wing beat frequency changes were transferred to Sigma Plot 12.5 to be time aligned. The presence or absence of double spikes during turning behaviour was analyzed using threshold detection in DataView. Double spikes indicate sustained depression of a wing and are associated with the generation of wing asymmetries.



**Figure 2.2: Body position, body orientation and muscle activity data from one locust producing a left turn.** Data in left panels are aligned to time of projected collision (TOC, red vertical line) of a 14 cm approaching disc. The bottom tether marker was used to represent changes in body position in the x, y and z planes ( $b_x$ ,  $b_y$  and  $b_z$ ). Tether markers were used to calculate yaw ( $\psi$ ), pitch ( $\chi$ ) and roll ( $\eta$ ), using the equations described in the text.  $R_m$  = right muscle electromyogram and  $L_m$  = left muscle electromyogram. Grey shaded region of traces on the left panel represents EMGs showing the onset of synchrony and latency and is expanded in the panels on the right. The red box in the right panel highlights a synchronization event, where all flight muscles fired within 3ms of each other. The blue box highlights negative and positive changes in latency between left and right flight muscle pairs. A negative latency results from the left flight muscles firing before the bilateral right flight muscles. In this example,  $L_m97$  fires before  $R_m97$  whereas  $L_m127$  and  $L_m99$  fire after  $R_m127$  and  $R_m99$ , respectively.

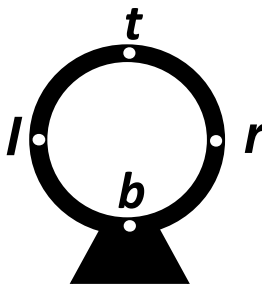


**Figure 2.3: Plots of synchrony versus time from one animal responding to a lateral looming disc.** Graphs indicate the inverted timing distances between spikes from flight muscles Lm127, Lm97, Lm99 and Rm127, relative to flight muscle Rm97. The distance between spikes is inverted, generating a positive inflection on the graph for spike time differences that are very small. The Y-axis represents the inverted time distance to the nearest spike in seconds.



### 2.3.6 VIDEO ANALYSIS

Three major behaviour types were recorded using high speed motion capture (stops, glides and turns). Cessation of wing beats in an open wing formation was considered a glide, whereas cessation with the wings closed against the body was considered a stop (McMillan et al., 2013). Body orientation changes were analyzed only for turning behaviours for three rotational degrees of freedom (yaw, pitch and roll). These body orientation changes were tracked within in 3-dimensional space based on 0.9 x 0.9 x 3m upwind section of a wind tunnel within a 15 x 15 cm area used to create a 32-point calibration box frame. Flight behaviours involving timing of turns (TOT) were classified by the locust tether data points deviating outside the 95% confidence interval of straight flight. Left and right camera video files were exported from MIDAS to WinAnalyze 3D motion analysis software (Mikromak, Berlin). Four-point tether (top, bottom, left and right, shown below) 3-dimensional auto-tracking was conducted on each 8.191s video (~2048 frames). Coordinates of x, y and z positions, measured for each frame, were converted to yaw ( $\psi$ ), pitch ( $\chi$ ) and roll ( $\eta$ ) using trigonometric equations (1, 2 and 3 respectively). This allowed for assessment of body orientation. l (left), r (right), b(bottom) and t(top) refer the positions of each tether mark on the tether disk. x, y and z refer to the position of that tether mark in relation to an axis. Yaw, Pitch and Roll values were transferred to Sigma Plot 12.5, where the timing of initiation of body orientation changes and their magnitude were measured and time aligned to TOC.

$$\begin{aligned}
 1. \quad \psi &= \tan^{-1} \left( \frac{l_z - r_z}{r_x - l_x} \right) \\
 2. \quad \chi &= \tan^{-1} \left( \frac{b_y - t_y}{t_z - b_z} \right) \\
 3. \quad \eta &= \tan^{-1} \left( \frac{b_x - t_x}{t_y - b_y} \right)
 \end{aligned}
 \tag{2.2}$$


Timing of body orientation changes were identified by coordinates leaving the upper or lower 95% confidence interval of a 1s second pre-behaviour epoch for longer than one wing beat cycle (Fig.2.4). Crossing of the upper or lower boundary indicates a right or leftwards yaw, respectively. An upper boundary crossing for pitch indicates an upwards pitch, whereas a lower boundary cross would indicate a downward pitch. A positive value of roll indicates a rightwards turn. Roll direction was indicated as leftwards if crossing the upper boundary and rightwards if crossing the lower boundary, determination of yaw direction followed the same criteria. Duration was measured from orientation change onset until orientation reversed direction (e.g leftwards yaw reverses to a rightwards yaw). The extent of roll, pitch and yaw was determined by examining the maximum change from a predetermined straight flight orientation epoch, calculated from the 95% confidence interval of a one second pre-behaviour epoch.

### **2.3.7 STATISTICAL ANALYSIS**

Statistical analysis was conducted using SigmaPlot 12.5 (Systat Software, Richmond, CA). All data was first analyzed for normality and equal variance. Measured EMG and body orientation parameters that were parametric were analyzed using a one-way ANOVA, parameters failing equal variance testing were analyzed using a Kruskal-Wallis ANOVA on ranks, followed by Dunn's method post hoc analysis. Data passing homogeneity of variance were tested using a Tukey test. Pearson's Product Moment Correlation was used to evaluate relationships between flight muscle synchrony, latency, wing beat frequency and body orientation changes. Conventions for the coefficient ( $\rho$ ) considered 0 to  $\pm 0.9$  to be non-correlative and  $\pm 0.1$  to  $\pm 0.29$ ,  $0.3\pm$  to  $\pm 0.49$  and  $\pm 0.5$  to  $\pm 1$  to be considered small, medium, and large correlations respectively (Cohen, 1988). All significance was assessed at ( $P < 0.05$ ).

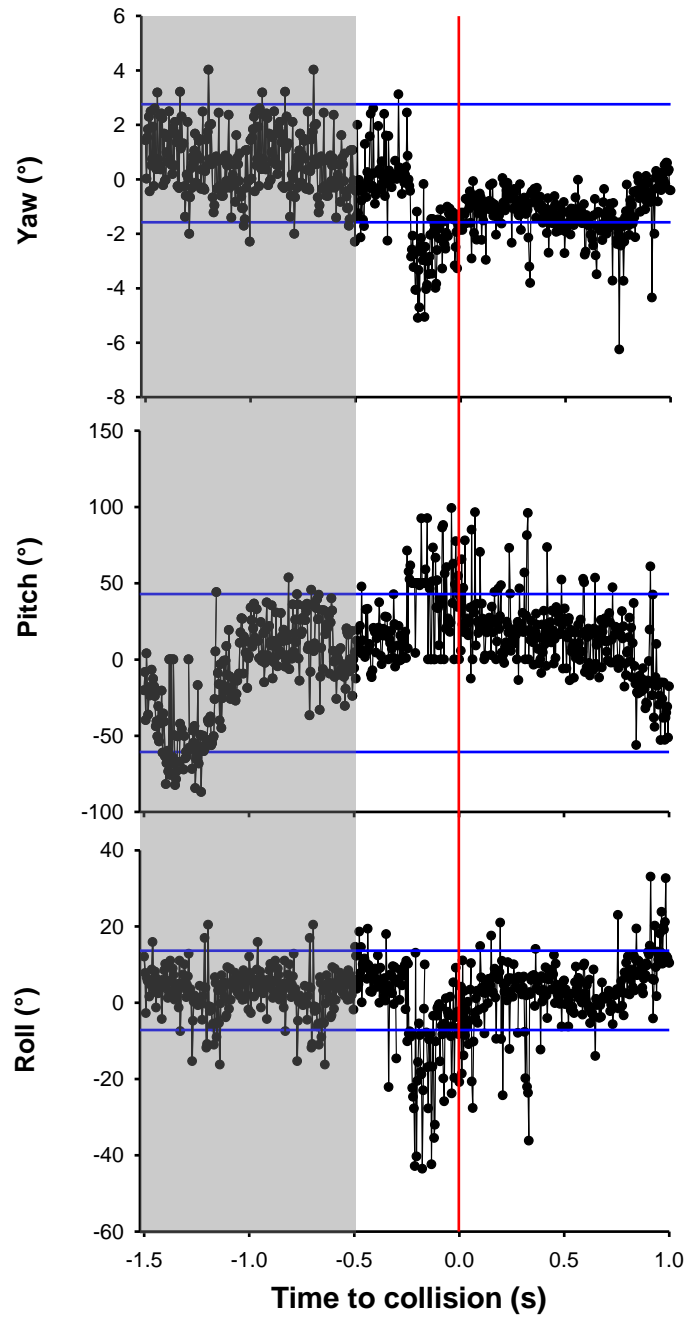


**Figure 2.4: Graphs showing body orientation changes over time in response to a lateral looming disc.** All times are in reference to TOC (red line). Blue lines indicate the upper and lower 95% confidence intervals of a one second pre-behaviour epoch (gray shaded region). This is an example of a leftwards yaw, upwards pitch, and a leftwards roll.

## 2.4 RESULTS

### 2.4.1 GENERAL BEHAVIOUR

Behaviours were classified into 3 groups. Left turns ( $N=14$ ), glides ( $N=3$ ) and stops ( $N=9$ ). Turning avoidance behaviours were defined as deviations from straight flight, occurring if the locust no longer demonstrated symmetrical beating of the forewings (Robertson & Rey, 1992). Turns ( $N=14$ ) occurred singularly ( $N=6$ ) or as the last action in a sequence of behaviours ( $N=8$ ) (Fig.2.5A). Within sequences, turns occurred after a glide ( $N=1$ ) or a stop ( $n=7$ ) (Fig.2.5B). All turns occurred in a leftwards direction, opposite the direction of the looming stimulus. Gliding behaviours were defined as an interrupt in normal wing beat cycle, with wings held in a symmetrical elevated position for longer than one wing beat cycle (Robertson & Reye, 1992, Santer et al., 2004, Santer et al., 2006). Glides occurred singularly ( $N=2$ ), or as the first behaviour in a sequence ( $N=1$ ). Stops were defined as the cessation of wing beats for more than one wing beat cycle ( $\sim 30\text{ms}$ ), where wings are tucked close to the body. Stopping ( $N=9$ ) occurred singularly ( $N=2$ ) or prior to left turns ( $N=7$ ) in a sequence. Turning was determined by the bottom tether marker position crossing the 95% confidence interval of the average straight flight marker position, created from a one second pre-behaviour epoch of straight flight. Eight flight behaviours were found to be in sequence, occurring in a consistent order of glide, stop and turn. Although the locusts exhibit different collision avoidance behaviours during loosely tethered flight (Chan and Gabbiani, 2013; McMillan et al., 2013), I focused analysis on the turns.

### 2.4.2 RESPONSE TIME AND DURATION

All behaviours were initiated before TOC, indicated by a negative time value. The initiation of behaviour occurred over a large range, the earliest behaviour occurring at  $-0.774\text{s}$  (turn) and the latest behaviour occurring at  $-0.111\text{s}$  (stop). Occurring over a large range, turns ( $-0.456\text{s} \pm 0.241\text{s}$ ,  $N=6$ ), glides ( $-0.538 \pm 0.111\text{s}$ ,  $N=3$ ) and stop timing ( $-0.236 \pm 0.088\text{s}$ ,  $N=8$ ) did not differ significantly (Kruskal-Wallis ANOVA on Ranks,  $N=3$ ,  $N=6$ ,  $N=8$ ,  $P=0.17$ ) (Fig. 2.5A). However, behavioural duration differed when comparing behaviours that occurred individually or in a sequence ( $H_3=11.5$ ,  $N=6$ ,  $P<0.05$ ) (Fig. 2.5B). Individual turns lasted for ( $0.693 \pm 0.0367\text{s}$ ,  $N=6$ ) and were significantly longer than turns in sequences of behaviours ( $0.448\text{s} \pm 0.084$ ) and stops followed by turns ( $0.340\text{s} \pm 0.175\text{s}$ ,  $N=6$ ).

Wing beat frequency changes occurred prior to the initiation of turns, initially increasing at  $-0.456s \pm 0.182s$  (N=6) and then decreasing at  $-0.424s \pm 0.06s$  (N=6) (Fig.2.6). Changes in wing beat frequencies were based on deviations from the 95% CI created from the average wing beat frequency of a one second, pre-behaviour epoch. Wing beat frequencies show a decrease ( $-1.947 \text{ Hz} \pm 0.746\text{Hz}$ ) (Holm-Sidak,  $P<.001$ ) followed by an increase ( $2.52\text{Hz} \pm 1.26\text{Hz}$ ) (Holm-Sidak,  $P<.001$ ) just prior to body orientation changes.

### **2.4.3 BODY ORIENTATION**

Due to the late onset (after TOC) of turn behaviours in a sequence, only individual turns (N=6) were analyzed for body orientation changes. A turning behaviour consisted of a combination of 3 rotational body orientation changes, executed in a consistent order of yaw, pitch, then roll. Yaw direction was leftwards and occurred earliest at a mean of  $-0.313s \pm 0.213$  (N=6) before TOC. During a yaw, a mean change in rotational angle of  $15.97^\circ \pm 3.91^\circ$  (N=6) occurred, and was held for a mean duration of  $0.285s \pm 0.112s$  (N=6, Fig. 2.7). Only 52ms later, the locust began to pitch upwards an average of  $20.96^\circ \pm 2.73^\circ$  (N=6, Fig.2.7) at a mean time of  $-0.261s \pm 0.183s$  (N=6). The upwards pitch was held slightly longer than the yaw, pitching for a mean of  $0.318s \pm 0.132s$  (N=6). During this upwards and leftwards deflection away from the looming stimuli, the final orientation change was initiated, a leftwards roll. The roll occurred 31ms after pitch was initiated at  $-0.230 \pm 0.180s$  (N=6) and extends  $-17.4^\circ$ , completing the full expression of the turn, lasting  $0.308s \pm 0.167s$  (N=6). From the time of initiation, the turning behaviour was completed within 0.391s, indicating rapid execution of turning behaviour in response to a potential collision.

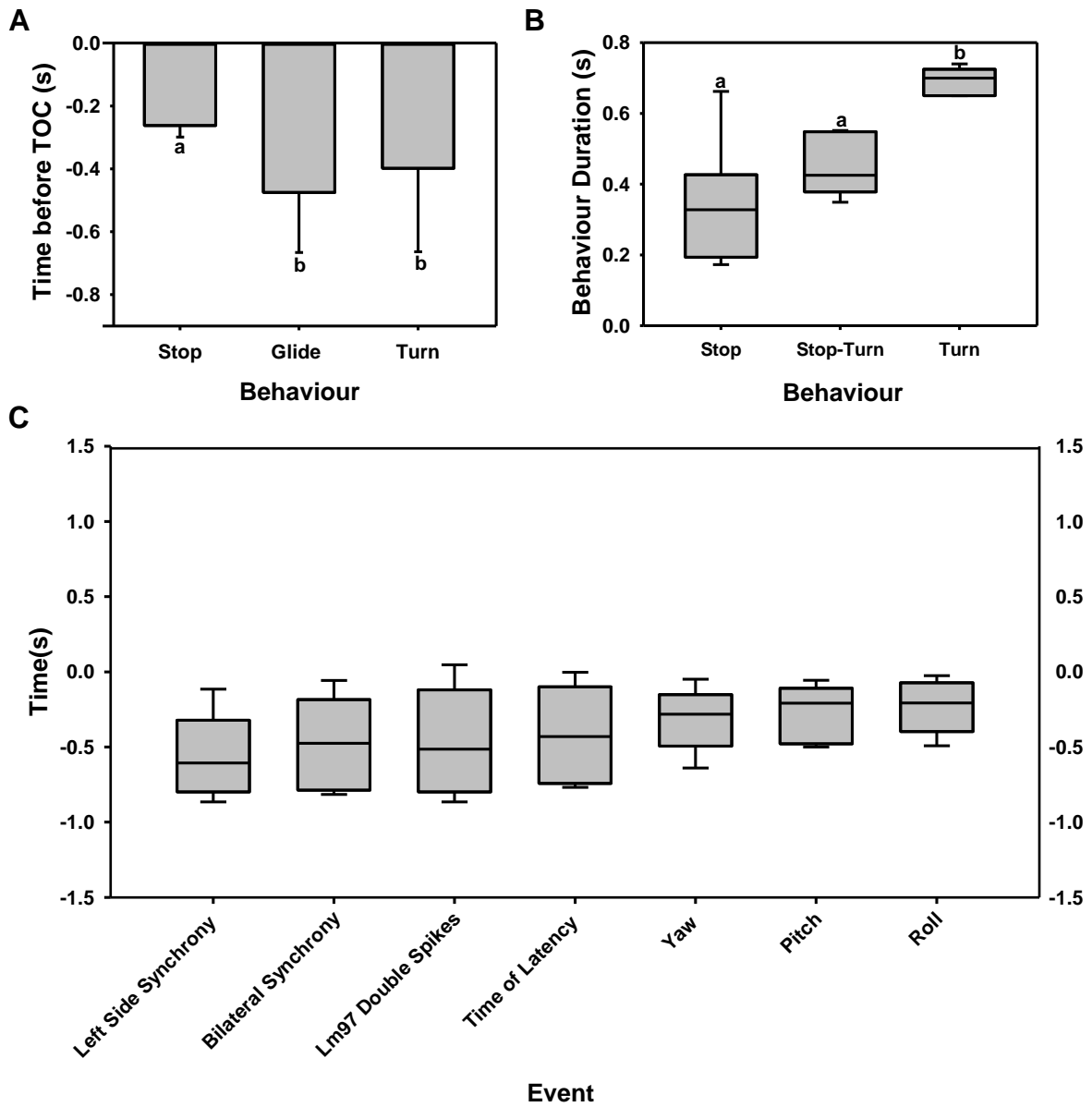


**Figure 2.5: Temporal properties of behaviour and body orientation parameters.** A) Initiation of stops (N=9), Glides (N=3) and turns (N=14), relative to time of collision (TOC = 0 s). B) Duration of stops (N=9), turns that occurred after a stop (N=7) and pure turns (n=6). See text for description of behavioural categories. C) Timing of changes in EMG and body orientation parameters (N=6). See text for details. Data in A are represented by bars showing the mean and error bars showing the -ve SD. Boxplots in (B) and (C) represent the median, 25th, and 75th percentiles and whiskers represent the 5th and 95th percentiles. Different letters associated with bars or boxes indicate significant differences.

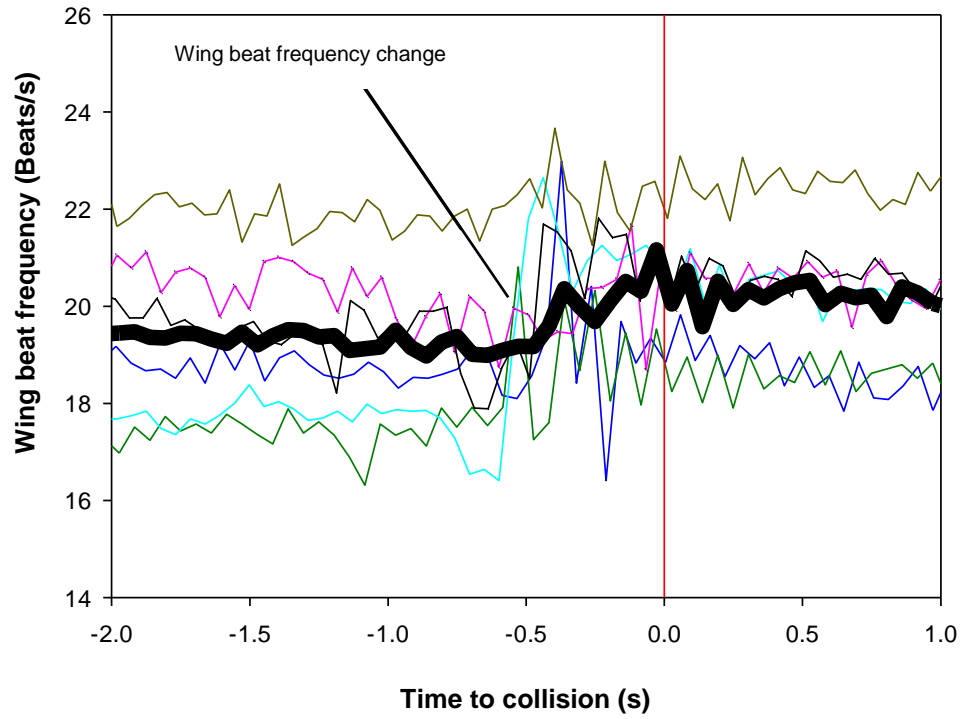


**Figure 2.6: Changes in instantaneous wing beat frequency for all pure left turns.** Data were time aligned to TOC (red vertical line). Each line is from a separate animal responding to a right lateral looming 14 cm disk. See text for calculation of instantaneous wing frequencies. The thick black line represents the average from all traces. Upwards inflections indicate increases in wing beat frequency.



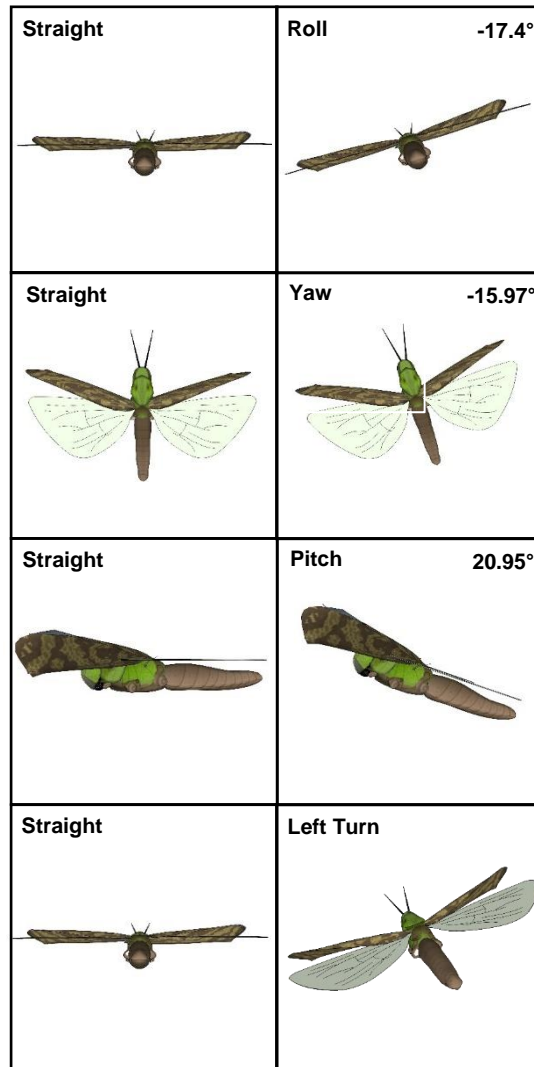


**Figure 2.7: Average changes in locust body orientation during initiation of a turn to the left.** Images show a 3D scaled representation of a locust during each rotational movement of yaw, pitch and roll. Numbers on the right indicate the extent of averaged angular movement during roll, yaw and pitch, respectively, compared to straight flight (N=6). Rotational angles were calculated from x, y and z coordinates from four tether markers, t (top), b (bottom), l (left) and r (right). Negative values indicate a leftward direction in the roll and yaw planes, and a downward direction in the pitch plane. Bottom right image represents the combined body orientation change of roll, pitch and yaw from straight flight orientation. See text for calculations of rotational angles. Note that wing positions were not measured and are presented here for scale.

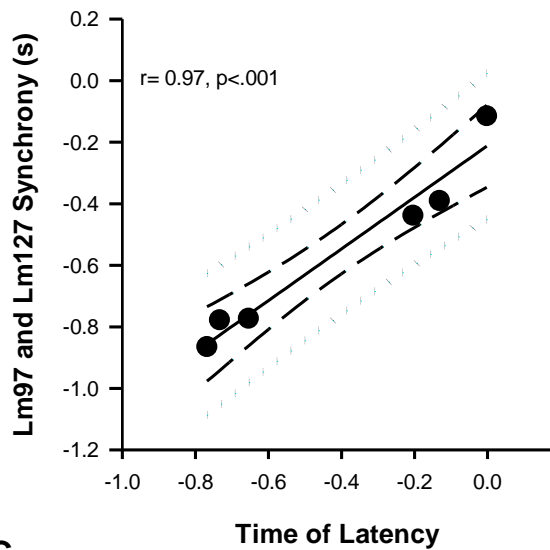
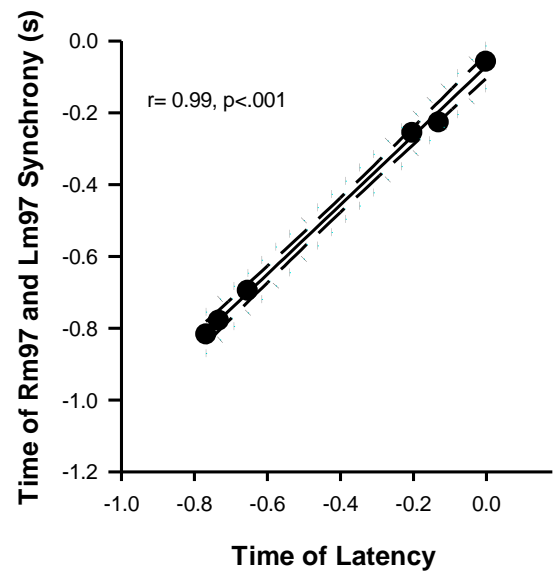
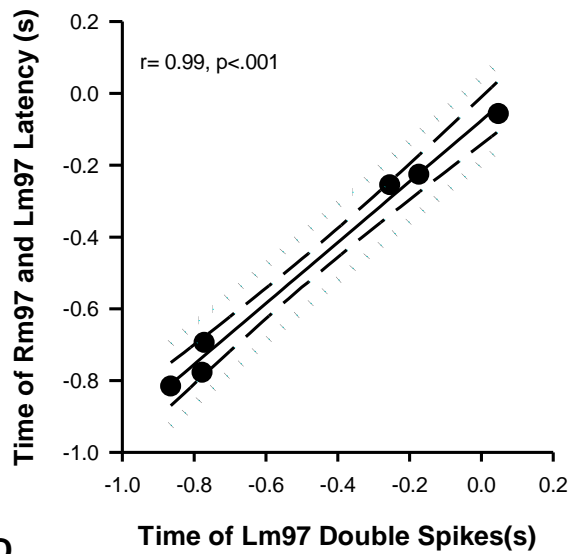
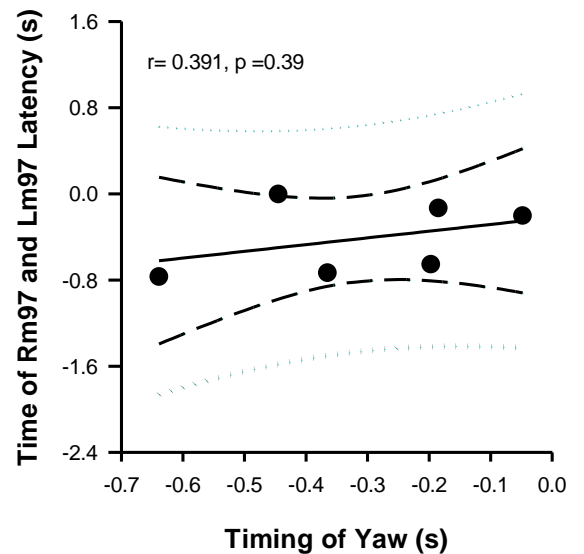
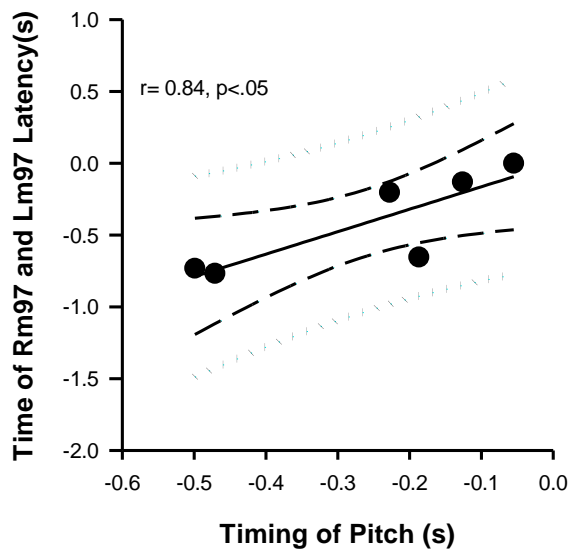
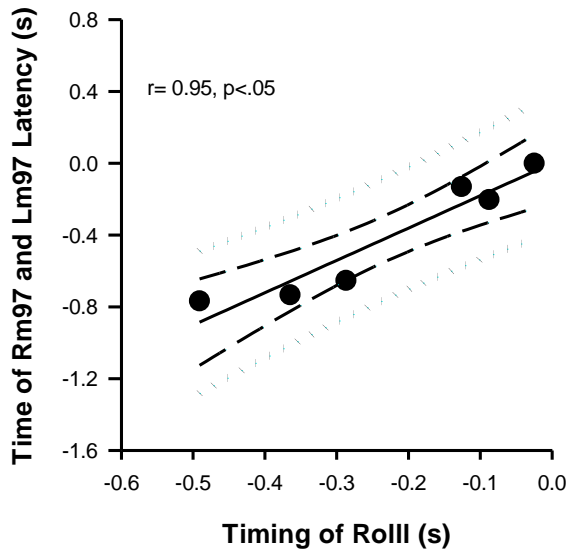
#### 2.4.4 DEPRESSOR MUSCLE ACTIVITY

Changes in depressor muscle timing were measured in relation to body orientation changes. Changes in bilateral muscle timing of the forewing flight muscles (m97) occurred prior to the initiation of body orientation changes (yaw 15.97°, pitch 20.96° and roll 17.4°) at -0.437s before TOC. Left EMG spikes consistently occurred before right EMG spikes during left turns, generating a mean negative latency of  $7.8 \text{ ms} \pm 2.4 \text{ ms}$  (N=6). Latencies could not be calculated for glides or stops, when forewing muscle activity ceased. During the onset of a left turn, double spiking occurred in the left m97 one wing beat cycle before (N=2) or during the onset of latency (N=4), which occurred at  $-0.466 \text{ s} \pm 0.184 \text{ s}$  (N=6). Latency was initiated between the left and right forewing m99 flight muscles later than m97 latency ( $-0.295 \text{ s} \pm 0.126 \text{ s}$ , N=6) and demonstrated a smaller negative latency ( $5.7 \text{ ms} \pm 1.8 \text{ ms}$ , N=6). Moreover, double spiking did not occur when turns were initiated in m99 muscles. During left turns, hind wing flight muscle activity (m127) preceded forewing latencies ( $-0.468 \text{ s} \pm 0.214 \text{ s}$ ) and created the shortest negative latency of  $3 \text{ ms} \pm 0.91 \text{ ms}$  (N=6). Uniquely, hind wing flight muscles demonstrated prevalent double spiking on both the left and right sides during the onset of hind wing latency ( $-0.468 \text{ s} \pm 0.247 \text{ s}$ , N=6). The earliest detectable muscle activity event was muscle synchronization between the forewing left m97 and the hind wing left m127 ( $-0.560 \text{ s} \pm 0.233$ , N=6). Lm99 did not demonstrate synchrony with either Lm97 or Lm127. Moreover, the right flight muscles did not demonstrate synchrony between the fore and hind wings. A second synchrony event occurred involving the synchronization of the right and left m97's just prior to the onset of forewing latency ( $-0.471 \text{ s} \pm 0.118 \text{ s}$ , N=6). Synchrony events occurred for only one wing beat cycle. Ipsilateralsal and bilateral synchrony events did not occur prior to or during glides and stops.

#### 2.4.5 TIMINGS AND CORRELATIONS

The timings of ipsilateral and bilateral flight muscle synchrony were compared to both timing of left-right flight muscle latency and body orientation changes (yaw, pitch, and roll). Ipsilateral synchrony of the left m97 forewing and left m127 hindwing correlated strongly with negative m97 latency ( $\rho = 0.97$ , N=6,  $P < .001$ ). Moreover, bilateral synchrony between the left and right m97's also correlated strongly with negative left-right latency ( $\rho = 0.99$ , N=6,  $P < .001$ ) (Fig.2.8A,B). Forewing flight muscles m99 did not share a clear relationship between synchrony and wing latency. Furthermore, ipsilateral synchrony was not present in the right flight muscles

during left turns. The timing of m97 negative latency strongly correlated with double spiking of the left m97 ( $\rho = 0.99$ ,  $N=6$ ,  $P<.001$ ) (Fig. 2.8C). Ipsilateral synchrony failed to show the same relationship. I also found that the onset of left ipsilateral synchrony correlated with the initiation of body orientations changes in the pitch and roll planes ( $\rho = 0.82$ ,  $N=6$ ,  $P<0.05$ ;  $\rho = 0.94$ ,  $N=6$ ,  $P<.001$ ). Concomitantly, bilateral m97 synchrony also correlated with body orientation changes in the roll and pitch plane ( $\rho = 0.84$ ,  $N=6$ ,  $P<0.05$ ;  $\rho = 0.95$ ,  $N=6$ ,  $P<0.05$ ) (Fig.2.8E,F). Despite strong correlations with roll and pitch changes, I observed no correlations between muscle activity and changes in the yaw plane for either synchrony events.

**A****B****C****D****E****F**

**Figure 2.8: Linear regressions of temporal properties of muscles activity and body orientation (N=6).** A) Correlation of timing of synchronization of left forewing flight muscle (m97) and left hindwing flight muscle (m127) with timing of left-right latency. Left-right latency was calculated by subtracting the timing of the Lm97 EMG spike times from the Rm97 EMG spike times. B) Correlation of synchronization timing of bilateral flight muscles Rm97 and Lm97 with left-right latency. C) Correlation between timing of left-right latency and occurrence of double spikes of the left m97. D - F) Correlation between time of left-right m97 latency and timing of body orientation changes in yaw (D), pitch (E), and roll (F). Pearson correlation coefficient values ( $\rho$ ) are presented on each graph with their respective p-values. Long dashed lines represent the 95% confidence interval of the regression line. Dotted lines represent the 95% confidence interval of the population. Dots closely grouped to the line and within the regression line 95% confidence interval represent a stronger correlation.

## 2.5 DISCUSSION

Although it is known that forewing depressor flight muscle activity corresponds with changes in locust flight kinematics during collision avoidance behaviour (McMillan et al., 2013), this is the first study to investigate putative synchrony between suites of forewing and hindwing muscles during responses to approaching objects. Understanding how flight muscles, both hindwing and forewing, are rapidly coordinated to produce complex aerial maneuvers, unlocks key components of a highly successful collision avoidance system. Using concurrent EMG and high-speed video analysis, I correlated fore and hindwing muscle activity with body orientation during presentations of a black disc looming within the locust's right visual field. I discovered a sequence of correlated events initiated during a turn, involving changes in wing beat frequency, spike timing of the forewing and hindwing flight muscles, and changes in the pitch and roll planes of the locust. Moreover, the crux of these findings revealed bilateral synchronization events between forewing flight muscles (m97s) and ipsilateral synchronization events between forewing flight muscles (m97s) and hindwing flight muscles (m127s) that highly correlated with the onset of forewing latency and, consequentially, turning behaviour. Flight muscle synchrony is the earliest detectable muscle activity event involved in locust collision avoidance behaviour during flight.

A loosely tethered preparation offers a unique balance of naturalistic elements of the locust's flight environment and refined experimental control of stimulus presentation (see Chan and Gabbiani, 2013; McMillan et al., 2013). Previous experiments investigating locust flight steering typically used a rigid tether set up (Hedwig and Becher, 1998; Robertson and Reye, 1992; Robertson and Johnson, 1993; Gray et al., 2001; Santer et al., 2005; Santer et al., 2006; Simmons et al., 2010; Ribak et al., 2012). More recently, loose tethers have been used, allowing the locust to orient in 3-dimensional space (Chan and Gabbiani, 2013; McMillan et al., 2013). Both studies involved the removal of the legs and the insertion of EMG electrodes. Leg removal is a necessary step to prevent removal of electrodes by the locust during experimentation. Despite this necessity, hind legs in particular have been shown to be involved in flight steering when extended (Robertson and Reye, 1992) and thus removal may introduce a slight confound in the timing and extent of turning behaviour. Furthermore, an important contributor to flight initiation is a lack of hind leg contact with the surface. Removal of the hind legs did not hinder

the locust's ability to initiate or sustain flight when exposed to wind. Although additional weight and wind resistance from the tether may have affected steering behaviours, improvements were made to increase the contrast of the markers for detection by the cameras. Furthermore, I reduced the tether weight by 2% (18% of total locust mass) compared to the most recent loosely tethered prep using *Locusta migratoria* (20%) (McMillan et al., 2013). Previous weight neutral tethers, where the tether is equal in weight to the weight lost from leg removal (Mohr and Gray, 2003), and non-weight neutral (McMillan et al., 2013), with identical procedures of leg removal, yielded response timings closely resembling what I recorded. Locusts were capable of performing consistent collision avoidance behaviours (stops, glides, and turns) within a 3-D calibrated space of 48 cm<sup>3</sup>, following stable pre-behaviour epochs of 10 seconds. Duration of turning behaviours (693ms) were also consistent with previous findings [560ms (McMillan et al., 2013)]. Locusts performed consistent aerial maneuvers within a behaviourally relevant time frame, correlating with stimulus parameters and flight muscle timing. Therefore, parameters associated with turn initiation were able to be reliably measured during flight in a 3D space.

Locusts consistently engage in a range of collision avoidance behaviours that change the flight trajectory towards or away from acoustic (Dawson et al., 1997; Dawson et al., 2004) or looming visual (Robertson and Johnson, 1993; Robertson et al., 1996; McMillan et al., 2013) stimuli. However, 100% of locusts in this study turned away from the looming object. The preference for left turns in my study may be a result of the looming object having double the diameter (14 cm) of visual objects used previously (7cm). The larger size may represent a decreased chance for the locust to effectively avoid interception by the predator, minimizing the chance of the locust to undercut the predators original trajectory. Despite turn direction variability, there is a clear preference for turning away from the stimulus in former studies (Ribak et al., 2012; Simmons et al., 2010; Robertson and Reye, 1992; Santer; Rind et al., 2008;). Furthermore, these studies demonstrate higher variability in turn choice than my study. Of the singular behaviours that occurred outside sequences, 75% were turns and 25% were stops, whereas unlike previous findings within sequential behaviours, turns composed the last behaviours in each sequence (87.5% following stops, and 12.5% following glides, McMillan et al., 2013). This confound may be a result of the tether design, biasing a preference for turning behaviour. I also found that the percentage of glides that occurred as the initial response in a behaviour sequence (33%) was consistent with previous findings (McMillan et al., 2013).

Although variability in collision avoidance behaviours for obstacles or conspecifics does not appear to have any particular benefit, predation avoidance likely benefits from variability by decreasing the chance of predators predicting the locust's movements (Card, 2012).

Traditionally, glides are considered a last ditch effort (Chan and Gabbiani, 2013a; Santer et al., 2005a) or occur before a turning behaviour in sequence (Ribak et al., 2012). Despite these findings, I observed only one glide occurring prior to a turn, and the other two occurred significantly earlier ( $t_8 = 4.39$ ,  $N=8$ ,  $N=2$ ,  $P < 0.05$ ) on par with the timings of turns, as was reported previously (McMillan et al, 2013). Frequencies of glides (20%, 7cm disk at 150cm/s at  $l/|v| = 23$  ms) were similar to frequencies found by Santer et al. (2005a) [15%], although their stimuli had a higher  $l/|v|$  value (40 ms; 8cm disk at approaching at 100cm/s. The most recent study showed higher glide frequencies [37%, (McMillan., et al, 2013)] with a lower  $l/|v|$  value (12 ms , 7cm disk approaching at 100cm/s). Therefore, differences in frequency may be a result of the  $l/|v|$  value used in my experiment. The remaining glides, that occurred singularly, held the glide for the duration of the experiment, long past TOC.

Although increases in wing beat frequency have been suggested to be one type of preparation for a turn (Ribak et al., 2012), and is known to increase following a glide (Santer et al., 2005a., McMillan et al., 2013), the low sample size of this particular behaviour in my study provides difficulty in drawing firm comparisons or contrasts with previous studies. Despite this, my results suggest that glides can occur as both a preparatory behaviour before a turn, and as an individual collision avoidance behaviour. Further experimentation, with more variation in object approach parameters, is needed to better understand the role of glides. My findings, however, do concur with previous studies that glides are not simply last-ditch efforts of avoidance, but are one of several viable collision avoidance behaviours (McMillan et al., 2013).

Animals employ a variety of wing beat manipulations to avoid obstacles. Pigeons can glide during straight flight or controlled descent, or pull the wings inwards during flight to reduce wing span and invoke rapid descent (Williams and Biewener, 2015). Flies are able to modulate wing beats to perform rapid saccades and escape behaviours (Dickinson and Muijres, 2016). Moreover, many insects evoke glides and stops to avoid obstacles, conspecifics, or to rapidly decrease altitude to avoid predators (Dawson et al., 2004; Miller and Surlykke, 2001; Santer et al., 2005a; Wehner et al., 2008). In my experimental setup, the constraints of the loose



tether may have introduced a confound during stopping behaviour. During an attempt for the animal to drop in altitude (e.g. stop), the animal could only drop as far as the length of the tether. In the most recent study, when the locusts drop in altitude abruptly stopped by the tether, it would rapidly initiate a turn (McMillan et al., 2013). In my study, stops within sequences of behaviours occurred at a high frequency (78%), and consistently before turns were initiated. Therefore, it is possible a similar confound previously found (McMillan et al., 2013) effected the frequency of initiation of turns in sequences. When I examined stop durations, I found considerably longer durations (340ms) than previously observed stops (~40ms) (McMillan et al., 2013). These durations resulted in turns, that followed stops, occurring very close to or after TOC. Moreover, stops occurred significantly later than glides and turns, inferring that stops are likely last resort behaviours, and not a vital precursor to other collision avoidance behaviours.

I found that the duration of turning behaviour may have been affected by the properties of the tether. During a turn, the locust would only be capable of turning as far leftwards as the arc of the tether would allow. Reaching the maximum extent leftwards would pull the locust back towards the center, ending the left turn. Although this may have resulted in a biased sampling of lower turn durations, values remained within a behaviourally relevant time frame with respect to TOC. Interestingly, the average timing of turns (-0.456s) occurred later than previously found [-0.659s (McMillan et al., 2013)]. Although individual turn timing was significantly earlier than stops, the turns did not occur significantly later than glides. However, I found significant differences in the median timings of turn durations between individual turns (~693ms) and turns in sequence (~448ms), whereas no differences were found by former studies (Santer et al., 2013, McMillan et al., 2013).

I found wing beat frequencies within the normal range of previous rigid tether (Robertson and Johnson, 1993; Santer et al., 2005a; Shoemaker and Robertson, 1998) and loose tether (McMillan et al., 2013) experiments. I did not observe wing beat frequency decreases prior to initiation of glides (as shown by Ribak et al. (2012)) or stops. However, I did find that increases in WBF correlated strongly with changes in pitch and roll. Therefore, I suggest that increases in wing beat frequency may provide the necessary thrust and flight stabilization during a turn during loosely tethered flight.

Previous timelines of collision avoidance behavior have stated that decreases in wing beat frequency were the first indicators of a turning behaviour (McMillan et al., 2013). My study has revealed an earlier indicator of turns, occurring during ipsilateral forewing and hind wing flight muscle synchronization between m127 and m97. Shortly after ipsilateral synchrony, bilateral synchrony of the forewing m97s occurs. Both synchronization events are strongly correlated with increases in m97 latency and changes of body orientation in the pitch and roll planes. Ipsilateral synchrony occurred consistently on the same side as the direction of the turn (left turn = left ipsilateral). Furthermore, m99 synchrony with m127 and m97 was not correlated with the onset of latency or body orientation changes. Locusts likely synchronize their flight muscles as a preparatory action to align the wings prior to increasing latency between the left and right forewing flight muscles. Given the dominance of leftwards turns, ipsilateral left side synchrony may be a predetermining factor for the onset of the leftwards turning. It is highly probable that left side synchrony influences the earlier firing of the left forewing muscles, and that right ipsilateral synchrony would occur and invoke a similar response during the execution of right turns to laterally looming stimuli from the left. Further experimentation with a larger sample size consisting of left and right turns could elucidate the relationship between right and left synchrony events and turn direction. Further along the timeline, forewing latency immediately and consistently followed ipsilateral and bilateral forewing synchrony events. Although average negative latency was consistent with former studies (McMillan et al., 2013), the timing, relative to TOC, of latency occurred later in my study (~100ms).

Relationships between flight muscle activity and body orientation changes are clear in my study, although concurrent with the most recent findings (McMillan et al., 2013), I found only weak correlations between m97 latency and yaw. Furthermore, I observed no correlation between either ipsilateral or bilateral flight muscle synchrony and yaw. As one of the three rotational degrees of freedom, change in the yaw plane is an integral part of a turn during collision avoidance behaviour. The low number of forewing muscles analyzed in this study could explain the lack of correlation of yaw to muscle activity, therefore, recording from more flight muscles simultaneously may reveal correlations with yaw initiation. Both pitch and roll correlated with ipsilateral and bilateral muscle synchrony and forewing increases in latency, suggesting that coordination of m97 flight muscle activity is involved in the execution of body orientation changes during collision avoidance.

Future experiments could incorporate more complex simulations of the environment. The use of complex backgrounds to simulate visual flow has been shown to elicit changes in looming sensitive neurons involved in collision avoidance behaviour (Silva et al., 2014). Furthermore, varying object trajectory and velocity could represent different levels of threat to a locust and demonstrate clear preferences for specific avoidance behaviours. Insect flight experiments have thus far been conducted in open loop conditions, with no feedback from the muscles to the virtual simulation generator. Furthermore, realistic changes in the visual environments of the insect's surroundings, in response to behaviours such as turns, would provide important information on how an insect reacts throughout collision avoidance behaviour. Thus, closing the loop and providing real time feedback to the locust would greatly increase the saliency of the locust's visual environment. We now know that flight muscle synchrony is the first detectable indicator of the onset of turning behaviour during collision avoidance behaviour, but we also know that prior to muscle activity changes, motor neurons that must synapse with flight muscles are synapsing with interneurons in the thoracic ganglia. This neural correlate is likely a looming sensitive neuron, known to respond looming objects. Investigating the roles of looming sensitive neurons that influence motor neuron output to the flight muscles could reveal insights into the role of the thoracic ganglia and the effects sensory motor integration during collision avoidance behaviour. The information presented here adds to a potential model for the order of events that occur leading up to a turn in response to a lateral looming object (McMillan et al., 2013). I suggest a modified time sequence (Fig 2.9), demonstrating the order of muscle activity and body orientation changes when evoking a left turn. Additions to these models, using data from future experiments described above, will assist in the creation of closed loop simulations that utilize muscle timings as predictors of body orientation changes, and add to our knowledge of physiological mechanisms underlying adaptive avoidance behaviours.

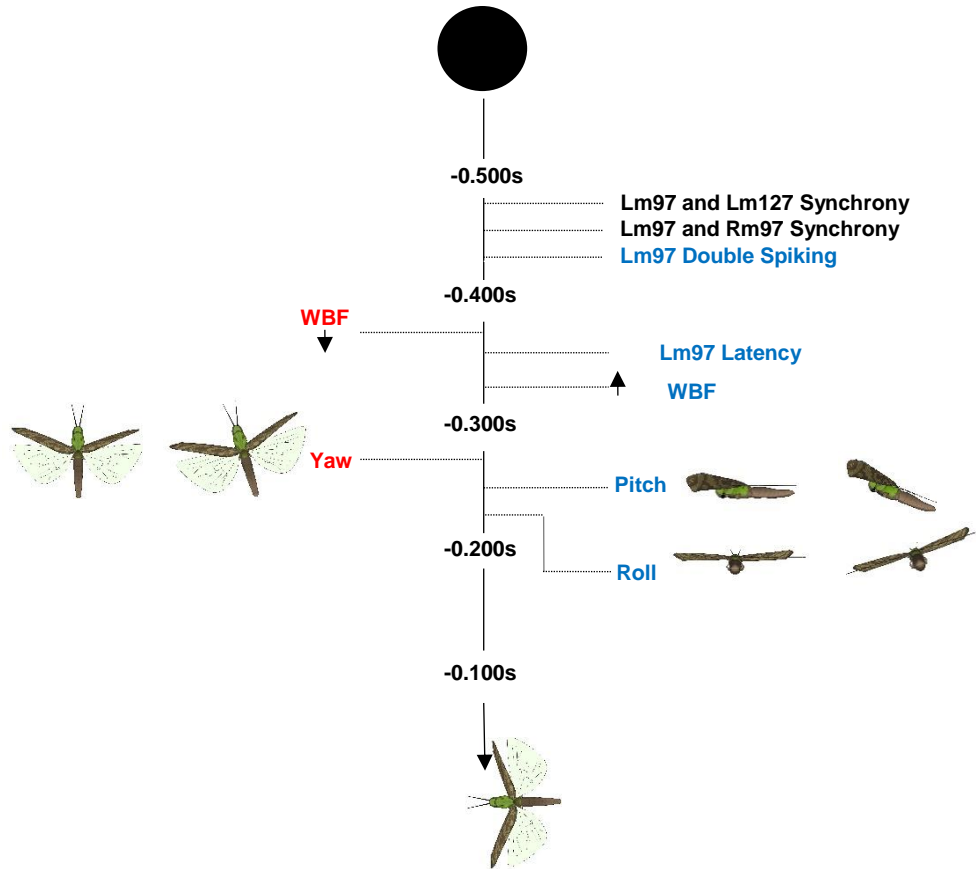


**Fig. 2.9: Order of muscle and body orientation events that occur during collision avoidance.** The black circle represents a looming 14 cm disc 500 ms before TOC and the black vertical arrow represents the timeline from -500 ms to TOC (locust image at bottom of diagram). All events in blue text represent events that were significantly correlated with Lm97 and Rm97 synchrony. Red events indicate no significant correlation to muscle activity.

## **CHAPTER 3**

### **RESPONSE OF A LOCUST MOTION SENSITIVE NEURON, FLIGHT MUSCLE ACTIVITY, AND WING ASYMMETRY DURING FLIGHT STEERING**

(Manuscript in preparation for eLife)

Gray. J.R., supervised the project and contributed to the formulation of the experimental design. Manchester, C.W., developed and carried out all experimentation and analysis. Results were discussed by both authors in the formulation of the final manuscript.

#### **3.1 ABSTRACT**

The locust Descending Contralateral Movement Detector (DCMD) is a well characterized motion-sensitive visual neuron that responds with an increased firing rate that peaks near the time of collision (TOC) of an approaching object. Increasing stimulus complexity (number and shape of objects or object trajectory changes) dynamically modulates the amplitude and temporal properties of the DCMD response profile. Furthermore, rate and time codes from DCMD bursts have been shown to be salient representations of the neurons response during collision avoidance behaviour. This is the first experiment to examine DCMD burst responses, EMG flight muscle activity and wing asymmetry during flight steering. Previously described DCMD bursting occurs in non-flying and flying locusts, suggesting that bursting is critical for coding object approach. When exposed to a looming 14 cm diameter sphere, DCMD burst responses showed dynamic changes that depended on background complexity and object trajectory. Flight also modulated the DCMD bursting responses. During flight, the DCMD peak burst firing rate, peak width at half height, and rise phase differed significantly compared to the non-flying conditions. Temporally, the timing of the first DCMD burst in response to a looming stimulus,

was found to be strongly correlated with flight muscle synchrony, left-right flight muscle latency and forewing asymmetry timing. My findings indicate an important neural correlate within the temporal coding of bursts in the initiation of intentional flight steering during collision avoidance behaviour in flight.

### **3.2 INTRODUCTION**

The neuronal control of behaviour is ubiquitous across the animal kingdom. Information regarding environmental stimuli is integrated in the CNS and transmitted to the peripheral nervous system in the form of rate codes, time codes, and population codes. When investigating the relationship between neuronal activity and environmental stimuli, rate codes have most commonly been used. Among vertebrates, for example, vision and locomotion in rats (Dipoppa et al., 2018), and vocal learning in zebra finches (Roberts et al., 2017) rely on intrinsic properties of firing rates. Moreover, in invertebrates, changes in firing rate properties have been shown to correlate with changes in locomotion in cockroaches (Bender et al., 2010) and navigation via central complex neurons in butterflies, beetles, bees, and locusts (Heinze and Reppert, 2011, el Jundi et al., 2015b, Stone et al., 2017, Homberg et al., 2011, Heinze, 2018). Currently, the interest and importance of the role of a specific type of rate code, found within bursts, has increased in recent studies (Eyherabide et al., 2008; Marsat and Pollack, 2012; McMillan and Gray, 2015; Zeldenrust et al., 2018). Bursts are series of high frequency neuronal spikes that occur in response to a stimulus. It has been postulated that the timing of bursting properties may lead to key correlations to behaviour output (McMillan and Gray., 2015). This brings to light the potential for a temporal code, associated with specific properties of bursting, which is responsible for evoking a collision avoidance response. As mentioned in chapter 2, flight muscle synchrony must be controlled by a neural correlate, responsible for beginning the cascade of muscle events, and body orientation changes correlated with flight steering during collision avoidance. These data lead to a neural candidate which is likely to contribute to flight muscle coordination and the onset of turning.

To successfully avoid an object, a locust must relay information regarding an object's velocity and trajectory to downstream neural circuitry responsible for controlling wing movement. The Descending Contralateral Movement Detector (DCMD), is a well characterized looming sensitive neuron, known to be associated with jumping (Fotowat and Gabbiani, 2007)

and gliding (Santer et al., 2006) collision avoidance behaviour. The DCMD carries information regarding looming stimuli to the thoracic ganglia, which are responsible for motor control of the legs and wings (Smarandache-Wellmann, 2016). As seen in chapter 2, outputs from the mesothoracic ganglia trigger bilateral flight muscle synchrony followed by left-right latency, causing an increased depression of one forewing. The increased depression of the wing creates a measurable asymmetry between the right and left wing positions, triggering the onset of a turn (McMillan et al., 2013). Despite the DCMDs involvement in jumping and gliding, the relationship between temporal properties of the DCMD, flight muscle activity, and wing asymmetry within a single flying animal has not been examined before. DCMD activity responds to different object trajectories (Dick et al., 2017a; Santer et al., 2008; Stott et al., 2018) and is affected by background complexity (Silva et al., 2014). Presenting different trajectories and manipulating the background complexity allows us to test a dynamic range of bursting properties during non-flying and flying conditions. Moreover, object trajectory and background complexity may affect temporal properties of flight muscle activity and wing asymmetry.

Neural recordings during flight introduces a new consideration of the effect of flight on the DCMD. Mechanosensory feedback from motor outputs generate efference copies, which modulate future motor outputs (von Holst and Mittelstaedt, 1950). In zebra fish, mechanosensory feedback enhances speed and stabilizes posture during locomotion (Knafo and Wyart, 2018), whereas in drosophila, feedback from the halteres are combined with visual feedback, in a weighted sum, to influence flight control (Sherman and Dickinson, 2003). Knowing that there is a clear influence of mechanosensory feedback from locomotion on behaviour, it is logical to assume that the locust's flight system modulates signals traveling to the motor system, by relaying the motor state of the wings to the CNS. Recording when flight motor output is active will result in a more realistic neural response during collision avoidance behaviour, as would be found in nature. The majority of experiments recording the DCMD response involved a rigid tether set up where the locusts are unable to (wings are removed) or are prevented from (wings are bound) flying (Gabbiani et al., 2001; Gray et al., 2010; Santer et al., 2005b; Silva et al., 2014; Yakubowski et al., 2016). This feedback may specifically modulate the DCMD response to different object trajectories in both simple and complex environments, therefore, comparing within the same animal, DCMD bursting parameters between non-flying and flying locusts could elucidate the importance sensory motor integration in collision avoidance behaviour.

Despite DCMD parameters such as peak firing rate, peak width at half height, peak timing, and rise and fall phases being commonly analyzed as response characteristics (Gray et al., 2010; Guest and Gray, 2005; Santer et al., 2005b; Santer et al., 2006), these parameters often occur after the initiation of the behaviour has taken place, centered around TOC. DCMD bursting activity presents us with a detectable parameter that is more behaviourally relevant, the timing of the first burst (TOFB) in a DCMD spike train. Occurring prior to the initiation of a collision avoidance behaviour, this event could be a predictive correlate. By correlating this event with downstream changes in muscle activity and wing asymmetry, it could yield the first detectable neural event responsible for the initiation of intentional flight steering during collision avoidance behaviour. I found that flying effected DCMD burst peak width at half height, rise phase and peak burst firing rate in both simple and complex visual environments. These data point to the potential necessity for inclusion of mechanosensory feedback when analyzing responses of looming sensitive neurons. Moreover, I found that the temporal bursting parameter (TOFB), is a neural correlate to not only the timing of wing asymmetry (TOWA), but also changes in muscle activity (bilateral muscle synchrony (TOS)), right-left muscle latency (TOL). This demonstrates a potential temporal code based on the arrival time of the first burst.



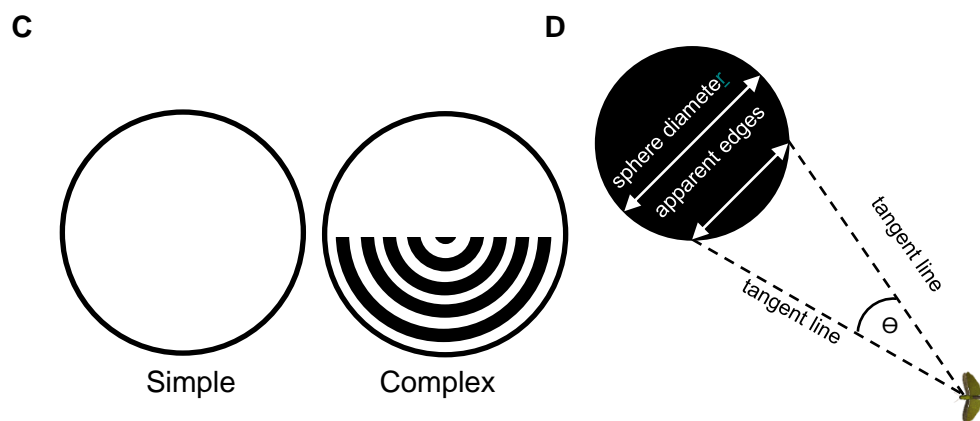
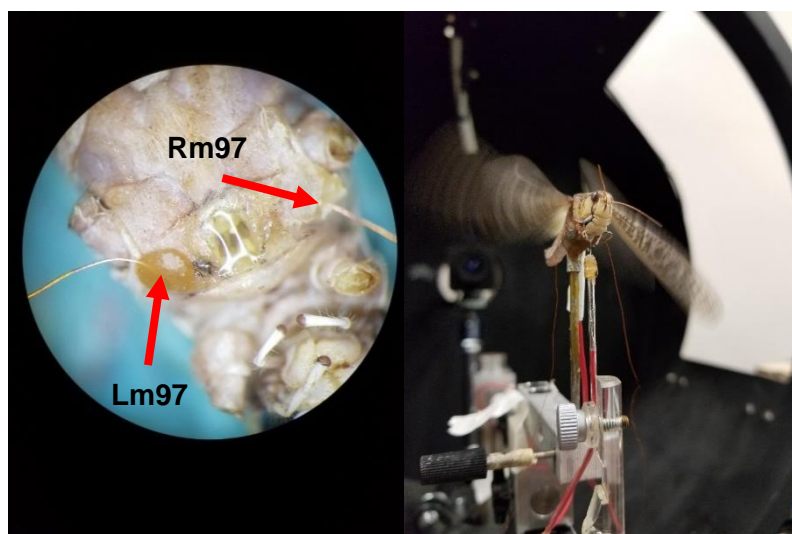
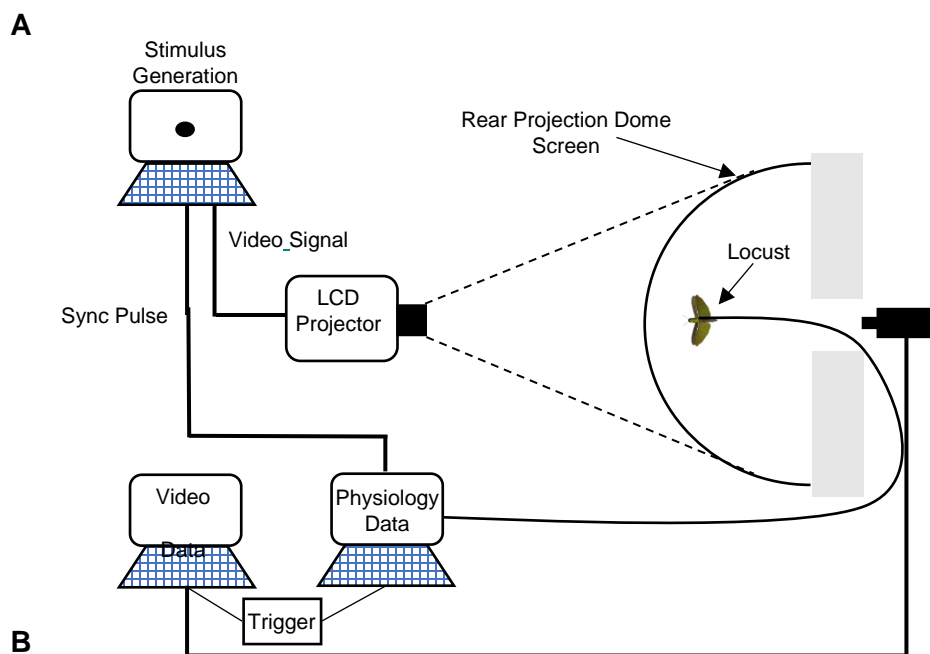


**Figure 3.1: A top and front view of the experimental set up** A) A LCD projector displayed, onto the rear projection dome screen, the image of a 14cm diameter looming sphere approaching at 3 m/s. A high speed motion camera positioned behind the locust recorded behaviors at 250fps. Video data were recorded and stored on the video data computer. A manual trigger was used to time sync the start of video recordings with the physiological data. B) A silver hook electrode and copper wire EMG electrodes inserted into the locust were recorded via a data acquisition (DAQ) board attached to a data collection computer. C) Examples of simple and complex backgrounds presented to the locust, see text for more information D) Example of subtense angle seen by a locust as a sphere approaches on a looming trajectory, see text for more information.

### 3.3 MATERIAL AND METHODS

#### 3.3.1 ANIMALS

Experiments were conducted on 23 adult male locusts (*L. Migratoria*). Animals were selected 3 weeks past their imaginal molt from a crowded colony maintained at the University of Saskatchewan in Saskatoon, Canada. The colony was maintained between 25-28°C and a 12h:12h light: dark cycle. Experiments were conducted at 28°C within a 10-hour period in the day to remove putative effects of locusts flying at night (Gaten et al., 2012).

#### 3.3.2 PREPARATION

Locusts were removed from their rearing cages and placed in a wire mesh container within the experimental room and acclimated for one hour. The legs of the locust were then removed to prevent dislodging of electrodes. Using a sapphire blade, a 2 x 2 mm square incision was made centrally on the upper ventral segment of the thorax, and the cuticle removed to grant access to the ventral nerve cord. Two 0.5 mm incisions were made on the ventral surface of the upper thorax where electromyograph (EMG) electrodes (100 µm gauge fine copper wire; Belden, St Laurent, QB, Canada) were inserted into the first basalar m97 flight muscles (Fig. 3.1B). The insertion site for EMG were the same used for the m97 sites in Chapter 2 (Fig. 2.B). A rigid tether was then attached with bee wax to the ventral side of the locust thorax, around the window to the ventral nerve cord. The locust was then transferred to the recording arena and the tether was secured. A silver hook electrode was hooked around the right or left ventral nerve cord, and preliminary recordings were made to confirm a clear signal from the DCMD. If a nerve cord failed to provide a clear signal, an attempt to hook the other nerve cord was made. Preparations that yielded no discernable electrophysiological response to stimuli (motion across the screen) were rejected from experimentation. The electrode hook site was then isolated with a mixture of Vaseline and mineral oil, and a ground wire was inserted into the ventral side of the abdomen. Following the isolation of the electrode hook site, the site was bathed in saline (147·mmol NaCl, 10·mmol KCl, 4·mmol·CaCl<sub>2</sub>, 3·mmol·NaOH, 10·mmol Hepes, pH·7.2) to prevent desiccation. The entire preparation was rotated 180°, orienting the locust dorsal-side up with its longitudinal axes perpendicular to the apex of the rear projection screen, where the eyes were aligned with the azimuthal and elevation axes of the dome apex (Fig. 3.1 A,B). This orientation presented 0°

directly in front of the locust, 180° was directly behind the locust, and 90° was aligned with center of the locust's eye. The locust was left for 10 minutes in front of a blank white screen (background luminance = 430 cd/m<sup>2</sup>) prior to the beginning of the experiment to allow for acclimatization.

### **3.3.3 VISUAL STIMULUS**

Visual stimuli were presented as 14cm diameter spheres traveling at 300 cm/sec, scaled in real-time at 85 frames/sec (fps), and projected onto a specialized rear projection dome screen using a Sony VPL-PX11 LCD data projector (NY, USA). A Quantum Instruments PMLX photometer (B & H Photo, New York, NY, USA) placed at the projection screen was used to measure the luminance of the black sphere and background, and thus calculate a Michelson contrast ratio of 0.962. Visual stimuli were coded using python in a program called Pyglet, a program used to write video graphics. This program also contained correctional factors for the curvature of the dome. Stimuli began at a size containing a subtense angle below the locust's ability to detect (<1°) (Horridge, 1978). The program output a 5V pulse at TOC, to synchronize electrophysiological data with the stimulus parameters. Spheres were presented at either 0° or 45° trajectories in the azimuthal plane at 0° elevation and began at a consistent virtual distance of 400 cm away from the locust for each presentation, reaching a final subtense angle of 180°. The simple background consisted of the stimulus against a solid white background, whereas the complex background consisted of concentric circles traveling at 100 cm/sec symmetrically outwards from the center of the dome below the horizon line (Fig.3.1C). The circle bar thicknesses was 5 cm with a spatial frequency of 5 cm and a Michelson contrast ratio of 0.812. Flying was initiated by a puff of air delivered to the locust's head or by mechanical stimulation of the abdomen. Trials consisted of presentations of 0° and 45° trajectory looms, each within a simple or complex background. Each presentation paradigm was replicated 3 times for a total of 32 presentations per trial. The time interval between each presentation was 2 minutes to prevent neural habituation.

### 3.3.4 RECORDING TECHNIQUES

Electromyogram and DCMD recordings were amplified using a differential AC amplifier (A-M Systems, model No. 1700, gain = 10,000, low cut-off = 1Hz, high cut-off = 5000hz). Neural, muscle, and stimulus pulse data was digitized using a Data Translation DT9818 data acquisition board (TechnaTron Instruments, Inc., Laval, QC) and recorded at 20 kHz with DataView version 11 (W.J. Heitler, University of St Andrews, Scotland). Electrophysiological recordings were exported to a data analysis computer following each trial. Video recordings of flight behaviour were collected by a monochrome digital camera (Flare, IO Industries, London, ON, Canada) located directly behind the locust (Fig.3.2A). The camera recorded at a resolution  $900 \times 900$  pixels at 250 frames/sec in conjunction with a digital video recorder (Express DVR, IO Industries, London, ON, Canada). Following each trial, recordings were exported to a data analysis computer.

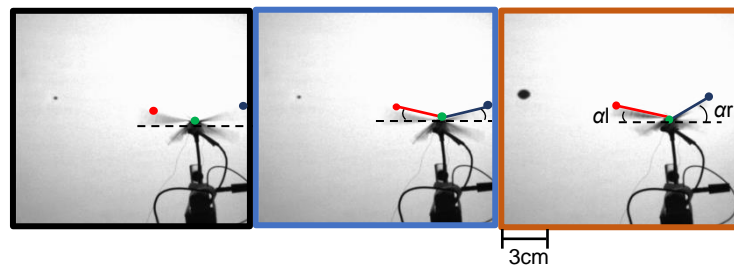
### 3.3.5 VISUAL ANALYSIS

Video recordings were imported in WinAnalyze3D motion analysis software (Mikromak, Berlin, Germany), which was calibrated for 2-D measurements. Three motion tracking points were digitally placed on each frame of the video recording. One point was placed on each of the locust's forewing tips, and one was placed on a stationary point of the locust, equidistant from the base of each forewing (Fig. 3.2A). Wing angles were calculated by measuring the change in position of the wing tip points (x,y, in a 2D plane) in reference to a central point, using the horizontal axis of the locust as a reference line. The angular difference ( $\theta_{diff}$ ) was calculated using the equation below.

$$(\theta_{diff}) = \text{atan}\left(\frac{y_r - y_o}{x_r - x_o}\right) - \text{atan}\left(\frac{y_l - y_l}{x_o - x_l}\right) \dots \dots \dots (3.1)$$

The *r* and *l* subscripts represent right and left-wing tips, whereas the *o* subscript represents the central point. Calculated values were then exported and processed in Sigma Plot 12.5 (Fig 3.2B). Timing of wing asymmetry was defined as a deviation of wing symmetry outside the 95% confidence interval (determined by a 0.5s second epoch of pre-turn wingbeats) (Fig.3.3). Maximum angular difference between left and right wings were calculated by subtracting the maximum angular change from the average angular difference of a 0.5s pre-turn epoch.

**A**



**B**

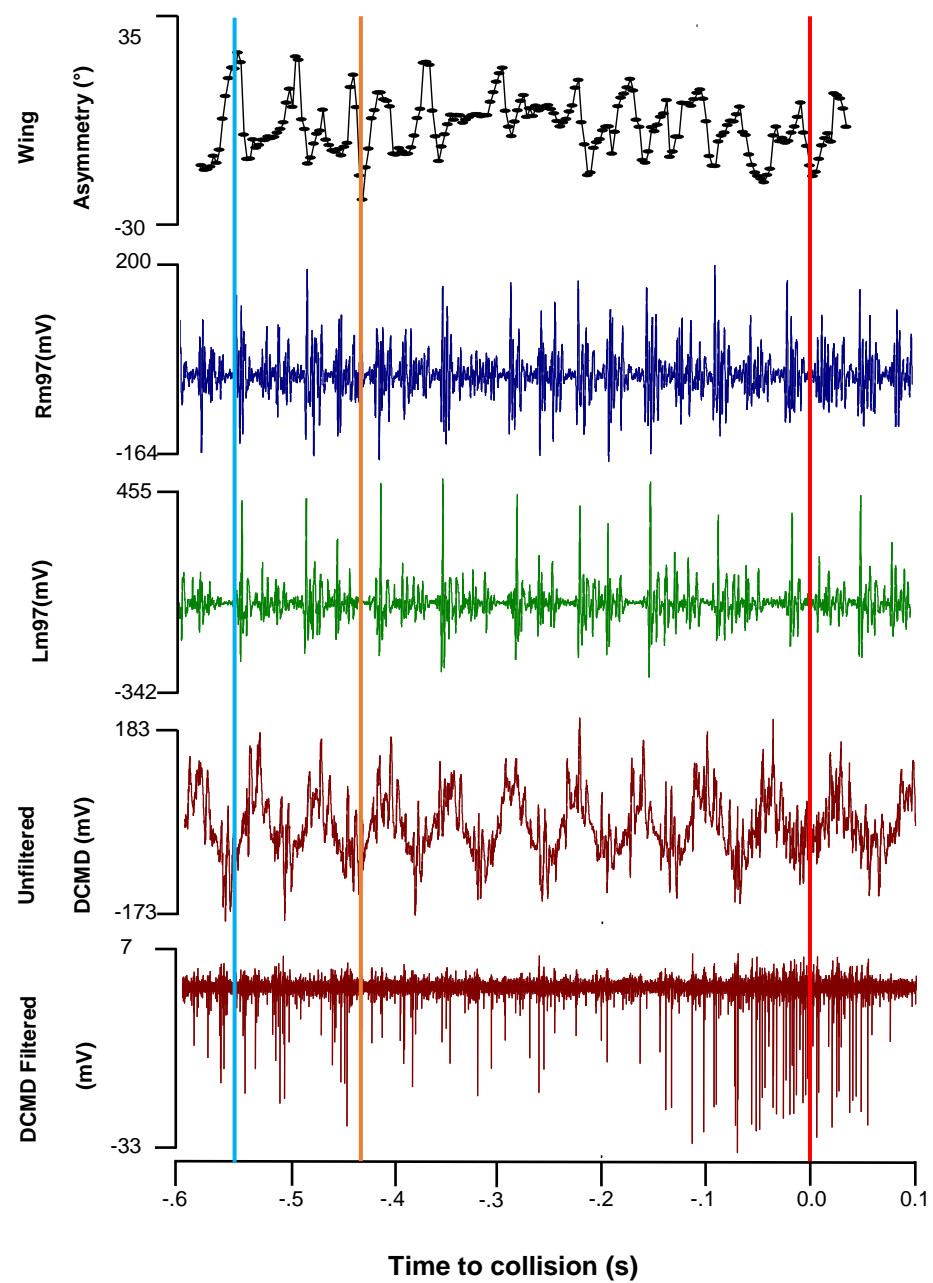


**Figure 3.2: Behavioural and physiological data from one locust during a left turn in response to a sphere looming 45° from the left.** A) Images were captured from video taken at 250 fps. Left two images represent pre-turn symmetry of the wings. Right image represents wing asymmetry during a left turn. Wing asymmetry was measured using the angular difference between  $\alpha_l$  and  $\alpha_r$ . Coloured borders of images correspond to the timing of the vertical coloured lines in (B). B) Wing asymmetry, extracellular recordings of Rm97 and Lm97 flight muscles, and unfiltered and filtered DCMD. The DCMD recording was filtered as described in the text. The red line represents TOC.

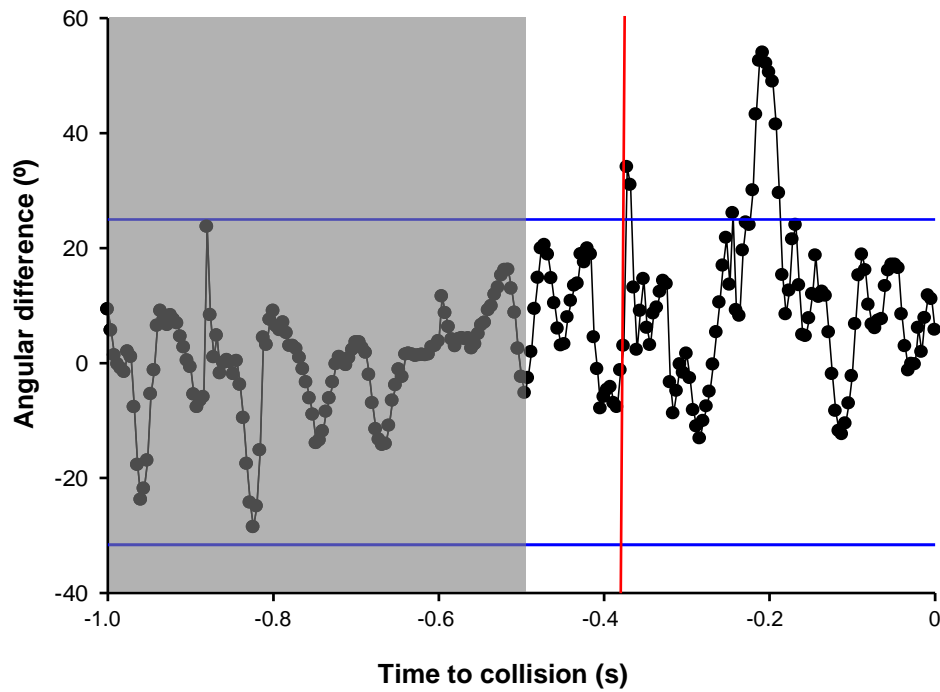


**Fig. 3.3: Change in angular difference between the left and right forewing, during a presentation of a leftwards 45° loom, in a simple background.** These data show a right turn, indicated by the crossing of the upper boundary of the 95% confidence interval (blue line). Confidence intervals were generated using a 0.5s pre-behaviour epoch (Gray shaded region). Red line represents time of increased wing asymmetry. Timeline is in reference to TOC (0s).



### 3.3.6 SPIKE TRAIN ANALYSIS

Electromyogram spike times were isolated using threshold analysis in DataView version 11.3.2 (W.J. Heitler, University of St Andrews, Scotland). Time stamps were exported to NeuroExplorer software (Version 4.0, Madison, AL, USA) to determine timing of bilateral synchrony using inverted synchrony versus time analysis. Bilateral flight muscle latency timings maximum extents were extracted using Sigma Plot 12.5 (Systat Software Inc., Richmond, CA, USA) and detected by deviations outside the 95% confidence interval of a pre-behaviour epoch. DCMD signal noise reduction was applied via a 60Hz debuzz and removal of DC filter. Flight muscle activity introduced considerable noise to the DCMD signal, therefore a 15kHz high pass filter was applied to obtain a clear DCMD signal (Fig 3.4B). The filtered DCMD channel time stamps were then extracted using threshold analysis in DataView. DCMD spike times were transformed into peristimulus time histograms with a 1 ms bin width and smoothed with 50ms gaussian filter. Bursting events were determined by a predetermined burst algorithm (McMillan and Gray, 2015). ISI analyses determined that the interspike interval used in the algorithm (8ms) was appropriate for my data (Fig.3.4). The sync pulse from the video recording used to time align with electrophysiology recordings, and the stimulus TOC pulse timing was also extracted using threshold analysis. All spike time events were time aligned to TOC. DCMD burst parameters were calculated using NeuroExplorer (Version 4.0, Madison, AL, USA). Rise phase was calculated using MATLAB (Version 9.2, MathWorks Inc., Natick, USA), from peristimulus time histograms, using the time of when the histogram last crossed the 95% confidence interval, with a positive slope, to the peak firing rate.

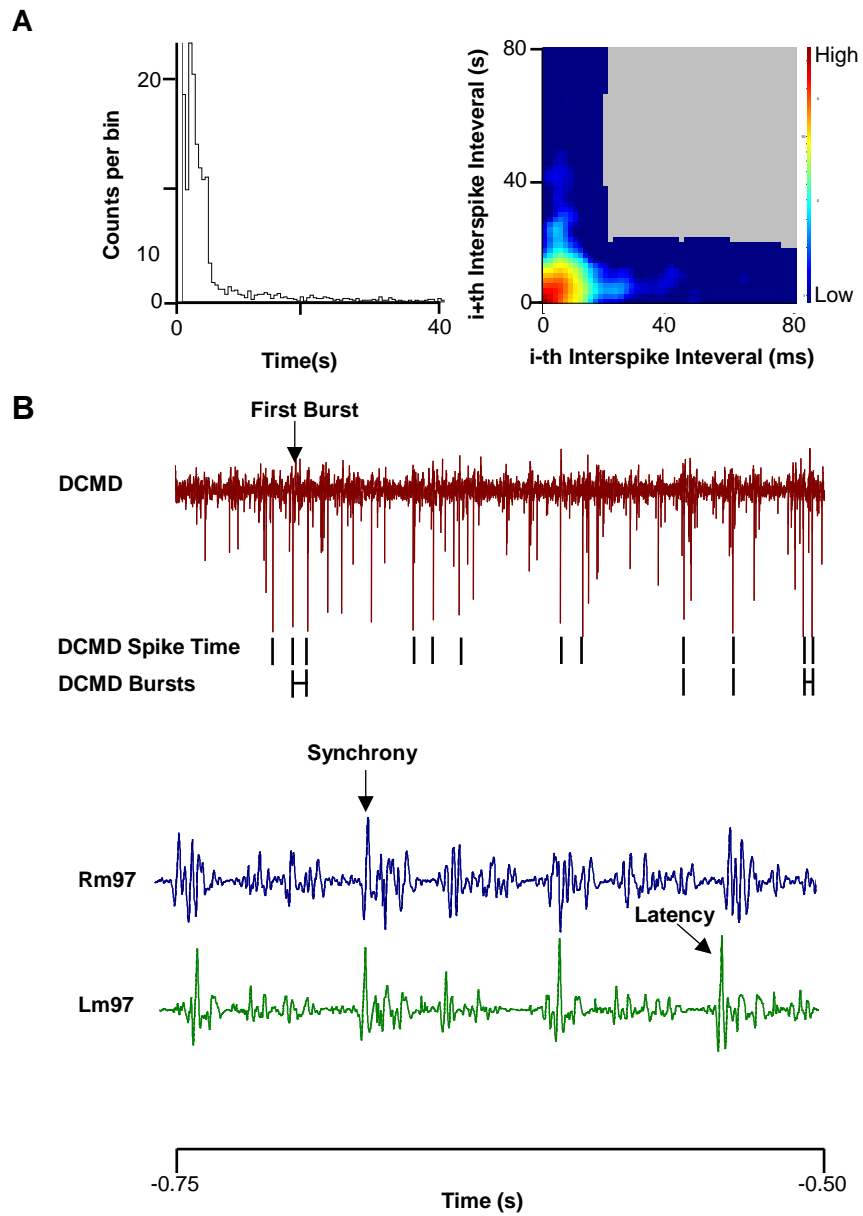


**Figure 3.4: EMG and DCMD recordings showing extractable parameters of muscle timing and DCMD bursting.** A) Average interspike interval diagrams of 12 locusts responding to 45° looms. The diagrams illustrate that the majority of spikes occur within 8 ms of each other, therefore the bursting algorithm used to create the bursting intervals seen in (B) uses a required maximum distance between spikes of 8 ms. B) Raw traces of DCMD and EMG activity during a left turn. The timing of the first burst can be seen on the filtered DCMD trace. Below, rasters show the timing of individual spikes and the occurrence of bursts. The locust responded to a 45° leftward looming 14 cm diameter sphere, approaching at 3m/s. Synchrony is represented by time-aligned right and left m97 EMG spikes. This was followed by a negative latency (left firing before the right).\_

### 3.3.7 STATISTICAL ANALYSIS

Statistical analysis was conducted using SigmaPlot 12.5 (Systat Software, Richmond, CA). All data were first analyzed for normality and equal variance. Measured DCMD, EMG, and wing asymmetry parameters that were parametric were analyzed using a one-way ANOVA and parameters failing equal variance testing were analyzed using a Kruskal-Wallis ANOVA on ranks, followed by Dunn's method post hoc analysis. Data passing homogeneity of variance were tested using a Tukey test. Pair comparison were conducted using student t tests. Pearson's Product Moment Correlation was used to evaluate relationships between ride phase, TOFB, TOS, TOL, and TOWA. Conventions for the coefficient ( $\rho$ ) considered 0 to  $\pm 0.9$  to be non-correlative and  $\pm 0.1$  to  $\pm 0.29$ ,  $0.3\pm$  to  $\pm 0.49$  and  $\pm 0.5$  to  $\pm 1$  to be considered small, medium, and large correlations respectively (Cohen, 1988). All significance was assessed at ( $P < 0.05$ ).

## 3.4 RESULTS

### 3.4.1 GENERAL BEHAVIOUR

Behaviours were only evaluated for locusts that generated flight-like beating of the wings (referred to as flight or flying in the text), and were classified into three behaviour groups: turns, glides, or stops. The behaviours were analyzed for differences in the occurrence of each behaviour (frequency) between different presentation conditions. In simple backgrounds, stops and glides occurred at a relatively lower frequency than turns for both 0° and 45° approach trajectories, respectively (Stops, 17% and 38%, and Glides, 10% and 11%, N=17, N=21). Within complex backgrounds (flow field), approaches from 0° evoked fewer glides (7%, n=17), and more stops (35%, N=17), whereas approaches from 45° evoked more stops (37%, N=16), and increases in glide frequency (13%, N=16) compared to 0°. Turn direction preference was also examined, to determine potential turn biases in the experiments. I found that 0° presentations evoked a leftward turn bias, composing 78% of the turns against a simple background and 40% of turns against a flow field. Furthermore, 45° presentations only evoked leftwards turning biases in simple backgrounds, consisting of 87% of the turns, whereas complex backgrounds evoked a rightwards bias of 68% of turns. When approaches were not straight (45°), and loomed from the left or right, 12.5% of locusts turned towards the approaching object when in simple backgrounds, and 10% within complex backgrounds. When analyzing the effect of presentation condition on the timing of behaviours, I found that background complexity and object trajectory had no effect on the timing of stops (One Way ANOVA, N=5, N=13, N=6, N=9, P=0.85). Moreover, the timings of stops and turns did not significantly differ across differing trajectories or background types ( $t_{13}=0.584$ , N=3, N=13,  $t_{11}=88.0$ , N=8, N=11,  $t_{11}=0.73$ , N=5, N=8,  $t_{12}=-1.71$ , N=6, N=8). Gliding behaviours occurred significantly earlier than stops for 0° presentations ( $t_3=4.98$ , N=3, N=2,  $P<0.05$ ,  $t_8=2.31$ , N=8, N=2,  $P=0.05$ ), although they did not differ from the timings of turns ( $t_{12}=-1.25$ , N=2, N=12,  $t_{11}=-0.46$ , N=2, N=11,  $t_8=-4.91$ , N=2, N=8). For approaches from 45°, glides occurred significantly earlier than stops ( $t_8=2.31$ , N=8, N=2,  $P<0.05$ ,  $t_6=-3.25$ , N=2, N=6,  $P<0.05$ ). Within complex backgrounds, I found that differing object trajectories resulted in glides occurring earlier than turns during 45° presentations ( $t_8=-4.91$ , N=2, N=8,  $P<.001$ ). I examined whether there was a relationship between the timing of wing asymmetry and turn direction. Although there was no relationship found in the timing of

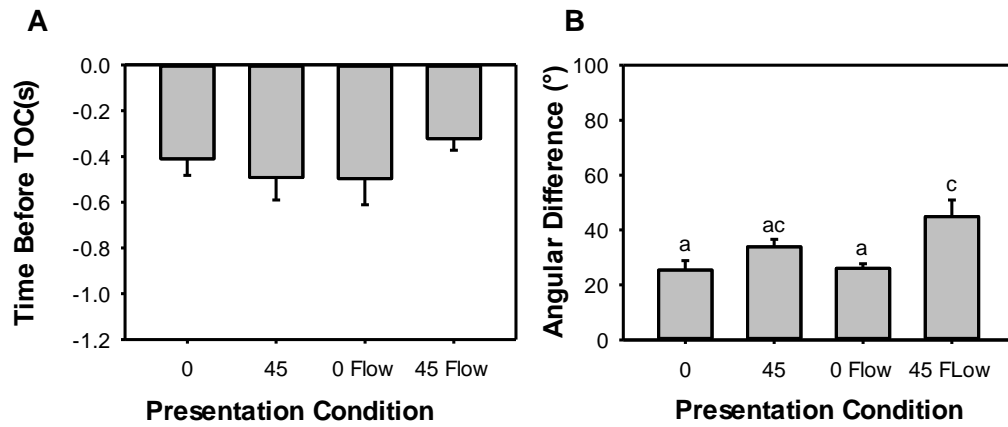


**Figure 3.5: Comparison of wing asymmetry timing and maximum angular difference between different stimulus conditions.** A) Timing of asymmetry did not significantly differ for either approach direction of background type. Times are in reference to TOC. B) Maximum extent of angular difference between left and right wings did not significantly differ for either approach direction of background type. Maximum angular extent was calculated by subtracting the maximum angular difference from the mean angular difference from a pre-turn epoch. See text for calculation. Data represent mean and standard error. Columns sharing the same letter do not significantly differ.

turns during 45° presentations, the extent of wing asymmetry increased in complex backgrounds compared to simple backgrounds, for left turns. The timing of wing asymmetry was not affected compared to simple backgrounds, for left turns. The timing of wing asymmetry was not affected by any of the presentation conditions. Timing of wing asymmetry was not affected by different presentation conditions (Kruskal-Wallis One Way ANOVA on Ranks, N=12, N=11, N=11, N=8, P=0.66) Fig(3.5A), although mean wing asymmetry evoked from 45° presentations within complex backgrounds ( $44.8 \pm 19.3^\circ$ ) were significantly greater than both 0° in simple backgrounds ( $25.8^\circ \pm 13.0^\circ$ ) and 0° in complex backgrounds ( $26.0^\circ \pm 4.7^\circ$ ) (One Way ANOVA on Ranks, N=12, N=11, N=11, N=8, P<0.05) (Fig 3.5B).

### 3.4.2 MUSCLE ACTIVITY AND TIMING

I quantified three muscle activity events for each presentation, the time of bilateral Lm97/Rm97 flight muscle synchrony, and properties of left-right m97 flight muscle latency (the timing of latency initiation and the maximum change in latency). First, I analyzed flight muscle synchrony, and found that synchrony events occurred singularly, over one wing beat cycle. Synchrony events occurred at an average of  $-0.518s \pm 0.237s$ , before TOC. There was no relationship found between the timing of synchrony and turn direction ( $t_{14} = 8.41$ , N=5, N=10,  $t_{15} = -1.17$ , N=6, N=11,  $t_8 = 2.8$ , N=3, N=6,  $t_{10} = -0.174$ , N=2, N=9, P>.05) ( Fig 3.6A). Furthermore, neither different trajectories nor background complexity was found affect the timing of muscle synchrony events (One Way ANOVA, N=15, N=11, N=16, N=8, P=0.26) (Fig.3.6E). Secondly, I analyzed the potential effect on muscle latency properties. Despite turn direction having no relationship to the timing of latency initiation ( $H_3 = 2.07$ , Dunn's) (Fig.3.6F), the latencies were longer in response to approaches from 45°, in simple backgrounds, and shorter during 0° approaches ( $t_{14} = 62.0$ , N=5, N=10,  $t_{15} = -0.30$ , N=6, N=11,  $t_8 = 6.02$  N=3, N=6, P,0.05) (Fig. 3.6C). Therefore, I examined differences in latency duration for both right turns and left turns separately (Fig.3.6D). Right turn durations had higher variability than lefts turns, with 45 ° presentations in simple backgrounds evoking significantly higher latency extents, and 0° presentations in complex backgrounds evoking lower latency extents than other presentation conditions (One Way ANOVA, N=15, N=11, N=16, N=8, P<.05). Conversely, the left turns did not demonstrate the same variability, and showed no significant differences (Kruskal-Wallis One Way ANOVA on Ranks, N=12, N=11, N=11, N=8, P=.66). When I examined the timing of

latency initiation, there was no effect by different trajectories or background complexity (Kruskal-Wallis One Way ANOVA on Ranks,  $N=12$ ,  $N=11$ ,  $N=11$ ,  $N=8$ ,  $P=.22$ ) (Fig.3.6F)

### 3.4.3 DCMD BURSTING ACTIVITY AND TIMING

Although behaviourally,  $45^\circ$  trajectories evoked later stops ( $-0.444s$ ) than turns ( $-0.773s$ ) (Mann-Whitney Rank Sum Test,  $N=13$ ,  $N=11$ ,  $P<0.05$ ) with respect to TOC, I found no bursting properties that confirm a relationship between the bursting and behaviour selection. DCMD burst responses showed no significant differences between stops and turns for maximum burst firing rate, peak position, peak width at half height, or rise phase (Mann-Whitney Rank Sum Test,  $N=15$ ,  $N=11$ ,  $N=16$ ,  $N=11$ ,  $P=0.29$ ,  $P=.12$ ,  $P=.67$ ,  $P=.09$ ). However, further analysis showed significant relationships between DCMD and muscle activity.

#### *Maximum firing rate and burst firing rate:*

Although my focus was on burst firing rate properties, I also investigated differences between the maximum DCMD burst firing rate and the maximum DCMD firing rate that included all spikes. I found that DCMD burst firing rate was consistently lower than DCMD peak firing rate (Fig.3.7). Specifically, peak burst firing rates were significantly lower for  $0^\circ$  trajectories during flight in simple backgrounds, (Kruskal-Wallis One Way ANOVA on Ranks,  $N=21$ ,  $N=16$ ,  $N=19$ ,  $N=19$ ,  $P<0.001$ ). Furthermore, I found that peak burst firing rates, during  $45^\circ$  presentations in simple backgrounds were significantly lower than DCMD peak firing rates (Kruskal-Wallis One Way ANOVA on Ranks,  $N=21$ ,  $N=16$ ,  $N=19$ ,  $N=19$ ,  $P<.001$ ). When focusing on bursting, I compared peak burst firing rates between different trajectories, background complexities, and flight conditions. I found that both background complexity and flight conditions affect the burst firing rate responses (Fig. 3.8A). Specifically, increasing background complexity elicits higher peaks for non-flying locusts presented with  $45^\circ$  looms (Kruskal-Wallis One Way ANOVA on Ranks,  $N=21$ ,  $N=16$ ,  $N=19$ ,  $N=19$ ,  $P<.001$ ) whereas within simple backgrounds,  $45^\circ$  trajectories elicited lower peaks in non-flying locusts compared to flying locusts presented with  $45^\circ$  trajectories and non-flying locusts presented with  $0^\circ$  looms (Kruskal Wallis One Way ANOVA on Ranks,  $N=19$ ,  $N=19$ ,  $N=21$ ,  $P<0.001$ ) (Fig.3.8A). Within the flight condition, in complex backgrounds,  $0^\circ$  looms evoked lower peaks than both flying and



non-flying locusts presented with 45° looms (Kruskal-Wallis One Way ANOVA on Ranks, N=16, N=19,  $P<0.001$ ).

***Peak Position:***

I compared peak positions of both DCMD and DCMD burst firing rates and found that burst firing rate peaks occurred significantly later than DCMD firing rate peaks ( $t_{21}= 504$ ,  $N=21$ ,  $P<0.05$ ). The peak position parameter was unaffected by any of my presentation conditions, or the presence or absence of flight like wing beats (Kruskal-Wallis One Way ANOVA on

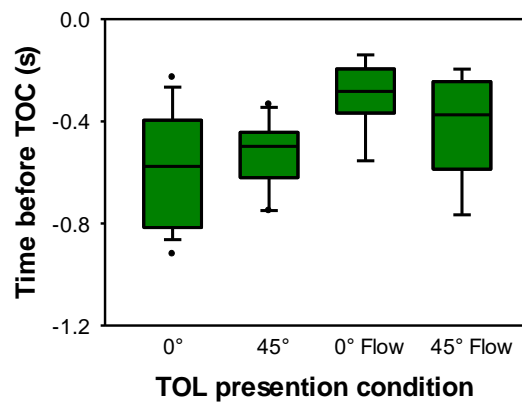
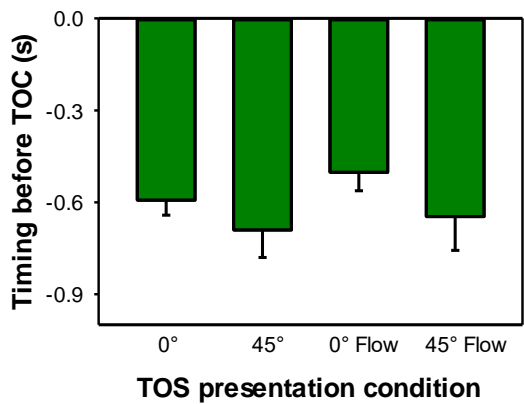
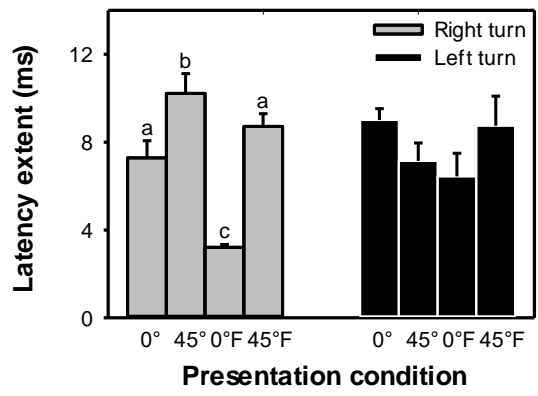
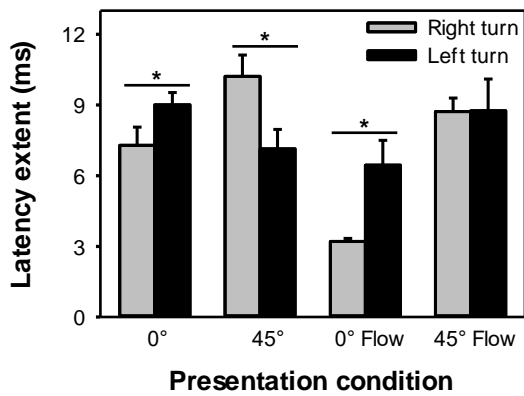
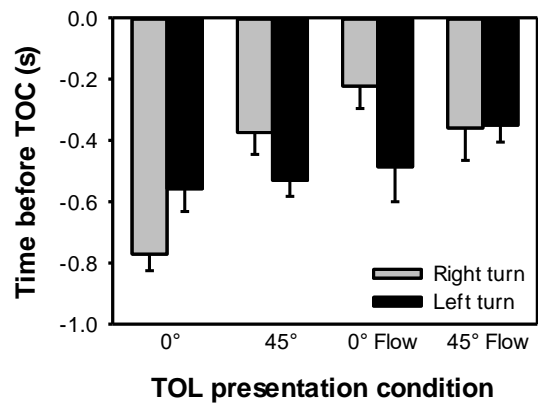
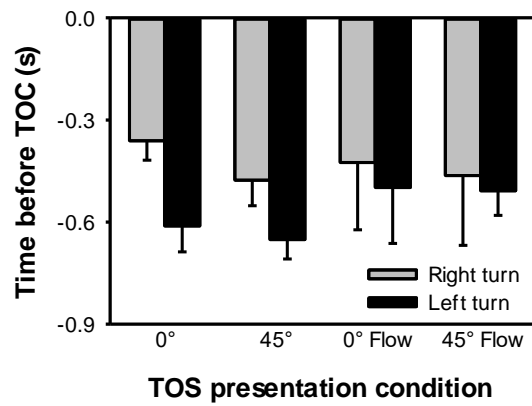


**Fig. 3.6: Comparisons of muscle activity properties across different presentation conditions.** A,B,C) Bar graphs comparing right and left turns for TOS, TOL, and latency extent across different presentation conditions, in reference to TOC (0s). Vertical bars indicate standard error, and horizontal bars with an asterisk indicate significant differences. Gray shaded bars are right turns and black bars are left turns. D) Histogram comparing latency extent within turn groups. Columns sharing the same letter are not significantly different from each other. E,F) Histograms and box plots comparing TOS and TOL. Boxplots in (F) represent the median, 25th, and 75th percentiles and whiskers represent the 5th and 95<sup>th</sup> percentiles.

Ranks N=16, N=19, N=19, N=21, P=0.14) (Fig 3.8B). When analyzing the bursting data, I noticed a consistent first burst that occurred at the beginning of each response to a presentation condition. Therefore, to investigate a potential fixed time delay between the first temporal bursting event and the timing of peak bursting, I measured the timing of the first burst in each spike train and compared them to the timing of peak bursting. I found small correlations for 0° and 45° presentations in simple backgrounds (N=12, N=11, N=11, N=8, N=8,  $\rho=0.14$ ,  $\rho=0.11$ ,  $\rho=0.09$ ,  $\rho=0.24$ ).

### ***Peak Width at Half Height:***

I compared the differences of peak width at half height between DCMD and DCMD bursts and found several differences. Presentation condition combinations, with the exception of flying locusts in simple backgrounds presented with 0° trajectories, and non-flying locusts within complex backgrounds presented with 45° trajectories, showed significantly wider DCMD burst peak width at half height than DCMD peaks width (Kruskal-Wallis One Way ANOVA on Ranks, N=21, N=16, N=19, N=19,  $P<.001$ ). I found that bursting responses were affected by both background complexity and flight. Animals presented 0° trajectories elicited wider peak widths in complex backgrounds compared to simple (Kruskal-Wallis One Way ANOVA on Ranks, N=21, N=16,  $P<0.001$ ) (Fig.3.8C), whereas 45° trajectories evoked the opposite response, showing lower peak widths in complex backgrounds (Kruskal-Wallis One Way ANOVA on Ranks, N=19, N=21,  $P<.001$ ) (Fig.3.8C). Furthermore, within non-flying animals in simple backgrounds, 45° trajectories elicit wider peaks than 0° trajectories (Kruskal-Wallis One

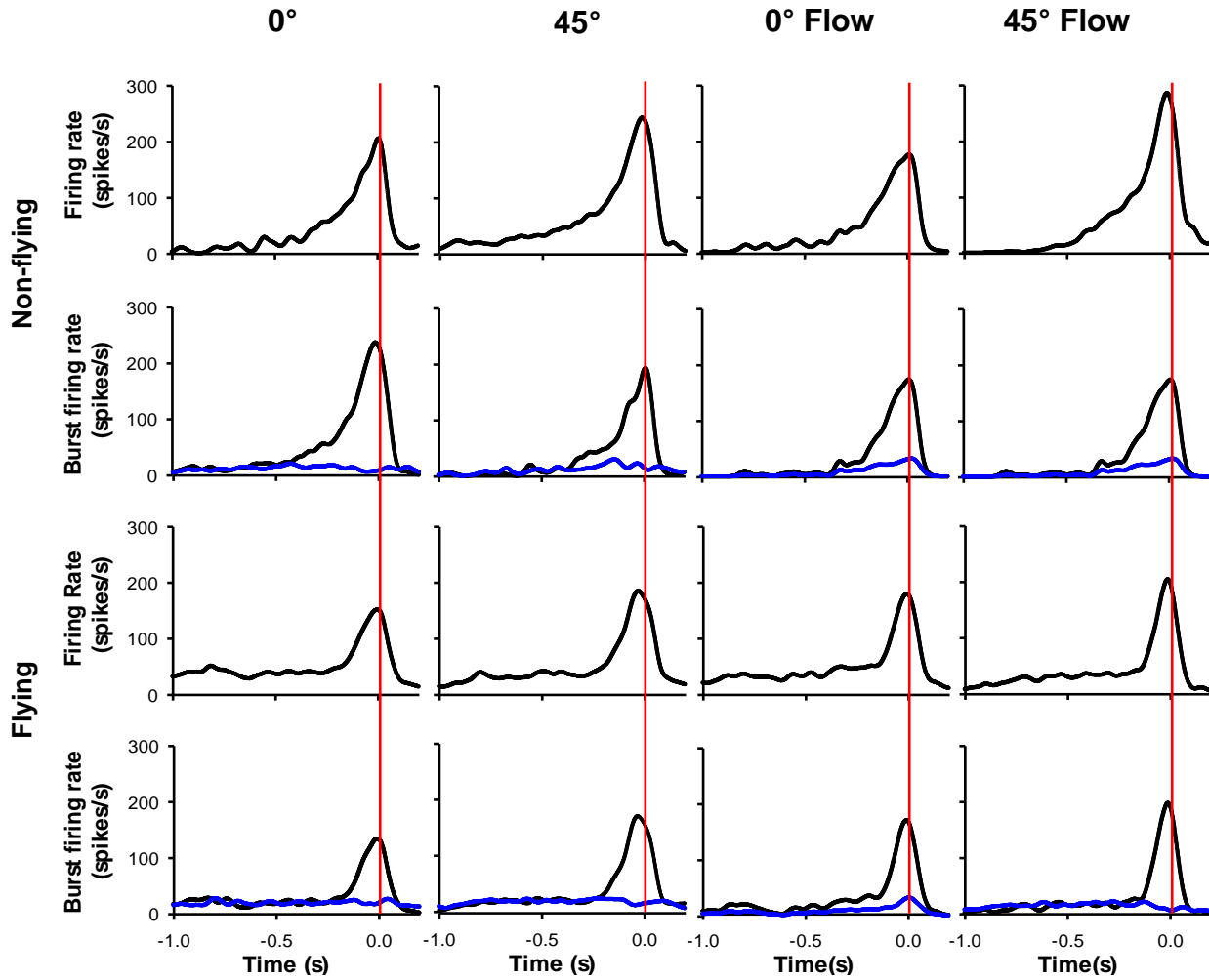


**Figure 3.7: DCMD firing rate and intraburst firing rate for each presentation and flight condition.** Perievent histograms were time aligned to TOC (vertical red lines) with a bin width of 1 ms and smoothed with a 50 ms gaussian filter. (A) Top panels show DCMD firing rate over time with reference to TOC (red vertical line). From left to right shows changes in DCMD activity for different direction of object approach and when adding a background flow field. Bottom panels show intraburst firing rate over time with reference to TOC. Blue lines indicate the isolated spikes, not included within the bursts, over time. (B) Shares the same comparisons as (A), but during flight.

Way ANOVA on Ranks,  $N=16$ ,  $N=21$ ,  $P<.001$ ). Moreover, I found that increasing background complexity, while flying, evokes wider peaks in  $0^\circ$  trajectories Kruskal-Wallis One Way ANOVA on Ranks,  $N=19$ ,  $N=16$ ,  $P<0.001$ ) (Fig.3.8C). The burst peak width at half height was the most highly affected parameter of the DCMD.

### ***Rise phase:***

The last DCMD bursting firing rate parameter examined was the rise phase. I found that only  $45^\circ$  looms in complex backgrounds evoked shorter mean rise phases of bursts in non-flying locusts ( $t_{36}= 6.47$ ,  $N=19$ ,  $N=19$   $P<.001$ ). When examining the rise phases of DCMD bursts, I found that background complexity, object trajectory, and flight all influenced the DCMD bursting response. When background complexity was increased, non-flying locusts presented  $0^\circ$  trajectories showed significantly shorter rise phases than simple backgrounds (Kruskal-Wallis One Way ANOVA on Ranks,  $N=16$ ,  $N=18$ ,  $P<0.001$ ) (Fig.3.8D). Furthermore, non-flying locusts exposed to  $45^\circ$  trajectories in complex backgrounds elicited longer rise phases than  $0^\circ$  trajectories (Kruskal-Wallis One Way ANOVA on Ranks,  $N=21$ ,  $N=16$ ,  $P<.001$ ) (Fig.3.8D). When the locust's wings are beating, the feedback elicits shorter rise phases when locusts presented with  $45^\circ$  trajectories, regardless of background complexity (Kruskal-Wallis One Way ANOVA on Ranks,  $N=17$ ,  $N=20$ ,  $N=20$ ,  $N=20$ ,  $P<0.001$ ). To investigate a potential temporal relationship between the timing of the first burst and the initiation of the rise phase, I measured the timing of the first burst in each spike train and compared the timing across different presentation conditions. I found that the timing of the first bursts only differed during  $45^\circ$  presentations in complex backgrounds during flight, when compared to non-flying locusts presented with the same trajectory (Kruskal-Wallis One Way ANOVA on Ranks,  $N=17$ ,  $N=11$ ,  $P<0.05$ ). I then investigated the potential relationship between the timing of the onset of the rise phase and the onset of asymmetry. I found medium correlations for within simple backgrounds for  $0^\circ$  and  $45^\circ$  presentations ( $N=12$ ,  $N=11$ ,  $\rho=0.64$ ,  $\rho=0.59$ ), ( $N=11$ ,  $N=8$ ,  $\rho=0.18$ ,  $\rho=0.22$ ).

## **4.4 DCMD BURSTING, MUSCLE ACTIVITY AND WING ASYMMETRY**

I examined the temporal relationships between all measured events across all presentation conditions. During flight, there was no effect on the median timing of first bursts from changes in background complexity or object trajectory (Kruskal-Wallis One Way ANOVA on Ranks,

N=21, N=19, N=19, N=16) occurring at median times (-0.715s, -0.773s, -0.788s, and -0.770s respectively before TOC). Furthermore, I found that the timing of the first bursts occurred consistently, and as the first event in a series of sequential neural and muscle events, that eventually lead to forewing asymmetry (Fig.3.9). I constructed a timeline based on the timings of each neural, muscles, and wing asymmetry event, in each presentation condition. I found that after an average of 72.4ms following the first burst, bilateral forewing flight muscle synchrony occurred across 0° and 45° trajectories within simple and complex backgrounds (-0.673s, -0.700s, -0.680s, -0.703s, before TOC). Rapidly, within 66 ms of flight muscle synchrony, forewing latency increased (-0.517s, -0.628s, -0.616, -0.630, before TOC), eliciting forewing asymmetry 205ms later (-0.410s, -0.492s, -0.367, -0.300), before TOC). Neither background complexity nor object trajectory affected the timings of these events. Once the order of events were established, I analyzed for potential temporal correlations in neural timing (timing of first burst), flight muscle activity changes (timing of flight muscle synchrony and latency) and the initiation of wing asymmetry. I found strong correlations in sequence, between neural and muscle events, and the initiation of wing asymmetry. Moreover, I found strong correlations between the timing of first bursts, and the initiation of wing asymmetry (Table 3.1). These correlations were held regardless of object trajectory or background complexity (Fig. 3.10). Firstly, the timing of first bursts correlated strongly with the timing flight muscle synchrony. In turn, flight muscle synchrony was strongly correlated with flight muscle latency. Lastly, flight muscle latency was strongly correlated with the initiation of forewing asymmetry (Table 3.1). Moreover, the timing of first bust correlated strongly with the onset of forewing asymmetry (gray shaded graphs, Fig. 3.10).

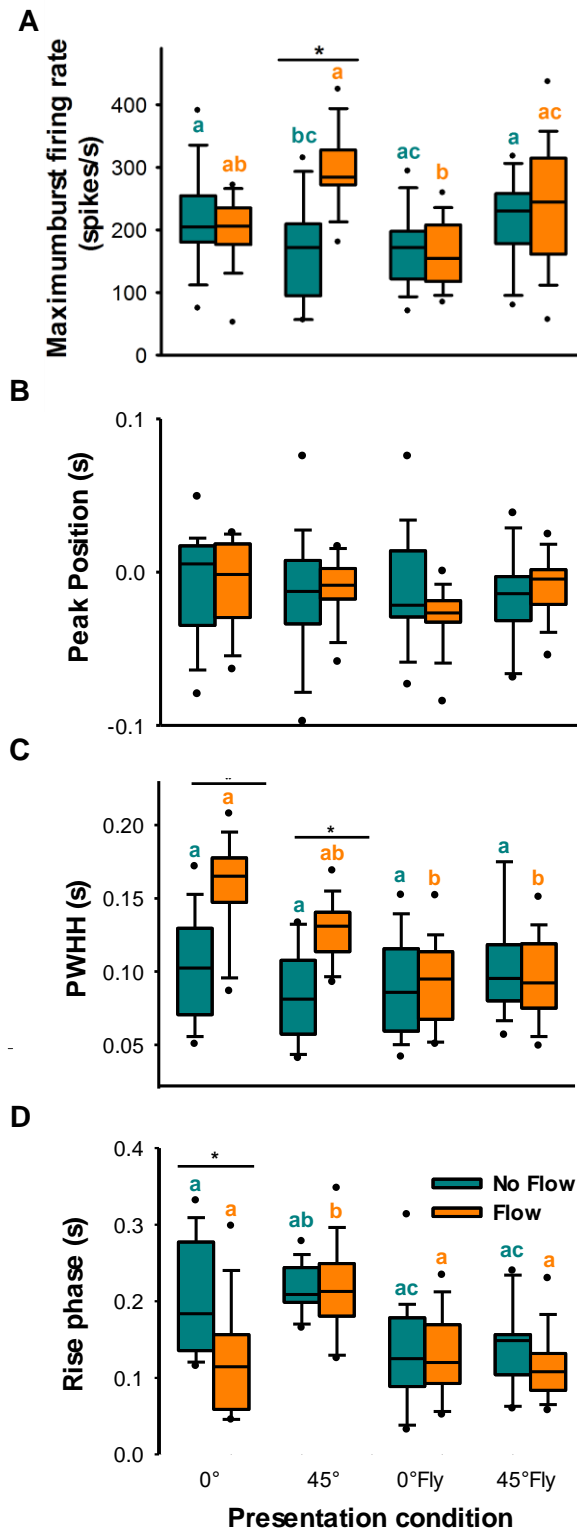




**Figure 3.8: Effects of stimulus trajectory, flight status, and background on DCMD burst parameters.** A) Comparisons of peak burst firing. B) Comparisons of the timing of peak position relative to TOC (0.0s). C) Comparisons of peak width at half height. D) Comparisons of rise phase. Boxplots show the median, 25th, and 75th percentiles, whiskers represent the 5th and 95th percentiles, and small filled circles represent outliers. Results are grouped into non-flying and flying groups (NF and F) and further separated within those groups by the direction of the looming stimulus ( $0^\circ$  and  $45^\circ$ ). The presence or absence of flow field is indicated by Cyan (no flow field) or orange (with flow field) coloured boxes. Black bars with dashes indicate significant differences within the trajectory groups. Boxes that share letters of the same colour do not differ significantly from each other.

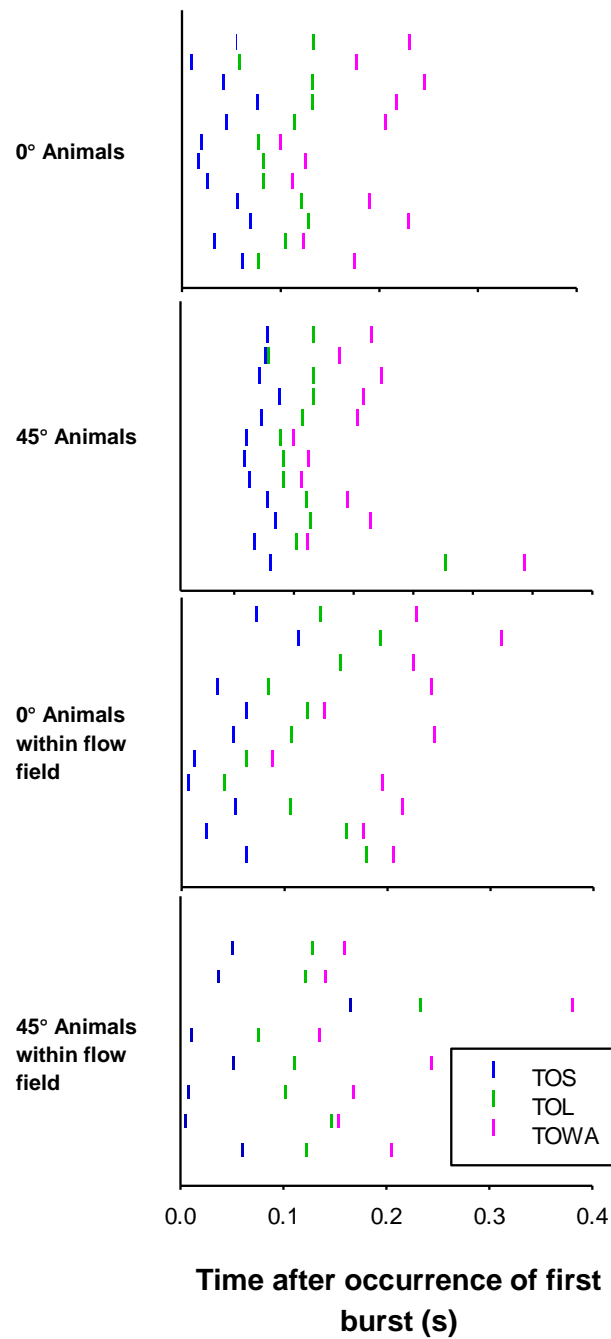


**Figure 3.9: Relative timing of DCMD bursting, flight muscle synchrony and latency, and behaviour during different presentation conditions.** Raster's show time of synchrony (TOS) and time of latency (TOL) of left and right m97 flight muscles, and time of wing asymmetry (TOWA) in reference to timing of the first burst of the DCMD (0.0s). Each line (left to right) represents data from one locust, and each muscle and behavioural event is coloured differently within each animal, TOS (blue), TOL (green) and TOWA (pink).

**Table 3.1: Neural, muscle, and wing asymmetry timing (PPM) correlations**

<b>Pearson Correlation</b>	<b>0 Fly (N=12)</b>	<b>45 Fly (N=11)</b>	<b>0 Flow Fly (N=11)</b>	<b>45 Flow Fly (N=8)</b>
TOFB VS TOS	0.99, P<0.05	0.97, P<.001	0.98, P<.001	0.97, P<.001
TOFB VS TOL	0.96, P<.001	0.98, P<.001	0.99, P<.001	0.99, P<.001
TOFB VS TOWA	0.96, P<.001	0.89, P<.001	0.99, P<.001	0.98, P<.001
TOS VS TOL	0.96, P<.001	0.98, P<.001	0.99, P<.001	0.97, P<.001
TOS VS TOWA	0.97, P<.001	0.86, P<.001	0.99, P<.001	0.97, P<.001
TOL VS TOWA	0.98, P<.001	0.90, P<.001	0.98, P<.001	0.99, P<.001

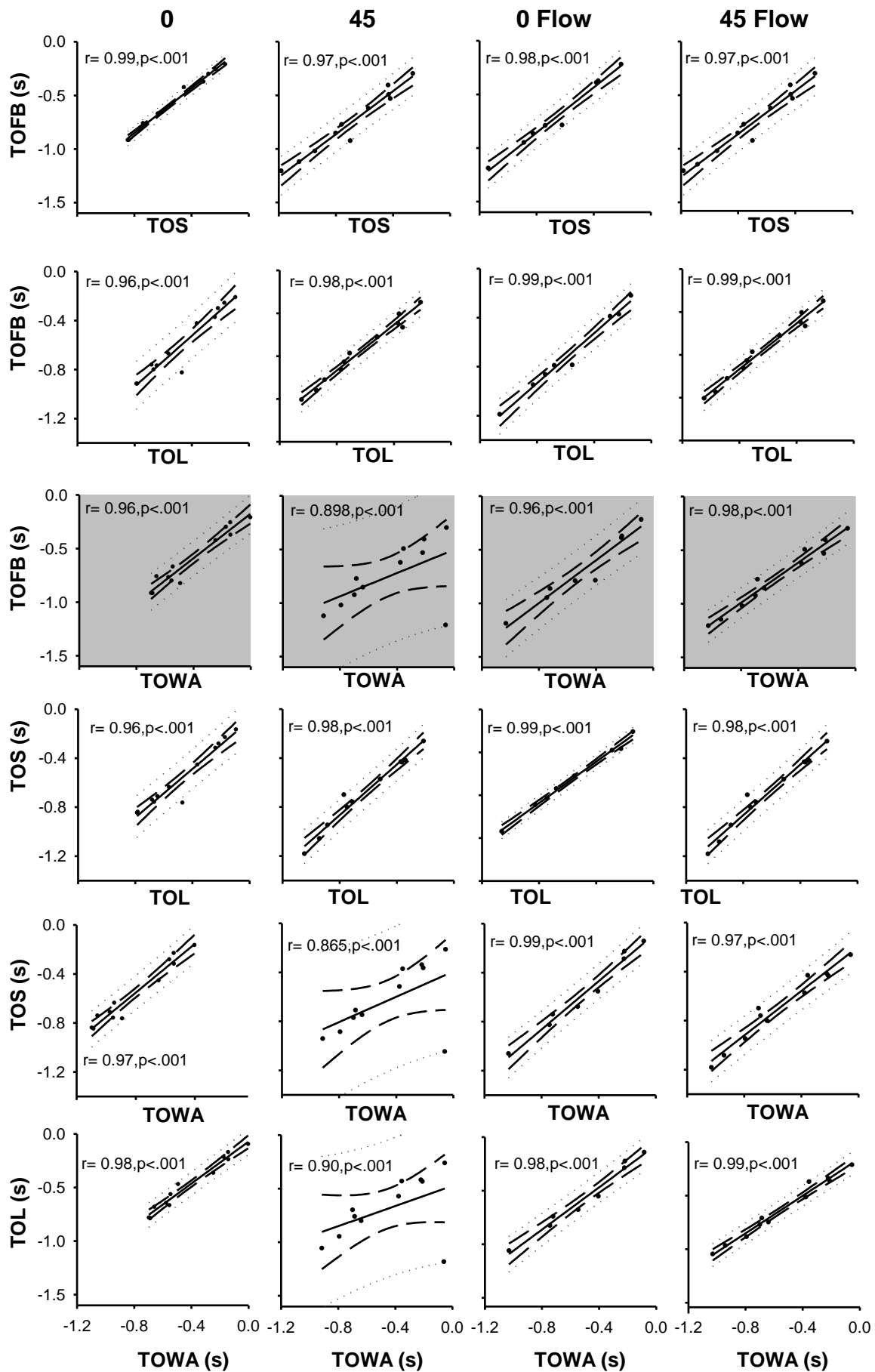


**Figure 3.10: Correlations between DCMD events, muscle events and wing asymmetry timings under varying presentation conditions.** Graphs show linear regressions trend lines. Long dashed lines represent the 95% confidence interval of the regression line. Dotted lines represent the 95% confidence interval of the population. Dots closely grouped to the line and within the regression line 95% confidence interval represent a stronger correlation. Pearson correlation coefficient values ( $\rho$ ) are presented on each graph with their corresponding p-values. Graphs highlighted in grey, show the strongest correlations in each presentation condition of timing of first burst and timing of wing asymmetry.

### 3.5 DISCUSSION

I sought out to investigate the relationships between neural coding, flight muscle coordination and the onset of wing asymmetry responsible for turning behaviour. To accomplish this, I utilized well established techniques in electrophysiology and behaviour, within a highly controlled experimental paradigm. I chose the DCMD as a potential neural correlate, because of its established and predictable responses to stimuli that elicit collision avoidance behaviour. Former studies using a rigid tether set up (Hedwig and Becher, 1998; Robertson and Reye, 1992; Robertson and Johnson, 1993; Gray et al., 2001; Santer et al., 2005; Santer et al., 2006; Simmons et al., 2010; Ribak et al., 2012), have successfully recorded from the DCMD whilst exposing locusts to various controlled stimuli. These have established a characteristic DCMD response of increasing firing rate as an object approaches on a collision with the locust. Further investigations into the role of the DCMD in collision avoidance behaviour have examined flight muscle activity during the elicitation of gliding collision avoidance behaviour (Santer et al., 2005, Chapter 2) and flexor and extensor muscles that are involved in jumping collision avoidance behaviour (Fotowat and Gabbiani, 2007). High bursting frequency in the DCMD, and the forewing elevator flight muscle M84, have been implicated in evoking gliding behaviour (Santer et al., 2005), whereas DCMD thresholds of 50 spikes/s have been shown to elicit preparatory stages of locust jumping behaviours (Fotowat and Gabbiani, 2005). Recordings of DCMD, flight muscle activity, and behavioural output (wing asymmetry) had yet to be recorded within a single animal during intentional flight steering. Recording from an actively behaving animal introduces many challenges. The selection of a rigid tether, although less naturalistic than free flight or a loose tether, was necessary to gain reliable signals from the locust during flight-like behaviour. My use of a rigid tether enabled successful recordings and behavioural results comparable to former studies that used both rigid and loose tethers.

In loosely tethered locusts, it has been postulated that glides are a last ditch effort that occur prior to turns (Chan and Gabbiani, 2013a; Santer et al., 2005a), although results from (McMillan et al., 2013) and Chapter 2, have shown that glides not only occur singularly, but also at a similar time to turns. In my study, higher burst firing rate did not result in higher occurrences of glides, as was suggested previously (Simmons and Rind 1992; Simmons and Rind 1997; Santer et al., 2005). However, intraburst firing rates between 30 spikes/s and 45 spikes/s

(occurring at the start of the rise phase) did show medium correlations to wing asymmetry. This may confirm the relationship of a firing rate threshold and the initiation of behaviours, as seen in locust jumping behaviours (Fotowat and Gabbiani, 2005). More similar to loosely tethered locusts (Chan and Gabbiani, 2013a; McMillan et al., 2013), despite the presence of gliding and stopping behaviours in response to my looming stimuli, turns occurred at the highest frequency regardless of increases in background complexity or object trajectories. Preference for turning behaviour has been demonstrated before (Chan and Gabbiani, 2013; McMillan et al., 2013), and emulates behavioural responses in previous loosely tethered experiments (Chan and Gabbiani, 2013; McMillan et al., 2013). Moreover, the frequencies of glides and stops fluctuated in response to changes in background complexity and object trajectory, whereas stops occurred later (-0.466s) than previous findings in loosely tethered locusts (-0.600s, McMillan et al., 2013), and earlier than found in Chapter 2 (-0.238s). In agreement with McMillan et al. (2013), glides were consistently the earliest occurring behaviour, although glides that occurred were singular and not followed by turns as previously reported by (Chan and Gabbiani, 2013a). Interestingly, locusts showed a higher preference for glides during 45° trajectories in the presence of complex backgrounds. This could allude to a combinative effect of trajectory and background complexity on gliding preference. Concomitantly, stop frequency increased considerably for both 0° and 45° trajectories when the background complexity was increased, suggesting that non-turn behaviours may be a more effective strategy within more complex environments. Furthermore, increased preference for stopping in complex backgrounds may be a result of the optic flow of the flow field, making a rapid drop in altitude appear more viable during avoidance. The timing of turns did not differ from stops, although, like stops in this experiment, turns occurred later than previously seen (-0.416s) (McMillan et al., 2013).

With the exception of the access point on the thorax to the ventral nerve cord, my preparation for extracellular recordings, emulated previous methods for recording DCMD signals. (Dick et al., 2017b; Fotowat and Gabbiani, 2007; McMillan and Gray, 2015; Santer et al., 2006; Yakubowski et al., 2016). Although not normally present in extracellular recording experiments of the DCMD, wind stimulation to the head was absent in my study. Despite this, locusts were capable of initiating and sustaining flight in the absence of wind, although the absence of feedback from wind detectors could have presented potential confounds during flight in comparison to previous loosely tethered preparations utilizing wind. The responses of the

DCMD to looming objects in my study showed characteristic increasing firing rate, with peak positions near TOC (Schlotterer 1977; Rind and Simmons 1992; Gabbiani et al. 1999; Gray et al. 2001).

I focused specifically on DCMD bursting in this study, and although studies have shown that bursting is involved in sensory processing (Lisman, 1997; Brenner et al., 2000) and also in encoding behaviourally relevant stimuli (Guido et al., 1995; Lesica and Stanley, 2004; Oswald et al., 2004; Marsat and Pollack, 2006; Eyherabide et al., 2008; Sabourin and Pollack, 2009), only one study has rigorously investigated bursting in this locust visual pathway (McMillan and Gray, 2015). The bursting responses and parameters shown here are consistent with those reported earlier (McMillan and Gray, 2015), which found a temporal code of bursts within the DCMD response that coincided with wing beat frequencies of the forewings (20-25 Hz) (Robertson and Johnson, 1993; McMillan et al., 2013). Moreover, burst frequencies increased with edge expansion of looming objects (McMillan and Gray, 2015), alluding to the involvement of bursting in coding properties of a looming object. When isolating spikes associated with bursts, intraburst firing rates emulated characteristic DCMD firing rates, whereas isolated spikes not associated with bursts did not (as seen in Fig 3.7). This bolsters previous findings that suggest that information of looming stimuli is reliably carried within bursts (McMillan and Gray, 2015). Moreover, the DCMD demonstrates multiplexing, which is likely responsible for initiating avoidance jump responses based on DCMD properties (firing rate threshold, peak firing time, and spike count) (Fotowat et al., 2011). It has also been suggested that multiplexing is involved with burst rate, detecting object approaches within behaviorally relevant time frames, and furthermore, detect changes in object velocity using intraburst firing rate (McMillan and Gray, 2015). Therefore, I focused on intraburst firing rates when looking at temporal properties, and rate properties of DCMD bursts when exposed to increases in background complexity, different object trajectories, and flight.

#### *Effect of Background Complexity:*

Flow fields can be used to simulate forward motion by providing a translating environment similar to what a locust would be exposed to in a free flying environment. Optic flow is used to stabilize flight in birds (Ros and Biewener, 2016) and ensure collision free



navigation in flies (Serres and Ruffier, 2017). Previous studies, using flow fields presented to a locust, used vertical bars that moved outwards in the azimuthal plane from the apex of the flight simulator dome (Silva et al., 2014; Yakubowski et al., 2016). The flow field used here imitated a horizon, and presented concentric circles emanating from the center of the dome downwards, leaving the top half of the dome white. Although differing in properties and presentation, both former and current flow fields simulated forward motion and increased the complexity of the background. DCMD responses associated with increased background complexity have been shown to be modulated when responding to looming objects (Silva et al., 2014; Yakubowski et al., 2016). Although burst firing rates were not analyzed in the previous studies, DCMD maximum firing rates during  $0^\circ$  trajectories were found to decrease and occur later, relative to TOC (Silva et al., 2015). Furthermore, non-flying DCMD responses showed no differences in maximum firing rate or peak position for  $0^\circ$  trajectories. Despite having no effect on peak position,  $45^\circ$  trajectories in my study evoked the opposite trend in firing rate, having significantly higher maximum firing rates. This was also reflected in peak burst firing rates in response to  $45^\circ$  trajectories. Differences from the former studies could largely be due to the differing trajectory choices, and the absence of translation or compound looms. Moreover, my study utilized a spherical object and a flow field with a more realistic optic flow pattern. My results show that burst firing rate is modulated by the presence of optic flow, and that within complex backgrounds trajectory changes modulate the maximum firing rate of bursts. Moreover, I saw that flow fields modulate the widths of peaks during changing trajectories, creating longer response profiles, more so for head on looms. Furthermore, rise phase was highly modulated, in both flying and non-flying paradigms for head on looms, regardless of flight. These changes were unaffected by the presence or absence of flight, representing a potential hierarchy of responses regardless of sensory feedback from the wings.

#### *Effect of flight on a looming sensitive neuron*

Due to the sensitivity of electrodes to vibrational and electrical noise, neuronal recordings are often conducted in the absence of movement. This can leave many questions unanswered in regard to how the neurons respond during naturalistic behaviours, when mechanosensory feedback is present. We know that during behavioural experiments when the locust is free to fly, locusts respond to looming stimuli by evoking collision avoidance behaviours such as stopping,

gliding, or turning towards or away from the object (Chan and Gabbiani, 2013a; McMillan et al., 2013; Ribak et al., 2012). Furthermore, the central pattern generators, active in the thoracic ganglia during flight, maintain a consistent rhythmic output to the wings. The flight rhythm outputs mechanosensory feedback which likely modulates incoming information from the CNS to successfully evoke collision avoidance behaviour. Mechanosensory feedback loops are vital to heading control and flight stability in flies (Lehmann and Bartussek, 2017) and attenuation of thorax body orientation for stable flight posture in moths (Dickerson et al., 2017). Compared to rigidly tethered non-flying locust (Fotowat and Gabbiani, 2011; Guest and Gray, 2005; McMillan and Gray, 2015; Santer et al., 2005b; Stott et al., 2018), inputs from looming sensitive neurons are likely modulated by efference copies sent to the CNS regarding the flight phases and wing positions. Although the locusts used here were on a rigid tether, they were capable of full wing motion, simulating regular wing beating patterns, and maintaining average wing beats frequencies of 19hz, within the range of normal previously loosely tethered studies (Chan and Gabbiani, 2013b; McMillan et al., 2013). Furthermore, during wing beating, clear EMG's from the right and left forewing flight muscles m97 were recorded. Flight introduced considerable vibrational and physiological noise into neuronal recordings. Vibrations stemmed from the motion of the wings beating, whereas the physiological noise originated from high amplitude, longer duration spikes of the flight muscles. High pass filtering, similar to that conducted by Santer (Santer et al., 2005a), was able to extract discernable DCMD spikes.

Although my focus was on burst firing rate responses, DCMD parameters were also found be affected by flight. I found that non-flying animals showed higher DCMD firing rates (200-220 spikes/s) than flying animals (150-180 spikes/s) (Kruskal-Wallis One Way ANOVA on Ranks,  $N=21$ ,  $N=19$ ,  $N=19$ ,  $N=16$   $P<0.05$ ). Non-flying animals showed similar peak firing rates to previous studies (Santer et al., 2005b; Simmons et al., 2010). This suggests that mechanosensory feedback may downregulate the firing rate of the DCMD during collision avoidance responses. It should be noted that former studies used slightly different approach parameters vectors ( $l/|v|$ ) for their stimuli, which were lower or higher than my study (23.3 ms) or differing trajectory (e.g 90° lateral). These could account for subtle difference in firing rate responses. It is interesting to note that for burst firing rates, although no affect was seen during approaches 0° looms, approaches from 45° showed a reverse effect with an increase in burst firing rate during flight. This alludes to how burst firing rate may gate information differently

and characterize differences in object trajectory via upregulation during flight. It has been shown, in the absence of a flow field, that the timing of peak position is little effected by stimulus changes. I found that both DCMD and DCMD bursts show no significant changes in peak position, and furthermore, I observed no relationship between timing of wing asymmetry and peak position timing. This suggests that peak position plays a negligible role in characterizing collision avoidance behaviour. For peak width at half height, I observed a combinative effect of background complexity and flight. DCMD peak widths were shorter for 45° trajectory responses during flight ( $H_3=57.5$ ,  $N=19$ ,  $P<0.05$ ) whereas burst peak widths were greater for both 0° and 45° against a complex background when the locust wasn't flying. However, there is no effect of background complexity. Furthermore, 0° trajectories showed thinner peak widths within complex backgrounds during flight. There may be an interplay between optic flow feedback and mechanosensory feedback from the wings. Furthermore, within complex backgrounds 45° trajectories evoked shorter burst rise phases during flight, indicating an increase in activity over shorter periods of time, causing a more fine-tuned response.

#### *The role of the DCMD in the coordination of flight steering*

The DCMD plays a role in the elicitation of gliding collision avoidance behaviour, through high frequency EPSPs onto the MN84 (Santer et al., 2005b). Similar to what has been observed in jumping collision avoidance behaviour, the position of peak firing rate does not seem to influence the motor system during collision avoidance behaviour (Fotowat and Gabbiani, 2007), and temporally, peak firing occurs after collision avoidance behaviors have been initiated. Although DCMD response parameters may represent a screenshot of what a response to a particular stimulus looks like, peak width at half height and rise phase are the only parameters that occur in a time frame that encompasses the initiation of a behaviour. If we want to predict the behavioural output, it is important to study parameters that occur in a behaviourally relevant time frame.

Compared to bilateral flight muscle synchrony timing found in Chapter 2, synchronization times occurred ~70ms earlier, but showed no effect of trajectory direction. However, with increasing azimuthal angle of trajectories (0°→45°→90°), the timings of bilateral flight muscle latency occurred later in reference to TOC. Despite this effect, latencies occurred within the range of previous studies [~400ms-600ms before TOC, (McMillan et al, 2013; Chan

and Gabbiani, 2013)]. Concomitantly, the timing of forewing asymmetry occurred within the time frame of previously measured values of loosely tethered set ups (McMillan et al., 2013).

The DCMD has a strong association with avoidance behaviour, although it has not been shown to be required to trigger behavioural responses, e.g. triggering hindleg flexion in locusts during jumping avoidance responses (Fotowat and Gabbiani, 2007). The coactivation of muscles involved in jump phases is a relatively time consuming processes, and has been shown to occur around the same time as peak DCMD position (Hatsopoulos et al., 1995). Despite this, jumping phases do not have a fixed delay between jump phases and DCMD peak firing (Fotowat and Gabbiani, 2007). A later study found correlations between flexion timing and the occurrence of high frequency DCMD spikes, postulating that rapid increases in firing rate-initiated leg flexion (Santer et al., 2008). Concomitantly, my study yielded no direct connection between behaviours and timing of DCMD peaks. However, similar to previously studies, I found that the start of the rise phase of the DCMD peaks showed medium correlations with the initiation of wing asymmetry regardless of object trajectory or background complexity. This relationship appears plausible in reference to previous work done on the relationship between the DCMD and initiation of motor outputs associated with behaviours. The temporal changes in rise phase could play an important neuronal role in how turning is initiated.

I have discovered a temporal DCMD burst event that occurs within a behaviourally relevant time frame, prior to the onset of both muscle activity changes and the output of collision avoidance behaviour. The timing of the first burst in a DCMD spike train may be a catalyst that begins the cascade of muscle activity changes, and the creation of wing asymmetry. First bursts are strongly correlated with increases in wing asymmetry associated with turns, and moreover, first bursts are correlated with timings of forewing flight muscle synchrony and latency. Each event is strongly correlated in sequence and represents collision avoidance from the level of the neuron to the level of behaviour. Although many properties and events are comparable to what I found in Chapter 2, the necessary next step is to conduct neuronal recordings while the locust is flying loosely tethered, and in a closed loop system. The importance of the effect of mechanosensory feedback, and real time dynamic changes in the visual environment are essential to more naturalistic collision avoidance responses during flight. Furthermore, the importance of temporal coding is clear, inferring that temporal relationships between single

neurons, populations of neurons, and behavioural outputs deserve more in-depth investigation, and would greatly increase our knowledge of the neuronal control of behaviour.

## CHAPTER 4. GENERAL DISCUSSION

### 4.1 FLIGHT MUSCLE COORDINATION IN COLLISION AVOIDANCE BEHAVIOR

This thesis addresses three major questions regarding the neuronal control and coordination of flight steering during collision behavior. Firstly, how are flight muscles coordinated to influence body orientation changes during intentional flight steering during collision avoidance behaviour? Secondly, what role does the looming sensitive neuron, DCMD, play in coordination of flight muscles, and production of wing asymmetry. Thirdly, how does putative mechanosensory feedback from the wings modulate the properties of looming sensitive neurons involved in collision avoidance behaviour?

Findings from Chapter 2 revealed pivotal muscle activity events that occurred in sequence to coordinate flight muscles to produce turns. Locusts responded robustly to lateral looming stimuli, and produced turns away from the looming object, both singularly or in sequences of behaviours. The behavioural responses I report coincide with previous work (McMillan et al., 2013, Chan and Gabbiani, 2013), and confirmed the potential existence of a hierarchy of collision avoidance behaviour type (stops, glides, or turns). Despite this, more diverse stimuli are required to test this behavioural hierarchy. Singular turn behaviours involved important relationships between two muscle activity events, (ipsilateral side of the turning direction and bilateral flight muscle synchronization, and left-right forewing flight muscle latency) and pitch and roll body orientation changes. The importance of forewing latency to the initiation of turns agreed with previous findings involving loosely tethered experiments (McMillan et al., 2013, Chan and Gabbiani, 2013). Furthermore, the importance of forewing flight muscle synchrony and latency was also seen in rigid tether experiments in chapter 3. I suggest that due to the strong correlation between flight muscle synchrony and forewing latency, the synchronization of the flight muscles is likely a preparatory stage, initiating further downstream muscle activity changes and body orientation changes. The speed of coordination of these events alludes to the impressive efficiency of flight muscle coordination in initiating complex turns in comparison to the high energy requirements in birds (Biewener, 2011) and bats (Hedenström and Johansson, 2015)

The absence of correlations between flight muscle synchrony and changes in yaw orientations, suggests that more neurons are involved in influencing body orientation changes, as the presence of other looming sensitive neurons active during collision avoidance behaviour have been shown (Dick et al., 2017b). Furthermore, since both ipsilateral and bilateral flight muscle synchrony, and latency are strongly correlated with pitch and roll body orientation changes, these muscle events must have neural correlates that initiate the sequence of events that lead to collision avoidance behaviour.

In Chapter 3, I aimed to elucidate a neural correlate to collision avoidance behaviour. In invertebrates, neural correlates have been found that are responsible for feeding behaviour in flies (Sun et al., 2014), and navigation behaviour in dung beetles (el Jundi et al., 2015). Although only a handful of studies have attempted to connect neural activity with behavioural output within the same animal. The DCMD is a likely candidate for involvement in flight muscle coordination, given its robust responses to stimuli that trigger collision avoidance behaviours. Furthermore, although other neurons are likely involved, the DCMD likely effects other suites of flight muscles beyond what I tested.

The bursting response parameters of the DCMD changed dynamically in response to differing looming object trajectories and increases in background trajectory. This further reinforces that DCMD bursting not only encodes properties of looming stimuli, but also changes in visual environment complexity. I observed a tentative temporal relationship between burst rise phase and the initiation of wing asymmetry. Given the early average timing of rise phase initiations within a collision avoidance response, this could contribute to the execution or maintenance of behaviours. This also reinforces previous findings that certain spike thresholds may exist, that when surpassed, initiate specific behaviours (Santer, 2006). Rate codes contribute greatly to the output of behaviour, although in my study, I was able to connect activity of a single neuron to turning behaviour through a temporal code. The timing of first bursts represents a neural correlate to muscle activity changes and turning collision avoidance behaviour. It is the first indicator event in the sequence of neural, muscle and behavioural output, and correlates with each muscle and behavioural event. These data infer that the temporal arrival of DCMD bursts coordinates flight muscles activity and the initiation of wing asymmetry that leads to a turn in response to a looming stimulus.

## **4.2 THE EFFECT OF BEHAVIOUR ON THE SENSORY SYSTEM**

Sensory motor integration shapes active locomotion in zebra fish larva (Yang et al., 2016) and modulates flight posture stabilization in moths (Dickerson et al., 2014) and likely plays an important role in naturalistic flight behaviours in locusts. In my experimental paradigm, I was able to assess the effect of DCMD responses to mechanosensory feedback from the wings during flight. The thoracic ganglia are often referred to as the black boxes of the locust nervous system, modulating ingoing and outgoing signals from the CNS and motor systems. Sensory motor integration takes place in the presence of mechanosensory feedback from the wings and modulates signals destined for the motor system. This feedback may have affected responses of the DCMD to looming and, therefore flight effects may more accurately represent a natural environment and should be integrated into future experiments. I found that during flight, firing rates of both the DCMD and DCMD bursts were downregulated and peak widths shortened in the absence of visual complexity. When visual complexity increased, peak heights remained unchanged, but peak widths were wider and rise phases were longer. This suggests that sensory motor integration in the thoracic ganglia may modulate signals from the DCMD in a context dependent manner, representing a potential hierarchy of information that is carried through to motor output. Furthermore, the DCMD response appears to be finely tuned after modulation from feedback, meaning that information for muscle coordination is gated differently during flight. Fine tuning a response for more accurate behaviour execution is utilized across species, from human dexterity (Ackerley et al., 2016) to adaptive filtering in electric fish (Ackerley et al., 2016). Therefore, sensory motor integration is an integral part of the neuronal control of behaviour.

## **4.3 FUTURE DIRECTIONS**

While we know that the DCMD plays an important role in collision avoidance, it also likely effects more muscles than were included in this study. Investigating DCMD activity with larger groups of muscles may elucidate a larger role it plays in collision avoidance behaviour. Furthermore, the DCMD is not the sole contributor to this system. Flight muscle coordination is very likely a result of multiple inputs, contributing both individual rate codes, time codes, and population codes. It has been shown that discrete units of looming sensitive neurons respond to



variations in trajectory in locusts (Dick and Gray, 2015). Neurons within populations can also be ranked by order of arrival, representing a population time code. Multichannel recordings conducted when the locust is in flight could elucidate extremely valuable information regarding the suites of neurons involved in coordinating collision avoidance behaviour. Traditionally with locusts, open loops systems have been used, lacking real time visual feedback from the environment. Closing the loop and using temporal information from flight muscle activity during flight, could be used to change the visual environment of the locust in real time, portraying a more accurate collision avoidance response.

This study demonstrated that: 1) Flight muscles are coordinated through ipsilateral and bilateral synchronization and the creation of forewing asymmetry to initiate turning behaviours. 2) Temporal coding within the arrival of first bursts in the DCMD initiates flight muscle coordination and, in turn, wing asymmetry and 3) Mechanosensory feedback from the flight system modulates DCMD bursting properties. These results provide further insight into the neural control of collision avoidance behaviour, and a snapshot from neuron to behaviour. I have compiled a timeline of neuronal, muscle, and behavioural events that result in a turn during collision avoidance behaviour (Fig. 4.1) These data bring us closer to modeling flight behaviour and generating biological inspired algorithms that can be applied to robotic systems and future addition will bring us closer to understanding the neuronal control of behaviour.

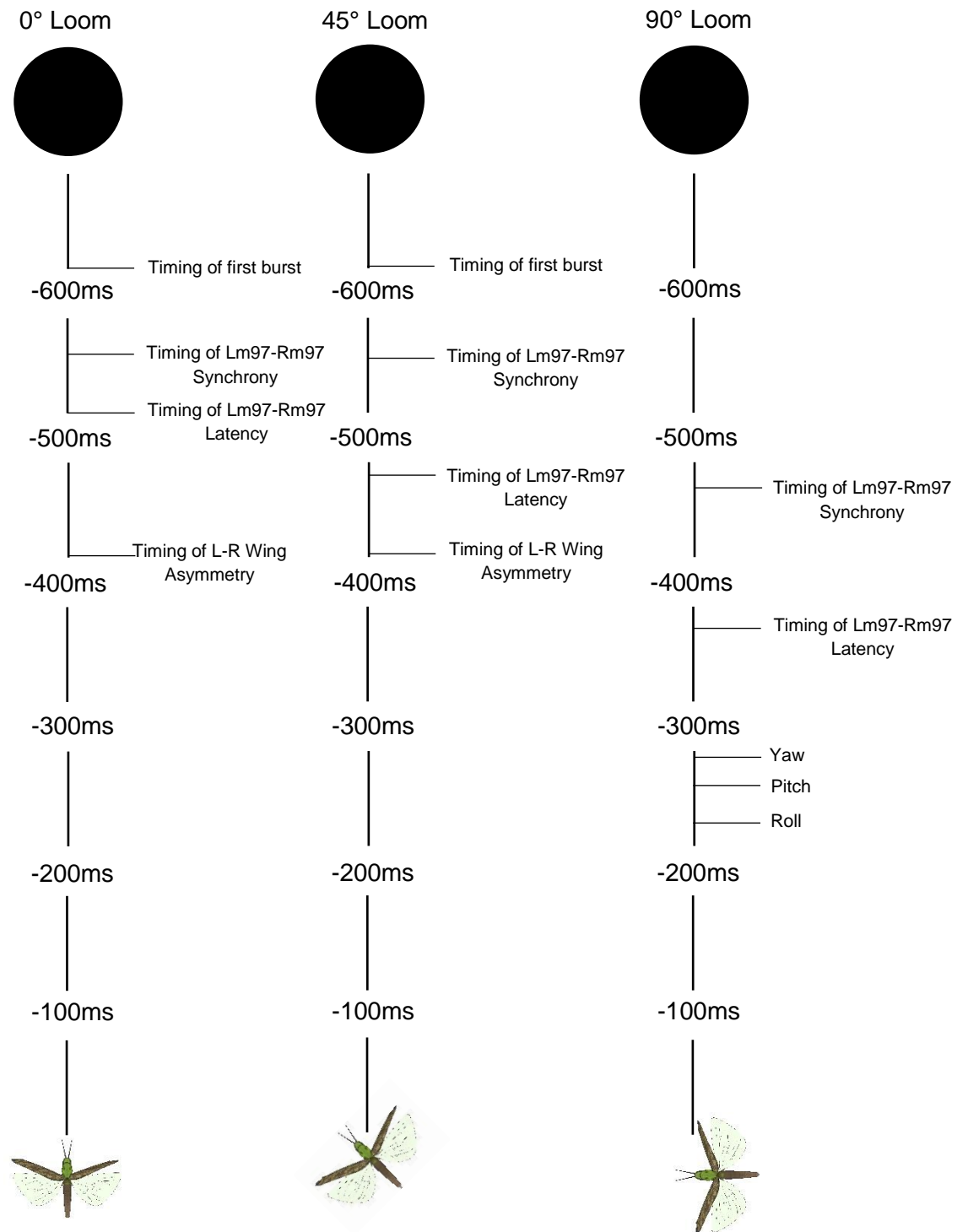


**Figure 4.1: Diagram illustrating the timing of events leading to collision avoidance behaviour for three looming trajectories.** The 90° loom was in a free flying tether prep, 0° and 45° were in a rigid tether flight prep. The black disk represents looming 14cm disks 600 ms before TOC and the black vertical lines represents the timeline from -600 ms to TOC (locust images at bottom of diagram).

## REFERENCES

- Ackerley, R., Borich, M., Oddo, C. M. and Ionta, S.** (2016). Insights and Perspectives on Sensory-Motor Integration and Rehabilitation. *Multisens. Res.* **29**, 607–633.
- Anstey, M. L., Burrows, M., Ott, S. R., Rogers, S. M. and Simpson, S. J.** (2009). Serotonin Mediates Behavioral Gregarization Underlying Swarm Formation in Desert Locusts. *Science* (80-. ). **323**, 627–630.
- Arbas, E. A.** (1986). Control of hindlimb posture by wind-sensitive hairs and antennae during locust flight. *J. Comp. Physiol. A* **159**, 849–857.
- Arshavsky, V. Y., Lamb, T. D. and Pugh, E. N.** (2002). G Proteins and Phototransduction. *Annu. Rev. Physiol.* **64**, 153–187.
- Bass, A. H., Bodnar, D. A. and McKibben, J. R.** (1997). From neurons to behavior: Vocal-acoustic communication in teleost fish. *Biol. Bull.* **192**, 158–163.
- Bässler, U.** (1993). The walking-(and searching-) pattern generator of stick insects, a modular system composed of reflex chains and endogenous oscillators. *Biol. Cybern.* **69**, 305–317.
- Bender, J. A., Pollack, A. J. and Ritzmann, R. E.** (2010). Neural Activity in the Central Complex of the Insect Brain Is Linked to Locomotor Changes. *Curr. Biol.* **20**, 921–926.
- Bernard, E.** (2005). *Dover Books on Aeronautical Engineering*. 1st ed. Dover Publications.
- Berry, R. P., Warrant, E. J. and Stange, G.** (2007). Form vision in the insect dorsal ocelli: An anatomical and optical analysis of the Locust Ocelli. *Vision Res.* **47**, 1382–1393.
- Biewener, A. A.** (2011). Muscle function in avian flight: Achieving power and control. *Philos. Trans. R. Soc. B Biol. Sci.* **366**, 1496–1506.
- Burrows, M.** (1975). Monosynaptic connexions between wing stretch receptors and flight motoneurons of the locust. *J. Exp. Biol.* **62**, 189–219.
- Burrows, M.** (1996). *The neurobiology of an insect brain*. Oxford University Press.
- Cayley, G.** (1809). On Aerial navigation. *J. Nat. Philos. Chem. Arts*.
- Chan, R. W. and Gabbiani, F.** (2013a). Collision-avoidance behaviors of minimally restrained flying locusts to looming stimuli. *J. Exp. Biol.* **216**, 641–655.
- Chan, R. W. and Gabbiani, F.** (2013b). Collision-avoidance behaviors of minimally restrained flying locusts to looming stimuli. *J. Exp. Biol.* **216**, 641–655.
- Chapman, R. F.** (1998). *The Insects: Structure and function*. 5th ed. (ed. Simpson, S. J.) and Douglas, A. E.) Cambridge University Press.

- Cheer, A. Y. L. and Koehl, M. A. R.** (1987). Paddles and Rakes : Fluid Flow Through Bristled Appendages of Small Organisms Department of Mathematics , University of California ,. *J. Theor. Biol.* **129**, 17–39.
- Chin, D. D. and Lentink, D.** (2016). Flapping wing aerodynamics: from insects to vertebrates. *J. Exp. Biol.* **219**, 920–932.
- Cofer, D., Cymbalyuk, G., Heitler, W. J. and Edwards, D. H.** (2010). Neuromechanical simulation of the locust jump. *J. Exp. Biol.* **213**, 1060–1068.
- Cohen, J.** (1988). *Statistical power analysis for the behavioural sciences*. 2nd ed. Lawrence Erlbaum Associates.
- Cohen, A. H. and Wallen, P.** (2004). The neuronal correlate of locomotion in fish. *Exp. Brain Res.* **41**, 11–18.
- Combes, S. A., Salcedo, M. K., Pandit, M. M. and Iwasaki, J. M.** (2013). Capture success and efficiency of dragonflies pursuing different types of prey. *Integr. Comp. Biol.* **53**, 787–798.
- Connors, B. W. and Gutnick, M. J.** (1990). Intrinsic firing patterns of diverse neocortical neurones. *TINS* **13**, 99–104.
- Cooter, R. J. and Baker, P. S.** (1977). Weis-Fogh clap and fling mechanism in *Locusta*. *Nature* **269**, 53–54.
- Dacke, M., Baird, E., Byrne, M., Scholtz, C. H. and Warrant, E. J.** (2013). Dung beetles use the milky way for orientation. *Curr. Biol.* **23**, 298–300.
- Dawson, J. W., Dawson-Scully, D. and Robertson, R. M.** (1997). Forewing asymmetries during auditory avoidance in flying locusts. *J. Exp. Biol.* **200**, 2323–2335.
- Dawson, J. W., Leung, F. H. and Robertson, R. M.** (2004). Acoustic startle/escape reactions in tethered flying locusts: Motor patterns and wing kinematics underlying intentional steering. *J. Comp. Physiol. A Neuroethol. Sensory, Neural, Behav. Physiol.* **190**, 581–600.
- De valois, R. L. and Jacobs, G. H.** (1986). Primate color vision. *Science* (80-. ). **162**, 533–540.
- Deora, T., Singh, A. K. and Sane, S. P.** (2015). Biomechanical basis of wing and haltere coordination in flies. *Proc. Natl. Acad. Sci. U. S. A.* **112**, 1481–1486.
- Dick, P. C. and Gray, J. R.** (2014). Spatiotemporal stimulus properties modulate responses to trajectory changes in a locust looming-sensitive pathway. *J. Neurophysiol.* **111**, 1736–1745.
- Dick, P. C., Michel, N. L. and Gray, J. R.** (2017a). Complex object motion represented by context-dependent correlated activity of visual interneurons. *Physiol. Rep.* **5**, 1–21.
- Dick, P. C., Michel, N. L. and Gray, J. R.** (2017b). Complex object motion represented by context-dependent correlated activity of visual interneurons. *Physiol Rep* **5**, 1–21.
- Dickerson, B. H., Aldworth, Z. N. and Daniel, T. L.** (2014). Control of moth flight posture is mediated by wing mechanosensory feedback. *J. Exp. Biol.* **217**, 2301–2308.

- Dickinson, M. H. and Muijres, F. T.** (2016). The aerodynamics and control of free flight Manoeuvres in *Drosophila*. *Philos. Trans. R. Soc. B Biol. Sci.* **371**,.
- Dickinson, M. H. and Tu, M. S.** (1997). The function of dipteran flight muscle. *Comp. Biochem. Physiol. - A Physiol.* **116**, 223–238.
- Dickinson, M. H., Lehmann, F. O. and Sane, S. P.** (1999a). Wing rotation and the aerodynamic basis of insect flight. *Science* (80-. ). **284**, 1954–1960.
- Dickinson, M. H., Lehmann, F. and Sane, S. P.** (1999b). Wing rotation and the aerodynamic basis of flight. *Science* (80-. ). **284**, 1954–1960.
- Dipoppa, M., Ranson, A., Krumin, M., Pachitariu, M., Carandini, M. and Harris, K. D.** (2018). Vision and Locomotion Shape the Interactions between Neuron Types in Mouse Visual Cortex. *Neuron* **98**, 602-615.e8.
- Dong, D., Jones, G. and Zhang, S.** (2009). Dynamic evolution of bitter taste receptor genes in vertebrates. *BMC Evol. Biol.* **9**, 1–9.
- Dudchenko, P. A. and Wallace, D.** (2018). Neuroethology of spatial cognition. *Curr. Biol.* **28**, R988–R992.
- Dudley, R.** (2000). *The Biomechanics of Insect Flight*. Princeton: Princeton University Press.
- Dugard, J. J.** (1967). Directional change in flying locusts. *J. Insect Physiol.* **13**, 1055–1063.
- el Jundi, B., Warrant, E. J., Byrne, M. J., Khaldy, L., Baird, E., Smolka, J. and Dacke, M.** (2015). Neural coding underlying the cue preference for celestial orientation. *Proc. Natl. Acad. Sci.* **112**, 11395–11400.
- Ellington, C. P.** (1985). Power and efficiency of insect flight muscle. *J. Exp. Biol.* **115**, 293–304.
- Ellington, C. P., den Berg, C. Van and Willmott, A. P.** (1996). Leading-edge vortices in insect flight. *Lett. to Nat.* **384**, 626–630.
- Erber, J.** (1985). Response characteristics and after effects of multimodal neurons in the mushroom body area of the honey bee. **53**, 423–426.
- Eyherabide, H. G., Rokem, A., Herz, A. V. M. and Samengo, I.** (2008). Burst firing is a neural code in an insect auditory system. *Front. Comput. Neurosci.* **2**,.
- Flanders, M.** (2011). What is the biological basis of sensorimotor integration? *Biol. Cybern.* **104**, 1–8.
- Fotowat, H. and Gabbiani, F.** (2007). Relationship between the Phases of Sensory and Motor Activity during a Looming-Evoked Multistage Escape Behavior. *J. Neurosci.* **27**, 10047–10059.
- Fotowat, H. and Gabbiani, F.** (2011). Collision Detection as a Model for Sensory-Motor Integration. *Annu. Rev. Neurosci.* **34**, 1–19.

- Gabbiani, F. and Krapp, H. G.** (2006). Spike-Frequency Adaptation and Intrinsic Properties of an Identified, Looming-Sensitive Neuron. *J. Neurophysiol.* **96**, 2951–2962.
- Gabbiani, F., Metzner, W., Wessel, R. and Koch, C.** (1996). From stimulus encoding to feature extraction in weakly electric fish. *Nature* **564–567**,.
- Gabbiani, F., Krapp, H. G. and Laurent, G.** (1999). Computation of object approach by a wide-field, motion-sensitive neuron. *J. Neurosci.* **19**, 1122–41.
- Gabbiani, F., Mo, C. and Laurent, G.** (2001). Invariance of Angular Threshold Computation in a Wide-Field Looming-Sensitive Neuron. *J. Neurosci.* **21**, 314–329.
- Gabbiani, F., Krapp, H. G., Koch, C. and Laurent, G.** (2002). Multiplicative computation in a visual neuron sensitive to looming - Supplementary Material. *Nature* **420**, 320–324.
- Gaten, E., Huston, S. J., Dowse, H. B. and Matheson, T.** (2012). Solitary and gregarious locusts differ in circadian rhythmicity of a visual output neuron. *J. Biol. Rhythms* **27**, 196–205.
- Genzel, D., Yovel, Y. and Yartsev, M. M.** (2018). Neuroethology of bat navigation. *Curr. Biol.* **28**, R997–R1004.
- Gewecke, M. and Phillippen, J.** (1978). Control of the horizontal flight-course by air-current sense organs in *Locusta migratoria*. *Physiol. Entomol.* **3**, 43–52.
- Gibson, J.** (1979). The Ecological approach to visual perception.
- Glantz, R. M.** (1974). Visually Evoked Defense Reflex of the crayfish: Habituation, facilitation, and the influence of picrotoxin. *Dev. Biol.*
- Gray, J. R., Blicow, E. and Robertson, R. M.** (2010). A pair of motion-sensitive neurons in the locust encode approaches of a looming object. *J. Comp. Physiol. A Neuroethol. Sensory, Neural, Behav. Physiol.* **196**, 927–938.
- Grillner, S.** (1981). Control of locomotion in bipeds, tetrapods, and fish. *Handbook of Physiol. Nerv. Syst. II* 1179–1236.
- Guest, B. B. and Gray, J. R.** (2005). Responses of a Looming-Sensitive Neuron to Compound and Paired Object Approaches. *J. Neurophysiol.* **95**, 1428–1441.
- Guest, B. B. and Gray, J. R.** (2006). Responses of a Looming-Sensitive Neuron to Compound and Paired Object Approaches. *J. Neurophysiol.* **95**, 1428–1441.
- Guo, X., Ma, Z. and Kang, L.** (2013). Serotonin enhances solitariness in phase transition of the migratory locust. *Front. Behav. Neurosci.* **7**, 1–12.
- Guthrie, B. D. M.** (1964). Observations on the nervous system of the flight apparatus in the locust *Schistocerca gregaria*. *Quart. J. micr. Sci* **105**, 183–201.
- Harris-Warrick, R. M.** (1991). Modulation of neural networks. *Annu. Rev. Neurosci.* **14**, 39–57.

- Hatsopoulos, N. G., Gabbiani, F. and Laurent, G.** (1995). Elementary computation of object collision by a wide-field visual neuron. *Science* (80-. ). **270**, 1–8.
- Hawryshyn, C. W. and McFarland, W. N.** (1987). Cone photoreceptor mechanisms and the detection of polarized light in fish. *J. Comp. Physiol. A* **160**, 459–465.
- Hedenström, A.** (2014). How Insect Flight Steering Muscles Work. *PLoS Biol.* **12**, 1–4.
- Hedenström, A. and Johansson, L. C.** (2015). Bat flight: aerodynamics, kinematics and flight morphology. *J. Exp. Biol.* **218**, 653–63.
- Hemmi, J. M.** (2005). Predator avoidance in fiddler crabs: 2. The visual cues. *Anim. Behav.* **69**, 615–625.
- Horridge, F. R. .** (1978). The separation of visual axes in apposition compound eyes. *Philos. Trans. R. Soc. London* **285**, 1–59.
- Horsmann, U., Heinzl, H. G. and Wendler, G.** (1983). The phasic influence of self-generated air current modulations on the locust flight motor. *J. Comp. Physiol. □ A* **150**, 427–438.
- Hoyle, G.** (1955). The anatomy and innervation of locust skeletal muscle. *R. Soc. London* **143**, 281–292.
- Ijspeert, A. J.** (2008). Central pattern generators for locomotion control in animals and robots: A review. *Neural Networks* **21**, 642–653.
- Isreal, Z. and Burchiel, K.** (2004). *Microelectrode Recordings in Movement Disorder Surgery*. Thieme Medical Publisher.
- Judge, S. and Rind, C. F.** (1997). The locust DCMD, a movement-detecting neurone tightly tuned to collision trajectories. *J. Exp. Biol.* **200**, 2209–2216.
- Kalmus, H.** (1972). A new model describing the coordination of the legs of a walking stick. *Nature* **237**, 55–56.
- Kiehn, O.** (2006). Locomotor Circuits in the Mammalian Spinal Cord. *Annu. Rev. Neurosci.* **29**, 279–306.
- Knafo, S. and Wyart, C.** (2018). Active mechanosensory feedback during locomotion in the zebrafish spinal cord. *Curr. Opin. Neurobiol.* **52**, 48–53.
- Konishi, M.** (1998). How the owl resolves auditory coding ambiguity. *Proc. Natl. Acad. Sci.* **95**, 10932–10937.
- Körding, K. P. and Wolpert, D. M.** (2004). Bayesian integration in sensorimotor learning. *Nature* **427**, 244–7.
- Krahe, R. and Gabbiani, F.** (2004). Burst firing in sensory systems. *Nat. Rev. Neurosci.* **5**, 13–23.
- Kramer, B.** (1996). *Electroreception and Communication in Fishes*. Gustav Fischer, Germany.



- Krieger, J., Braun, P., Rivera, N. T., Schubart, C. D., Müller, C. H. G. and Harzsch, S.** (2015). Comparative analyses of olfactory systems in terrestrial crabs (Brachyura): Evidence for aerial olfaction? *PeerJ* **2015**,.
- Kruyt, J. W., Van Heijst, G. J. F., Altshuler, D. L. and Lentink, D.** (2015). Power reduction and the radial limit of stall delay in revolving wings of different aspect ratio. *J. R. Soc. Interface* **12**, 1–7.
- Kullander, K.** (2012). Role of EphA4 and EphrinB3 in Local Neuronal Circuits That. *Proc. R. Soc. London Ser. B* **299**, 1889–1893.
- Lee, D. N.** (1976). A theory of visual control of breaking based on information about time to contact. *Perception* **5**, 437–459.
- Lehmann, F. O.** (2004). The mechanisms of lift enhancement in insect flight. *Naturwissenschaften* **91**, 101–122.
- Lentink, D. and Dickinson, M. H.** (2009). Rotational accelerations stabilize leading edge vortices on revolving fly wings. *J. Exp. Biol.* **212**, 2705–2719.
- Li, W.-C., Merrison-Hort, R., Zhang, H.-Y. and Borisyuk, R.** (2014). The Generation of Antiphase Oscillations and Synchrony by a Rebound-Based Vertebrate Central Pattern Generator. *J. Neurosci.* **34**, 6065–6077.
- Lighthill, M. J.** (1973). On the Weis-Fogh mechanism of lift generation. *J. Fluid Mech.* **60**, 1–17.
- Lissmann, H. W. and Machin, K. E.** (1958). The Mechanism of Object Location in *Gymnarchus Niloticus* and Similar Fish. *J. Exp. Biol.* **35**, 451–486.
- Marder, E. and Bucher, D.** (2001). Central pattern generators and the control of rhythmic movements. *Curr. Biol.* **11**, R986–R996.
- Marsat, G. and Pollack, G. S.** (2012). Bursting neurons and ultrasound avoidance in crickets. *Front. Neurosci.* **6**, 1–9.
- Martinez-Conde, S., Macknik, S. L. and Hubel, D. H.** (2002). The function of bursts of spikes during visual fixation in the awake primate lateral geniculate nucleus and primary visual cortex. *Proc. Natl. Acad. Sci.* **99**, 13920–13925.
- Matheson, T., Rogers, S. M. and Krapp, H. G.** (2004). Plasticity in the Visual System Is Correlated With a Change in Lifestyle of Solitarious and Gregarious Locusts. *J. Neurophysiol.* **91**, 1–12.
- McClamroch, N. H.** (2011). *Steady Aircraft Flight and Performance*. 1st ed. Princeton: Princeton University Press.

- McConney, M. E., Schaber, C. F., Julian, M. D., Eberhardt, W. C., Humphrey, J. A. C., Barth, F. G. and Tsukruk, V. V.** (2009). Surface force spectroscopic point load measurements and viscoelastic modelling of the micromechanical properties of air flow sensitive hairs of a spider (*Cupiennius salei*). *J. R. Soc. Interface* **6**, 681–694.
- McMillan, G. A. and Gray, J. R.** (2012). A looming-sensitive pathway responds to changes in the trajectory of object motion. *J. Neurophysiol.* **108**, 1052–1068.
- McMillan, G. A. and Gray, J. R.** (2015). Burst Firing in a Motion-Sensitive Neural Pathway Correlates with Expansion Properties of Looming Objects that Evoke Avoidance Behaviors. *Front. Integr. Neurosci.* **9**, 1–13.
- McMillan, G. A., Loessin, V. and Gray, J. R.** (2013). Bilateral flight muscle activity predicts wing kinematics and 3-dimensional body orientation of locusts responding to looming objects. *J. Exp. Biol.* **216**, 3369–3380.
- MIALL, R. C.** (1978). The flicker fusion frequencies of six laboratory insects, and the response of the compound eye to mains fluorescent ‘ripple.’ *Physiol. Entomol.* **3**, 99–106.
- Miller, L. A. and Peskin, C. S.** (2009). Flexible clap and fling in tiny insect flight. *J. Exp. Biol.* **212**, 3076–3090.
- Miller, L. A. and Surlykke, A.** (2001). How Some Insects Detect and Avoid Being Eaten by Bats: Tactics and Countertactics of Prey and Predator. *Bioscience* **51**, 570–581.
- Miller, G. A., Dodgson, T., Simpson, S. J., Claridge, T. D. W. and Islam, M. S.** (2008). Swarm formation in the desert locust *Schistocerca gregaria*: isolation and NMR analysis of the primary maternal gregarizing agent. *J. Exp. Biol.* **211**, 370–376.
- Möhl, B. and Zarnack, W.** (1977). Activity of the direct downstroke flight muscles of *Locustamigratoria* (L.) during steering behaviour in flight. 2. Dynamics of the time shift and changes in the burst length. *J. Comp. Physiol.* **1118**, 235–247.
- Mohr, N. A. and Gray, J. R.** (2003). Collision Avoidance in Flying Locusts. *Neurosci. Abstr. Program nu*, 403.2.
- Money, T. G. A., Anstey, M. L. and Robertson, R. M.** (2004). Heat Stress–Mediated Plasticity in a Locust Looming-Sensitive Visual Interneuron. *J. Neurophysiol.* **93**, 1908–1919.
- Montell, C.** (2012). *Drosophila* visual transduction. *Trends Neurosci.* **35**, 356–363.
- Nalbach, H.-O.** Visually Elicited Escape in Crabs. *Front. Crustac. Neurobiol.* 165–172.
- Nordstrom, K.** (2013). Robust prey detection in a small nervous system. *Proc. Natl. Acad. Sci.* **110**, 389–390.
- O’Shea, M. and Williams, J. L. D.** (1974). The anatomy and output connection of a locust visual interneurone; the lobular giant movement detector (LGMD) neurone. *J. Comp. Physiol.* **91**, 257–266.

- Olberg, R. M.** (1986). Identified target-selective visual interneurons descending from the dragonfly brain. *J. Comp. Physiol. A* **159**, 827–840.
- Olberg, R. M., Worthington, A. H. and Venator, K. R.** (2000). Prey pursuit and interception in dragonflies. *J. Comp. Physiol. - A Sensory, Neural, Behav. Physiol.* **186**, 155–162.
- Oliva, D., Medan, V. and Tomsic, D.** (2007). Escape behavior and neuronal responses to looming stimuli in the crab *Chasmagnathus granulatus* (Decapoda: Grapsidae). *J. Exp. Biol.* **210**, 865–880.
- Pener, M. P. and Yerushalmi, Y.** (1998). The physiology of locust phase polymorphism: An update. *J. Insect Physiol.* **44**, 365–377.
- Pesavento, U. and Wang, Z. J.** (2009). Flapping wing flight can save aerodynamic power compared to steady flight. *Phys. Rev. Lett.* **103**, 1–4.
- Pringle, J. W. S.** (1954). The mechanism of the myogenic rhythm of certain insect striated muscles. *J. Physiol.* **124**, 269–291.
- Pringle, J. W. .** (1957). *Insect Flight*. Cambridge University Press.
- Pynn, L. K. and DeSouza, J. F. X.** (2013). The function of efference copy signals: Implications for symptoms of schizophrenia. *Vision Res.* **76**, 124–133.
- Reichel, S. V, Labisch, S. and Dirks, J.-H.** (2017). What goes up must come down  
Biomechanical impact analysis of jumping locusts. *bioRxiv* 1–15.
- Ribak, G., Rand, D., Weihs, D. and Ayali, A.** (2012). Role of wing pronation in evasive steering of locusts. *J. Comp. Physiol. A Neuroethol. Sensory, Neural, Behav. Physiol.* **198**, 541–555.
- Rillich, J., Stevenson, P. A. and Pflueger, H. J.** (2013). Flight and Walking in Locusts- Cholinergic Co-Activation, Temporal Coupling and Its Modulation by Biogenic Amines. *PLoS One* **8**, 1–11.
- Rind, F. C. and Simmons, P. J.** (1992). Orthopteran DCMD neuron: a reevaluation of responses to moving objects. I. Selective responses to approaching objects. *J. Neurophysiol.* **68**, 1654–1666.
- Rind, F. C. and Simmons, P. J.** (1996). Signaling of Object Approach by the DCMD Neuron of the Locust. *J. Neurophysiol.* **77**, 1029–1033.
- Rind, F. C., Wernitznig, S., Pölt, P., Zankel, A., Gütl, D., Sztarker, J. and Leitinger, G.** (2016). Two identified looming detectors in the locust: Ubiquitous lateral connections among their inputs contribute to selective responses to looming objects. *Sci. Rep.* **6**, 1–16.
- Roberts, T. F., Hisey, E., Tanaka, M., Kearney, M. G., Chattree, G., Yang, C. F., Shah, N. M. and Mooney, R.** (2017). Identification of a motor-to-auditory pathway important for vocal learning. *Nat. Neurosci.* **20**, 978–986.

- Robertson, R. M. and Johnson, A. G.** (1993). Retinal image size triggers obstacle avoidance in flying locusts. *Naturwissenschaften* **80**, 176–178.
- Robertson, R. M. and Pearson, K. G.** (1982). The distributed nature of the locust flight motor. *Soc. Neurosci.* 736.
- Robertson, R. M. and Pearson, K. G.** (1983). Interneurons in the flight system of the locust: Distribution, connections, and resetting properties. *J. Comp. Neurol.* **215**, 33–50.
- Robertson, R. M. and Reye, D. N.** (1992). Wing movements associated with collision-avoidance manoeuvres during flight in the locust *Locusta migratoria*. *J. Exp. Biol.* **163**, 231–258.
- Robertson, M., Kuhnert, C. and Dawson, J.** (1996). Thermal avoidance during flight in the locust *Locusta migratoria*. *J. Exp. Biol.* **199**, 1383–1393.
- Rogers, S. M.** (2004). Substantial changes in central nervous system neurotransmitters and neuromodulators accompany phase change in the locust. *J. Exp. Biol.* **207**, 3603–3617.
- Ros, I. G. and Biewener, A. A.** (2016). Optic flow stabilizes flight in ruby-throated hummingbirds. *J. Exp. Biol.* **219**, 2443–2448.
- Rowell, C. H. F. and Reichert, H.** (1991). Mesothoracic interneurons involved in flight steering in the locust. *Tissue Cell* **23**, 75–139.
- Ryckebusch, S. and Laurent, G.** (1993). Rhythmic patterns evoked in locust leg motor neurons by the muscarinic agonist pilocarpine. *J. Neurophysiol.* **69**, 1583–95.
- Salcedo, E., Zheng, L., Phistry, M., Bagg, E. E. and Britt, S. G.** (2003). Molecular basis for ultraviolet vision in invertebrates. *J. Neurosci.* **23**, 10873–8.
- Salinas, E. and Sejnowski, T.** (2010). Correlated neuronal activity and the flow of neural information. *Neuroscience* **2**,.
- Sandoz, J. C.** (2011). Behavioral and Neurophysiological Study of Olfactory Perception and Learning in Honeybees. *Front. Syst. Neurosci.* **5**, 1–20.
- Sane, S. P.** (2003a). Review The aerodynamics of insect flight. *J. Exp. Biol.* **206**, 4191–4208.
- Sane, S. P.** (2003b). The aerodynamics of insect flight. *J. Exp. Biol.* **206**, 4191–4208.
- Sane, S. P. and Dickinson, M. H.** (2001). The control of flight force by a flapping wing: lift and drag production. *J. Exp. Biol.* **204**, 2607–26.
- Sane, S. P. and Dickinson, M. H.** (2002). The aerodynamic effects of wing rotation and a revised quasi-steady model of flapping flight. *J. Exp. Biol.* **205**, 1087–1096.
- Sanger, T. D.** (2003). Neural population codes. *Curr. Opin. Neurobiol.* **13**, 238–249.
- Santer, R. D.** (2006). Role of an Identified Looming-Sensitive Neuron in Triggering a Flying Locust's Escape. *J. Neurophysiol.* **95**, 3391–3400.

- Santer, R. D., Simmons, P. J. and Rind, F. C.** (2005a). Gliding behaviour elicited by lateral looming stimuli in flying locusts. *J. Comp. Physiol. A Neuroethol. Sensory, Neural, Behav. Physiol.* **191**, 61–73.
- Santer, R. D., Simmons, P. J. and Rind, F. C.** (2005b). Response of the locust descending movement detector neuron to rapidly approaching and withdrawing visual stimuli. *J. Comp. Physiol. A Neuroethol. Sensory, Neural, Behav. Physiol.* **55**, 1–4.
- Santer, R. D., Rind, F. C., Stafford, R. and Simmons, P. J.** (2006). Role of an Identified Looming-Sensitive Neuron in Triggering a Flying Locust's Escape. *J. Neurophysiol.* **95**, 3391–3400.
- Santer, R. D., Yamawaki, Y., Rind, F. C. and Simmons, P. J.** (2008). Preparing for escape: An examination of the role of the DCMD neuron in locust escape jumps. *J. Comp. Physiol. A Neuroethol. Sensory, Neural, Behav. Physiol.* **194**, 69–77.
- Satterlie, R. A.** (2002). Neuronal control of swimming in jellyfish: a comparative story. *Can. J. Zool.* **80**, 1654–1669.
- Schmidt, J. and Zarnack, W.** (1987). Biological Cybernetics. *Biol. Cybern.* **56**, 397–410.
- Schürmann, F.-W. and Elekes, K.** (1987). *Synaptic Connectivity in the Mushroom Bodies of the Honeybee Brain: Electron Microscopy and Immunocytochemistry of Neuroactive Compounds*. Berlin Heidelberg: Springer-Verlag.
- Serres, J. R. and Ruffier, F.** (2017). Optic flow-based collision-free strategies: From insects to robots. *Arthropod Struct. Dev.* **46**, 703–717.
- Sherman, A. and Dickinson, M. H.** (2003). Summation of visual and mechanosensory feedback in *Drosophila* flight control. *J. Exp. Biol.* **207**, 133–142.
- Shoemaker, K. L. and Robertson, R. M.** (1998). Flight motor patterns of locusts responding to thermal stimuli. *J. Comp. Physiol. - A Sensory, Neural, Behav. Physiol.* **183**, 477–488.
- Silva, A. C., McMillan, G. A., Santos, C. P. and Gray, J. R.** (2014). Background complexity affects response of a looming-sensitive neuron to object motion. *J. Neurophysiol.* **113**, 218–231.
- Simmons, P. J., Rind, F. C. and Santer, R. D.** (2010). Escapes with and without preparation: The neuroethology of visual startle in locusts. *J. Insect Physiol.* **56**, 876–883.
- Smarandache-Wellmann, C. R.** (2016). Arthropod neurons and nervous system. *Curr. Biol.* **26**, R960–R965.
- Sobel, E. C. and Tank, D. W.** (2006). In Vivo  $Ca^{2+}$  Dynamics in a Cricket Auditory Neuron: An Example of Chemical Computation, Published by: Ameri. *Science* (80-. ). **263**, 823–826.
- Sommerfeld, A.** (1908). A Contribution to Hydrodynamic Explanation of Turbulent Fluid Motions. *Int. Congr. Math.* 116–124.

- Speck-Hergenröder, J. and Barth, F. G.** (1987). Tuning of vibration sensitive neurons in the central nervous system of a wandering spider, *Cupiennius salei* Keys. *J. Comp. Physiol. A* **160**, 467–475.
- Stein, R. B., Gossen, E. R. and Jones, K. E.** (2005). Neuronal variability: Noise or part of the signal? *Nat. Rev. Neurosci.* **6**, 389–397.
- Stevens, S. S.** (1966). Duration, luminance, and the brightness exponent. *Percept. Psychophys.* **1**, 96–100.
- Stott, T. P., Olson, E. G. N., Parkinson, R. H. and Gray, J. R.** (2018). Three-dimensional shape and velocity changes affect responses of a locust visual interneuron to approaching objects. *J. Exp. Biol.* **221**, jeb191320.
- Straw, A. D.** (2008). Vision Egg: An open-source library for realtime visual stimulus generation. *Front. Neuroinform.* **2**, 1–10.
- Sun, F., Wang, Y. J., Zhou, Y. Q., Van Swinderen, B., Gong, Z. F. and Liu, L.** (2014). Identification of neurons responsible for feeding behavior in the *Drosophila* brain. *Sci. China Life Sci.* **57**, 391–402.
- Sunada, S., Kawachi, K., Watanabe, I. and Azuma, A.** (1993). Performance of a butterfly in take-off flight. *J. Exp. Biol.* **183**, 249–277.
- Taube, J. S.** (2007). The Head Direction Signal: Origins and Sensory-Motor Integration. *Annu. Rev. Neurosci.* **30**, 181–207.
- Taylor, G. K.** (2001). Mechanics and aerodynamics of insect flight control. *Biol. Rev.* **76**, 449–471.
- Thüring, D. A.** (1986). Variability of motor output during flight steering in locusts. *J. Comp. Physiol. A* **158**, 653–664.
- Topaz, C. M., Bernoff, A. J., Logan, S. and Toolson, W.** (2008). A model for rolling swarms of locusts. *Eur. Phys. J. Spec. Top.* **157**, 93–109.
- Troy Zars** (2000). Behavioral functions of the insect mushroom bodies. *Curr. Opin. Neurobiol.* **10**, 790–795.
- Usherwood, J. R. and Lehmann, F. O.** (2008). Phasing of dragonfly wings can improve aerodynamic efficiency by removing swirl. *J. R. Soc. Interface* **5**, 1303–1307.
- Uvarov, B.** (1977). *Grasshopper and locusts. A handbook of general acridology Vol.2*. London: Centre for Overseas Pest Research.
- Van Hiel, M. B., Depuydt, G., Schoofs, L., Boerjan, B., Ernst, U. R. and De Loof, A.** (2015). Epigenetics and locust life phase transitions. *J. Exp. Biol.* **218**, 88–99.
- VanRullen, R., Guyonneau, R. and Thorpe, S. J.** (2005). Spike times make sense. *Trends Neurosci.* **28**, 1–4.



- Vitzthum, H., Müller, M. and Homberg, U.** (2002). Neurons of the Central Complex of the Locust *Schistocerca gregaria* are Sensitive to Polarized Light. *J. Neurosci.* **22**, 1114–1125.
- Volman, S. F.** (1994). *Directional Hearing in Owls: Neurobiology, Behaviour and Evolution*. Berlin: Springer Berlin Heidelberg.
- von Holst, E. and Mittelstaedt, H.** (1950). Das Reafferenzprinzip. *Naturwissenschaften* **37**, 464–476.
- Wakeeling, J. M. and Ellington, C. P.** (1997). Dragonfly flight. *J. Exp. Biol.* **200**, 557–582.
- Wang, X.-J.** (1998). Calcium Coding and Adaptive Temporal Computation in Cortical Pyramidal Neurons. *Am. Psychol. Soc.* **79**, 1549–1566.
- Wang, Y. and Frost, B. J.** (1992). Time to collision is signalled by neurons in the nucleus rotundus of pigeons. *Nature* **356**, 236–238.
- Wang, Y., Gupta, A., Toledo-Rodriguez, M., Wu, C. Z. and Markram, H.** (2002). Anatomical, Physiological, Molecular and Circuit Properties of Nest Basket Cells in the Developing Somatosensory Cortex. *Cereb. Cortex* **12**, 395–410.
- Warrant, E. J.** (1999). Seeing better at night: Life style, eye design and the optimum strategy of spatial and temporal summation. *Vision Res.* **39**, 1611–1630.
- Wehner, R.** (1987). “Matched filters” - neural models of the external world. *J. Comp. Physiol. A* **161**, 511–531.
- Wehner, R., Warrant, E. J., Processing, V. M., Smooth, I. F. O. R., Movements, P. E. Y. E., Warrant, E. J., Sperry, R., Lorenz, K., Guthrie, B. D. M., Derby, C. D., et al.** (2008). Central pattern generators and the control of rhythmic movements. *Neuroscience* **56**, 1–8.
- Weis-fogh, B. Y. T.** (1973). Fitness in Hovering Animals , Including Novel. *J. Exp. Biol.* **59**, 169–230.
- Whiting, M. F., Carpenter, J. C., Wheeler, Q. D. and Wheeler, W. C.** (1997). The strepsiptera problem: Phylogeny of the holometabolous insect orders inferred from 18S and 28S ribosomal DNA sequences and morphology. *Syst. Biol.* **46**, 1–68.
- Willi, U. B., Bronner, G. N. and Narins, P. M.** (2006). Ossicular differentiation of airborne and seismic stimuli in the Cape golden mole (*Chrysochloris asiatica*). *J. Comp. Physiol. A Neuroethol. Sensory, Neural, Behav. Physiol.* **192**, 267–277.
- Williams, C. D. and Biewener, A. A.** (2015). Pigeons trade efficiency for stability in response to level of challenge during confined flight. *Proc. Natl. Acad. Sci.* **112**, 3392–3396.
- Wilson, D. M.** (1966). Central nervous mechanisms for the generation of rhythmic behaviour in arthropods. *Symp Soc Exp Biol* 199–228.
- Wilson, D. M.** (1968a). The flight-control system of the locust. *Sci. Am.* **218**, 83–90.

- Wilson, D. M.** (1968b). The Nervous Control of Insect Flight and Related Behavior<sup>1</sup>. *Adv. In Insect Phys.* **5**, 289–338.
- Wilson, D. M.** (1968c). Inherent asymmetry and reflex modulation of the locust flight motor pattern. *J. Exp. Biol.* **48**, 631–41.
- Wilson, M.** (1978). Journal of Comparative Physiology. A The Functional Organisation of Locust Ocelli. *Physiol* **124**, 297–316.
- Wilson, D. M. and Weis-Fogh, T.** (1962). Patterned Activity of Co-Ordinated Motor Units, Studied in Flying Locusts. *J. Exp. Biol.* **39**, 643–667.
- Wilson, M., Garrard, P. and McGinness, S.** (1978). The unit structure of the locust compound eye. *Cell Tissue Res.* **195**, 205–226.
- Yakubowski, J. M., Mcmillan, G. A. and Gray, J. R.** (2016). Background visual motion affects responses of an insect motion-sensitive neuron to objects deviating from a collision course. *Physiol. Rep.* **4**, 1–15.
- Yang, H., Yang, J., Xi, W., Hao, S., Luo, B., He, X., Zhu, L., Lou, H., Yu, Y., Xu, F., et al.** (2016). Laterodorsal tegmentum interneuron subtypes oppositely regulate olfactory cue-induced innate fear. *Nat. Neurosci.* **19**, 283–289.
- Zeldenrust, F., Wadman, W. J. and Englitz, B.** (2018). Neural Coding With Bursts—Current State and Future Perspectives. *Front. Comput. Neurosci.* **12**, 1–14.
- Zucker, R. S.** (1971). Crafish Escape Behaviour and Central Synapses I. Neural Circuit Exciting Lateral Giant Fiber. *Dep. Biol. Sceinces Progr. Neurol. Sceinces* 599–620.